INFORMATION TO USERS

This manuscript has been reproduced from the microfilm master. UMI films the text directly from the original or copy submitted. Thus, some thesis and dissertation copies are in typewriter face, while others may be from any type of computer printer.

The quality of this reproduction is dependent upon the quality of the copy submitted. Broken or indistinct print, colored or poor quality illustrations and photographs, print bleedthrough, substandard margins, and improper alignment can adversely affect reproduction.

In the unlikely event that the author did not send UMI a complete manuscript and there are missing pages, these will be noted. Also, if unauthorized copyright material had to be removed, a note will indicate the deletion.

Oversize materials (e.g., maps, drawings, charts) are reproduced by sectioning the original, beginning at the upper left-hand corner and continuing from left to right in equal sections with small overlaps.

Photographs included in the original manuscript have been reproduced xerographically in this copy. Higher quality 6" x 9" black and white photographic prints are available for any photographs or illustrations appearing in this copy for an additional charge. Contact UMI directly to order.

Bell & Howell Information and Learning
300 North Zeeb Road, Ann Arbor, MI 48106-1346 USA
800-521-0600

INTERFACE ISSUES IN INDUCTION MOTOR DRIVES

Ali Hussein

A Thesis

in

The Department

of

Electrical and Computer Engineering

Presented in Partial Fulfillment of the Requirements
for the degree of Master of Applied Science at
Concordia University
Montreal, Quebec, Canada

August 1996

ABSTRACT

INTERFACE ISSUES

IN

INDUCTION MOTOR DRIVES

Ali Hussein

Adjustable speed induction motor drives are used more and more often in industry, particularly as an energy saving measure. Due to the presence of the power electronic drives, nonsinusoidal waveforms are injected into the electric distribution and the motor, affecting both the motor and the other loads connected to the same bus. In addition, the output voltage waveform of the converter feeding the motor has adverse effects on its insulation, particularly when long supply cables are used.

This thesis is a contribution to the study of these problems, associated with the use of adjustable speed drives. The motor drive circuit characteristics are studied when the speed of the motor is controlled using a pulse width modulated (PWM) inverter. The influence of cable length and power semiconductors switching times on motor overvoltages are studied for different rise times and cable lengths. Simulation studies are carried out using the EMTP software package. Simulation results are verified experimentally.

ACKNOWLEDGMENTS

I wish to express my sincere gratitude to my supervisor, Dr. Géza Joós for his guidance, help, encouragement and financial support during the course of this study.

I am also grateful to my many friends in the Power Electronics Laboratory, who made the period of this study more pleasant and fruitful. I will never forget the wonderful memory of working in the Power Electronics Laboratory. Special thanks to Mr. Jose Espinoza for many helpful discussions we shared.

I would also like to thank Mr. Alireza Bakhshai for his helpful suggestions in reading and correcting of this manuscript.

Special appreciation goes to my parents for their patience and encouragement.

TABLE OF CONTENTS

LIST OF FIGURES

Page

Chapter 4

Chapter 5

LIST OF TABLES

Page

LIST OF PRINCIPAL SYMBOLS

1. Voltage:

v_{d_s}	Stator voltage in *d*-axis
v'_{d_r}	Scaled rotor voltage in *d*-axis
v_{q_s}	Stator voltage in *q*-axis
v'_{q_r}	Scaled rotor voltage in *q*-axis
v_{0_s}	Stator voltage in *0*-axis
v'_{0_r}	Scaled rotor voltage in *0*-axis
V_e	Electrical equivalent voltage
V_s	Per phase rms motor input voltage
V_{dc}	The dc bus voltage
V_{LL_1}	Line to line rms fundamental voltage
E_s	Induced stator voltage
V_{th}	Thevinin equivalent voltage
V_{t_h}	Thevinin equivalent voltage for h^{th} *harmonic*
V_{base}	Base voltage
V_{al}	Motor rated voltage
E	Traveling wave voltage
e_1	Incident wave
e_2	Reflected wave
v_m	load voltage
$E_m(t)$	Voltage wave at node *m*
$E_n(t)$	Voltage wave at node *n*
V_{LL}	Supply input rms line to line voltage
V_{cc}	Coupling common voltage
V_{C_r}	Capacitor peak voltage

2. Current:

i_{d_s}	Stator current in *d*-axis
i'_{d_r}	Scaled rotor current in *d*-axis
i_{q_s}	Stator current in *q*-axis
i'_{q_r}	Scaled rotor current in *q*-axis
i_{0_s}	Stator current in *0*-axis
I_e	Injected current
i'_{0_r}	Scaled rotor current in *0*-axis
I_s	Per phase rms stator current
I_M	Per phase rms magnetizing current
I'_r	Per phase scaled rms current
I_{base}	Base current
I	Traveling wave current
i_1	Incident wave current
i_2	Reflected wave current
i_m	Load current
$i_{n,m}$	Current flowing from node *n* into node *m*
$i_{m,n}$	Current flowing from node *m* into node *m*
I_m	Current at node *m*
I_n	Current at node *n*
i_{dc}	The dc link current
I_c	Capacitor bank phase current
I_l	Linear load phase current
I_t	Resulting linear load phase current
I_{s_1}	Supply input phase current
I_{s_2}	Rectifier input phase current

3. Power

S_l	Apparent power
P_l	Active power
Q_l	Reactive power

4. Flux linkage:

λ_{d_s}	Stator flux linkage in *d*-axis
λ_{q_s}	Stator flux linkage in *q*-axis
λ'_{q_r}	Scaled rotor flux linkage in *d*-axis
λ'_{q_r}	Scaled rotor flux linkage in *q*-axis

5. Speed:

n	Machine speed
n_s	Synchronous speed
ω	Reference frame speed
ω_r	Rotor electrical speed
ω_m	Mechanical motor speed
v	Traveling wave speed

6. Torque:

T	Electromagnetic torque
T_L	Load torque
T_M	Useful mechanical torque

7. Frequency:

f	Motor input frequency

f_c	Carrier frequency
f_{base}	Base frequency
f_h	Harmonic frequency

8. Time:

t	Time
t_0	Traveling time

9. Resistance:

r_s	Per phase stator resistance
$r_r^{'}$	Per phase rotor scaled resistance
R_e	Electrical equivalent resistance
R_s	Line resistance
R_i	Sending end resistance
R_m	Load resistance
R_{max}	Maximum skin effect resistance
R_{min}	Cable resistance
R_L	Rectifier Load

10. Inductance:

L_{l_s}	Stator leakage inductance
$L_{l_r}^{'}$	Scaled rotor leakage inductance
L_e	Electrical equivalent inductance
L_s	Supply inductance
L	Cable inductance per meter
L_m	Load inductance

11. Capacitance:

C_e	Electrical equivalent capacitance
C_r	Rectifier filter capacitance
C	Cable capacitance per meter

12. Control Parameters:

V_{ref}	Reference wave
V_c	Carrier wave
m_a	Reference wave amplitude
m_f	Frequency modulation ratio

13. Miscellaneous:

J	Moment of inertia
B	Friction and windage coefficient
P	Number of pole pairs
S	Spring constant
θ_m	Mechanical angle
q_e	Electrical capacitor charge
s	Slip
φ	Air gap flux
D1, D2, D3, D4, D5, D6,	Rectifier bridge diodes
d1, d2, d3, d4, d5, d6	Inverter antiparallel diodes
T1, T2, T3, T4, T5, T6	Transistors
K, k	Integers
γ	Reflection coefficient

x	Distance
a, b, c	Three phase supply
a_1, a_2	Constants of integration

LIST OF ACRONYMS

EMTP	Electromagnetic Transient Program
PECAN	Power Electronic analysis Program
SPICE	Simulation Program With Integrated Circuit Emphasis
VSI	Voltage Source Inverter
PWM	Pulse Width Modulation
SPWM	Sinusoidal Pulse Width Modulated
PF	Power Factor
PF_i	Drive power factor
PF_m	Motor power factor

CHAPTER 1

INTRODUCTION

1.1 Introduction

The induction motor, particularly the squirrel cage type, is rugged, reliable, efficient, and has low maintenance requirements; therefore is the most widely used electric motor. However, until recently applications of the induction motor were limited to those requiring constant speed, as methods of speed control were either expensive, inefficient or limited.

With the advent of power semiconductor devices in 1950's and 60's, it has become possible to build cost effective variable speed induction motor drives. In the standard configuration for low and medium powers, the motor is fed from a voltage source inverter as shown in Fig. 1.1. The drive is a nonlinear load and therefore generates undesirable harmonics affecting the line and the other loads. Input effects include line current harmonics, line notching and distortion, and reduced power factor. Output effects are associated with the characteristics of the motor and the lines feeding the motor, namely heating, efficiency and overvoltages. Input considerations become more important as the use of solid state equipment increases and related standards are developed and applied. This increased concern is evident in the many questions put to equipment designers concerning line harmonics as well the possible adverse effects of

steep output voltage wave fronts on motor insulation and motor life when the motor is fed from the inverter using long cables.

Induction motor speed control, effect of the adjustable speed drive converter on line and motor, and motor overvoltages are the focus of this study. The simulation of the motor drive system is carried out using the Electromagnetic Transient Program (EMTP). The EMTP provides an appropriate environment for studying the behavior and the performance of adjustable speed drives. It allows representation of the drive and control system elements. Furthermore, the drive model developed in EMTP can be included in a broader power system study, particularly in harmonic penetration studies.

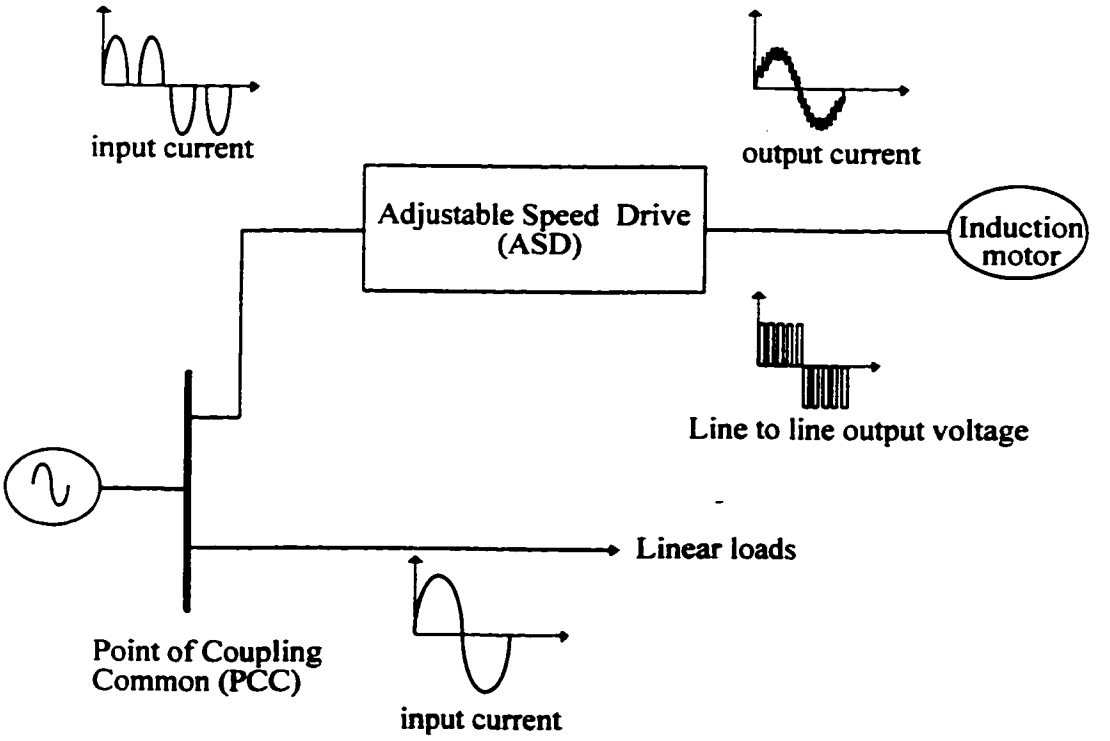

Fig. 1.1 Adjustable speed drive connected to a distribution bus.

1.2 Study of Induction Motor Drive Problems

Induction motor drive problems can be investigated by any of the following methods: (i) Laboratory tests, and (ii) Simulation studies.

The first method allows the most accurate analysis of the system behavior, but testing costs and availability of equipment remain an issue.

The second approach offers a good alternative since simulation is inexpensive and fast results are obtained. However, care must be taken when a physical system is studied by simulation. Correct modeling and appropriate simulation tools are crucial in obtaining correct and usable simulation results. However, the best validation method remains the experimental verification.

Simulation of adjustable speed induction motor drives involves modeling of the three major parts: motor, cable and converter unit. The EMTP with its exact models of cables [1], provides an excellent environment to study the motor terminal overvoltages. Moreover the program provides different models of induction machine, each one representing a special class of induction machine [2]. However, in EMTP there is no built in program models for either diode bridge rectifier or voltage source inverter thus, models need be developed for power converters.

1.3 Review of Previous Work

1.3.1 Induction Motor Speed Control and Modeling

The speed control of induction machines is the basis of industrial automation, quality control in production, increase in productivity and energy saving today[3] [4].

The interrelationship between the stator supply frequency and the synchronous speed of the induction motor indicates that frequency control is the most direct method to control the speed of the machine. Availability of solid state frequency converters with precise control of frequency has made possible variable speed induction motor drives for wide speed and power ranges [5]. To avoid motor saturation, the air gap flux can be maintained constant by varying the motor input voltage with frequency so that their ratio remains nearly constant [6] [7] [8]. At very low frequencies, the stator resistance dominates over the leakage inductance, and therefore additional voltage has to be impressed to compensate this effect [9].

Variable voltage variable frequency control can be obtained by using two kinds of inverters: square wave inverter and pulse width modulated inverter [10] [11]. Because of lower harmonic heating and torque pulsations compared to the square wave operation, the pulse width modulated (PWM) inverter is preferred for speed control.

The work on modeling of induction motors for electric drives is summarized in the following:

In [12], the model used for studying the steady state behavior of the machine is the single phase equivalent circuit. Klingshirn and Jordan have detailed the method of

calculating the currents and motor performance characteristics under steady state operation and nonsinusoidal source. Torque fluctuations have not been studied.

In [13], the method used to evaluate the torque fluctuations is the simplified motor per phase equivalent circuit. In addition, Robertson has neglected possible amplification of the harmonic torque due to rotor speed fluctuations.

In [14] [15], the motor is modeled using the back *emf* theory of the machines, and, the stator and rotor resistances are neglected for harmonic current calculations. The effect of machine resistances, in the harmonic equivalent circuit is negligible, except at low frequencies, where the resistances and harmonic leakage reactances become comparable.

In [16] [17], the motor is modeled using the *d-q* theory of machines. Therefore the machine can be represented either in the linear or saturation mode. This representation can be built in the EMTP program to simulate the motor drive system.

1.3.2 Simulation Techniques for Motor Drive Systems

Simulation of induction motor drive systems can be carried out using two kinds of electronic computers: (i) Analog, and (ii) Digital computers [18]-[24].

The effectiveness of an analog computer (electronic differential analyzer) for motor drive system is illustrated in [18]. It was used in 1960 where the system was represented using electronic devices [25] [26]. However, the analog computer simulation requires a substantial amount of computing equipment and has become obsolete.

Simulation techniques which yield a more direct means of simulating the system can be implemented using the digital computers.

Simulation of the motor drive systems using digital computer has been the standard for more than fifteen years [19-24]. Two categories using two different approaches of the representation of the system can be identified: (i) The state space approach [19] [20] [21], and (ii) The nodal approach [22] [23] [24].

In the state space approach, each switching stage of the circuit is described by a set of differential equations. However, following any change in the system topology, all differential equations have to be re-formulated resulting a longer execution time.

The nodal approach builds up the admittance matrix, and then solves voltages at each node. In nodal analysis approach, unlike the state space approach in which the state space equations have to be re-formulated after any change in a single branch, few elements in the admittance matrix must be changed for the same change in the same branch. This makes the nodal approach of PSPICE, PECAN and EMTP more convenient in a general simulation program.

The dynamic model for the induction motor can be built on the EMTP using the Universal Machine model available in the program [27] [28] in which the dynamics of the shaft is represented by an electric circuit, representing the mechanical shaft system [29] [30]. The nodal approach, therefore can be applied to both mechanical and electrical parts.

1.3.3 Converters Modeling

Static power converters used in the control of a drive can be analyzed by means of widely available circuit simulation packages such as PSPICE, PECAN, and EMTP.

In PSPICE, the switches in the converter circuit are usually modeled as a set of real switches, which results in long execution times and possible convergence problems in the case of complex circuits [31].

In PECAN and EMTP, the switches are modeled as ideal switches, and convergence problems are eliminated [32] [33].

Another representation of converters can be obtained using the transfer or switching function concept [34] [35] [36]. This representation is a powerful tool in understanding and optimizing the performance of converters such as the Voltage Source Inverter (VSI), Current Source Inverter (CSI) and Controlled PWM rectifier (CR).

1.3.4 Cable Modeling

As a first approximation, a cable connecting the motor and the inverter can be modeled with lumped parameters [37] [38].

In order to explain the oscillations and overvoltages, the connecting cable can no longer be treated using lumped parameter model. A distributed element equivalent circuit has to be used, leading to a cable representation as transmission line, characterized by a resistance R, and inductance L, a capacitance C and conductance G per unit length. The EMTP has the capability of representing cables as well as overhead lines using a

distributed parameter model [39]. The data for a study involving cables is normally obtained from the cable manufacturer [40]. If the manufacturer's data is not available, the EMTP auxiliary routines can be used to evaluate an approximate parameters for a cable [1].

1.3.5 Motor Terminal Overvoltages

One of the tendencies that can be observed over the years, is that the switching frequencies of the power electronic switches increase. This allows the manufacturers to built inverters with improved sinusoidal wave shape in output voltage and/or current. The increase in the switching frequency is made possible by the progress made in the domain of the switching devices.

One of the drawbacks of this new generation of inverters is that considerable overvoltages appear when supplying a motor with a long cable. These may damage the insulation of the motor.

The output voltage waveform obtained from pulse width modulated control is not a pure sine wave, rather it consists of step functions. When these step functions with high voltage rate of change are applied to the inductive circuit of the motor through a cable, distributed inductance and capacitance result in traveling waves between the inverter and the motor terminals which give overvoltage on the motor side. The peak value of the voltage may exceed the motor rated voltage. Furthermore, the short rise time of the voltage front may result in all of the voltage being initially applied to the first turn in the

phase coil. This results in a voltage stress across the insulation of the first turn and the adjacent turn, and may lead to insulation failure [41].

This phenomenon has previously been studied and a technical papers published.

In [41], the traveling wave phenomenon and its effect on motor terminal voltage are investigated for different inverter output rise times and cable lengths. The information provided is very useful for starting a study of the overvoltages across the motor terminals. However, Persson has assumed the reflection coefficient [42] at the point of connection between the motor and the cable as fixed rather than variable.

In [37], the study demonstrates the effect of the PWM inverter output rise time and cable length on the motor terminal voltage. This analysis is however, carried out without taking into account the skin effect of the cable. Also, the cable has been represented using lumped parameters.

An experimental study is reported in [43], for different system parameters, such as the type of inverter power switch and cable length.

Another experimental study reported in [44] shows that the reflections in an armoured power cable cause may double the motor terminal voltage. The proposed solution uses an L - C filter at the inverter terminals.

1.3.6 Harmonics in the Power System

1.3.6.1 Effect of Harmonics

The presence of harmonics in a power system can be a source of undesirable effects in electrical system. Their effect can be summarized as follows [45] [46] [47]:

(i) Harmonics can be amplified resonances associated with capacitors used for power factor correction.

(ii) Increased losses in power generation, transmission and distribution.

(iii) Increased heating leading to aging of the insulation of electrical components and shortening of useful life.

(iv) Additional losses in the stator and rotor circuits of rotating machines.

(v) Harmonics can distort or degrade the operating characteristics of protective relays.

1.3.6.2 Harmonic Standard and Recommended Practices

The factors that define the quality of the electrical supply include harmonic distortion. Limits on harmonic currents injected into the electric circuit have been specified by various international agencies. The revised IEEE 519/1992 [48] places new emphasis on the reduction of line harmonics and line distortion at the point of common coupling (PCC) of linear and nonlinear loads.

Table 1.2 shows the recommended values for the individual voltage distortion components (IVD) and the total harmonic voltage distortion (THD_v) at the PCC.

Table 1.1

Voltage Distortion Limits

Bus voltage at PCC	% IVD	% THD_v
69 kV and below	3 %	5 %

Table 1.2 lists the recommended harmonic current limits at different harmonic frequencies.

Table 1.2

Current Distortion Limits (120 V Through 69 000 V)

Individual harmonic order						
I_{sc}/I_L	h <11	11 < h < 17	17 < h < 23	23 < h < 35	35 < h	%THD_i
< 20	4	2	1.5	0.6	0.3	5
20< 50	7	3.5	2.5	1	0.5	8
50 < 100	10	4.5	4	1.5	0.7	12
100 < 1000	12	5.5	5	2	1	15
> 1000	15	7	6	2.5	1.4	20

I_{sc} = Short circuit current at PCC
I_L = Load current

1.4 Scope and Contribution of this Thesis

This thesis identifies and analyzes the problems associated with the use of adjustable speed drive converter on the supply and the induction motor.

In order to identify these problems, the motor drive circuit is presented, analyzed and verified with simulation and experimental results.

The main objectives of this thesis are:

(i) Modeling and simulation of the motor drive circuit, and, evaluating the system problems.

(ii) Modeling and simulation of traveling waves in induction motor drives.

(iii) Investigating the influence of cable length and power semiconductor switching times on the magnitude of motor terminal voltage and presenting different options for the feed cable modeling.

(iv) Studying the effect of the line inductance on the total harmonic distortion of the line.

(v) Investigating the effect of capacitor bank switching on the dc bus voltage.

1.5 Thesis Outline

The contents of this thesis are organized as follows:

The modeling of induction motor using the EMTP program is studied in Chapter 2. The transient and steady state operation of the induction motor are observed and, the behavior of induction motor under variable frequencies is discussed.

In Chapter 3, the speed control of the induction motor below its rated speed using the voltage/hertz control ratio for constant torque is investigated. Torque harmonics and variation of switching frequency for different motor frequencies is discussed.

In Chapter 4, the effects of long motor leads on PWM inverter fed induction motor are investigated. The overvoltages across the motor terminals are compared for different inverter output rise times and cable lengths from no load to full load. Finally, a filter is proposed to damp out these high frequency oscillations.

Chapter 5 describes the effect of the line inductance on the diode bridge rectifier output characteristic for the continuous and discontinuous modes of operation. Finally, the effect of line capacitor switching on the dc link voltage is obtained for different rectifier dc link capacitor and line inductor values.

Chapter 6 gives the summary and the conclusions of the thesis. Further work related to the thesis is suggested.

CHAPTER 2

INDUCTION MOTOR MODELING

2.1 Introduction

Induction machines are used in a wide variety of applications as a means of converting electrical power to mechanical power. Induction motors, particularly the squirrel cage type, have a number of advantages when compared with dc motors. Some of these are lower maintenance requirements, weight, volume, inertia and higher efficiency [3][4].

In addition to representing the induction motor using its electrical equivalent circuit, a representation of the induction motor with its mechanical elements can be defined in the EMTP program by using the Universal Machine model. Based on the Universal Machine model, the induction motor (or generator), can be described using the two axis theory of electrical machines in which the motor is represented by the direct (*d-axis*) and quadrature (*q-axis*) quantities.

In this chapter, modeling of the induction motor in EMTP program is studied. Motor characteristics during transient operation are presented and the behavior of induction motor, when fed from a non sinusoidal supply, is also discussed.

2.2 Induction Machine Theory

A three phase induction machine consists of three phase stator winding 120 degrees apart (with equivalent turns N_s and resistance r_s per phase) which are supplied by an alternating current from a balanced three phase supply, and, three phase rotor windings 120 degrees apart (with equivalent N_r turns and resistance r_r per phase), rotor currents are created by induction from the stator. The rotor may be a short circuited squirrel cage structure or a wound rotor.

With balanced three phase current flowing in the stator winding, a rotating air gap magnetic field is induced which rotates about the air gap at a speed determined by the frequency of the stator currents and the number of poles in the machine. The field induces current in the rotor, thereby giving rise to another rotating magnetic field which rotates with respect to the rotor at a speed corresponding to the frequency of rotor current. Due to the interaction of these two fields, a torque is produced in the machine. If the rotor is allowed to run under the torque developed by this interaction, the machine will operate as a motor. On the other hand, the rotor may be driven by an external source beyond a speed such that the machine begins to deliver electrical power and operates as an induction generator [4].

Fig. 2.1 shows the equivalent circuit of the machine in the *dq0* axis reference frame. L_{l_s} and L'_{l_r} are the stator and the scaled rotor leakage inductances. λ_{d_s} and λ_{q_s} are the stator flux linkages of the stator windings in *d* and *q* axis. λ'_{d_r} and λ'_{q_r} are the scaled

rotor flux linkages in *d* and *q* axis. *M* is the magnetizing inductance, ω is the reference frame speed, and ω_r is the rotor electrical speed [5].

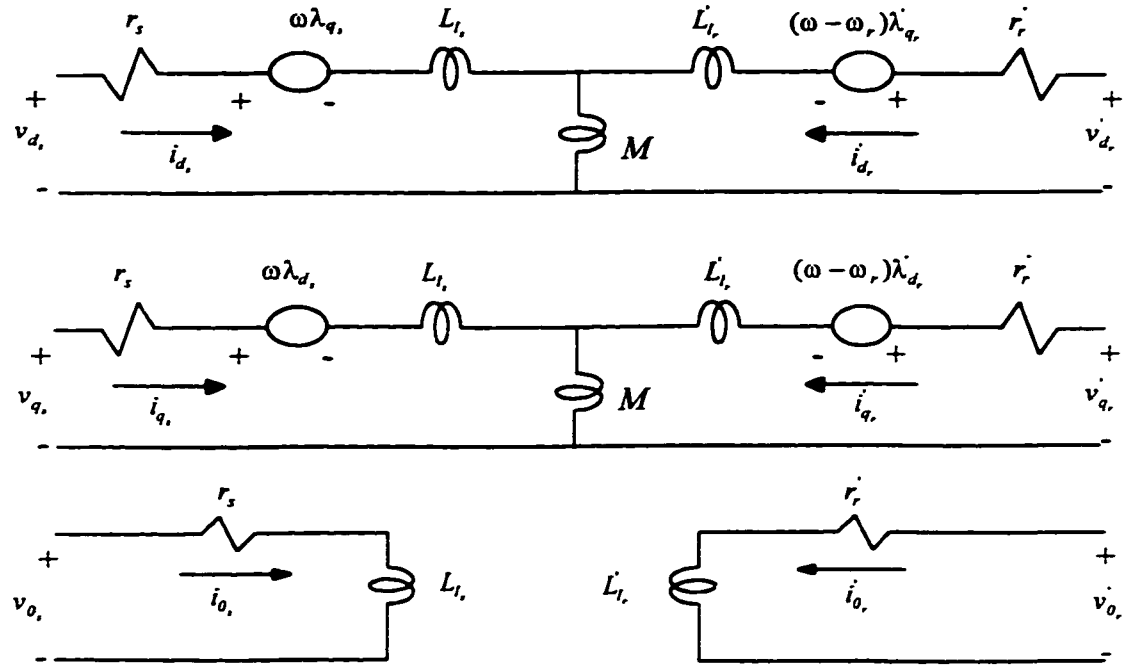

Fig. 2.1 Three phase symmetrical induction machine in *dq0* axis.

The electromagnetic torque produced by the machine in terms of an arbitrary reference frame is given by [5]:

$$T = (\frac{3}{2})(\frac{P}{2})(\lambda'_{q_r} i'_{d_r} - \lambda'_{d_r} i'_{q_r}) \tag{2.1}$$

where *P* is the number of poles in the machine.

If the machine is specified as a motor and J represents the moment of inertia of the motor load system referred to the motor shaft, and ω_m is the mechanical motor speed, then the electromagnetic torque can be written as:

$$T = J\frac{d\omega_m}{dt} + T_L \tag{2.2}$$

The first term in (2.2) represents the electromagnetic torque induced by the motor in N.m, and the second term represents the dynamic torque (inertial torque) which exists during the transient operation of the machine where J is in Kg.m^2. T_L represents the load torque induced by the motor in N.m.

The load torque has three components: friction, windage and mechanical torque. If windage and friction torques vary linearly with motor speed, then equation (2.2) can be written as:

$$T = J\frac{d\omega_m}{dt} + T_M + B\omega_m \tag{2.3}$$

where B is the friction and windage coefficient (N.m sec/rad), and T_M is the useful mechanical torque at the motor shaft.

The equivalent circuit diagram of Fig. 2.1 together with the torque equation of (2.1), and the dynamical equation of (2.3) are all we need to simulate an induction machine by an EMTP program to study the transient behavior of the machine.

2.3 The Universal Machine Model in the EMTP

The Universal Machine (UM) defined in EMTP is an electromechanical energy conversion device. Any type of rotating energy conversion devices connected to an

electrical network and mechanical system, can be modeled using it. The interface structure of the overall system can be divided into four parts [27][28][29]:

(i) The UM model which provides the system with information as to which type of electric machine is dealt with.

(ii) The electrical network such as supplies, transformers, transmission lines and cables which can be modeled by lumped parameters as well as distributed parameters.

(iii) The control system described by a block diagram with connections between the output terminals and the input terminals of the various blocks. Like all control systems some inputs to blocks are the measured variables sensed by the sensors and the outputs of some other blocks fed to the power system.

(iv) The mechanical system that is supposed to include the entire mechanical portion of the UM. The dual variables involved in the decomposition of the mechanical system and UM are the mechanical speed of the UM rotor mass and the electromagnetic torque produced by the electromagnetic system of the UM. The mechanical system that can be described by lumped parameters generates a mathematical model of the same form as the electrical and control circuits and in this case no special module needs to be developed for the mechanical system.

The schematic diagram of the general interface structure of the UM module with EMTP is shown in Fig. 2.2.

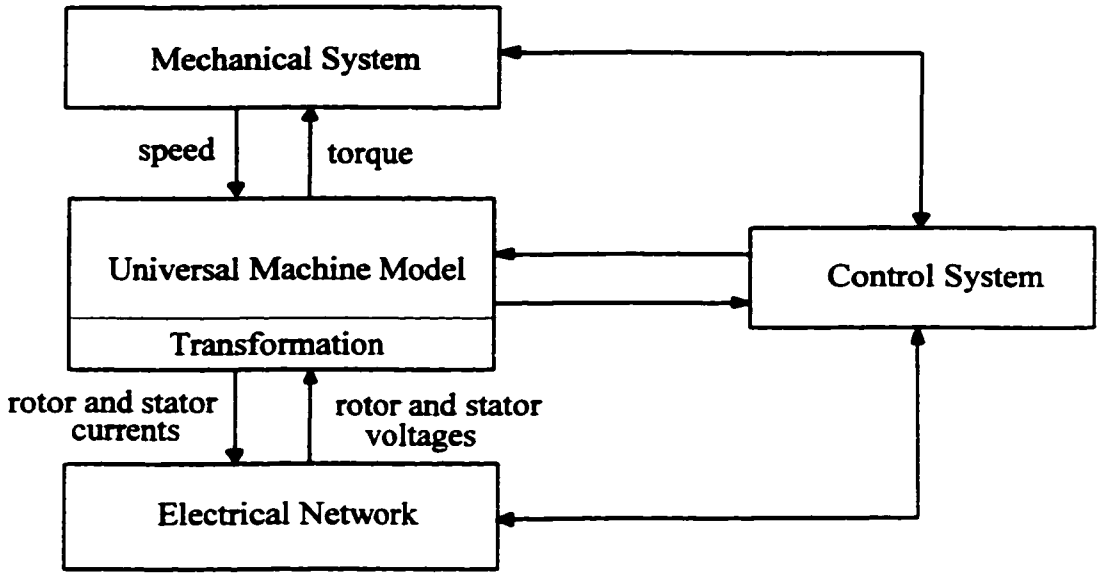

Fig. 2.2 UM schematic diagram.

The mechanical circuit of the drive can be described in the UM model and therefore can be represented using an equivalent electrical network, with lumped R_e, L_e and C_e, which is then specified as a part from the electric circuit network of the EMTP program. For each rotor mass, an equivalent node must be created in the overall electric circuit. All the mechanical data is transferred into electrical equivalent parameters at this node. The moment of inertia is represented by a capacitor (connected between the node and ground) of value J, and friction is represented by resistor (its value equals the inverse of the friction constant) connected in parallel with the capacitor. For two or more masses, an inductor (its value equals the inverse of the spring constant) connecting the adjacent capacitors is also added. Load torque will be a current injection into the bus with a

negative sign. There is no element providing the UM producing torque, since the EMTP provides this inherently [30].

Table 2.1 summarizes the relationship between mechanical quantities and electrical equivalents:

Table 2.1

Mechanical Quantities And Its

Electrical Equivalents Quantities

Mechanical quantities		Electrical equivalent quantities	
Shaft mass, J	$Kg.m^2$	Capacitance, C_e	F
Torque in shaft, T_S	N.m	Injected current, I_e	A
Friction, B	N.m.sec/rad	Conductance, $1/R_e$	Mho
Spring constant, S	N.m/rad	Inverse of inductance, $1/L_e$	1/H
Angular speed, ω_m	rad/sec	Voltage, V_e	V
Angle, θ_m	rad	Capacitor charge, q_e	Coulomb

The composition of the UM module with the electrical network and mechanical system modules involves the synchronization of the dual variables voltage and current at each electrical terminal separating the UM from the electrical network; for the mechanical side the dual variables are the electromagnetic torque and the rotor mechanical speed. The control of the information flow between the UM model and the electric network can be obtained using the processors *Transformation*. The information

flow concerns the voltages from the electric network to the UM and the currents from the UM to the electric network [28][29].

2.4 EMTP UM Representation of Induction Machines

Using the Universal Machine module in EMTP, induction machines can be represented with an arbitrary number of rotor circuits in the *d-q* axes. Types available in EMTP include [30]: *type 3* (three phase stator with arbitrary number of rotor circuits), *type 4* (three phase stator and three phase rotor), *type 5* (two phase stator with an arbitrary number of rotor circuits), *type 6* (single phase stator and single phase rotor) and *type 7* (single phase stator and two phase rotor). *Type 40* induction machine, could be used as a special application to obtain machine parameters from machine name plate data.

The saturation effect can be added in the simulation program using the UM approximation for the saturation curve. The saturation curve is represented as two linear segments with residual flux in the machine and can be included in the *d-q* axis [2][30].

2.5 Induction Motor Free Acceleration Characteristics

Free acceleration of induction motor is obtained when a three phase balanced voltage supply is applied directly to induction motor using contactor.

A 3 hp, 3-phase, 4 poles, 1740 RPM, 208 V, 10 A class B star connection induction motor was simulated using EMTP program and the results were studied. Motor parameters resulting from motor testing at rated frequency are shown in Table 2.2 with the rotor's resistance and leakage inductance referred to the stator side. The

magnetization curve of the motor is assumed to be linear (magnetization losses are neglected), the measured equivalent moment of inertia is 0.03 Kg.m^2 and the friction and windage losses assumed to vary linearly with the speed and at rated speed they are equal to 164 W. The variation of the rotor resistance during acceleration, due to the nonuniform current distribution between the layers, is approximated as linear variation and its maximum value equals 3.6 times the rotor steady state value [4]. Motor characteristics during free acceleration are shown in Fig. 2.3.

Table 2.2

3 hp Induction Motor Parameters Values

Per phase stator resistance, r_s	0.40 Ω
Per phase stator leakage inductance, L_{l_s}	1.80 mH
Per phase rotor resistance referred to the stator, $\dot{r_r}$	0.50 Ω
Per phase rotor leakage inductance referred to the stator, $\dot{L_{l_r}}$	2.70 mH
Per phase magnetizing inductance, M	48.3 mH

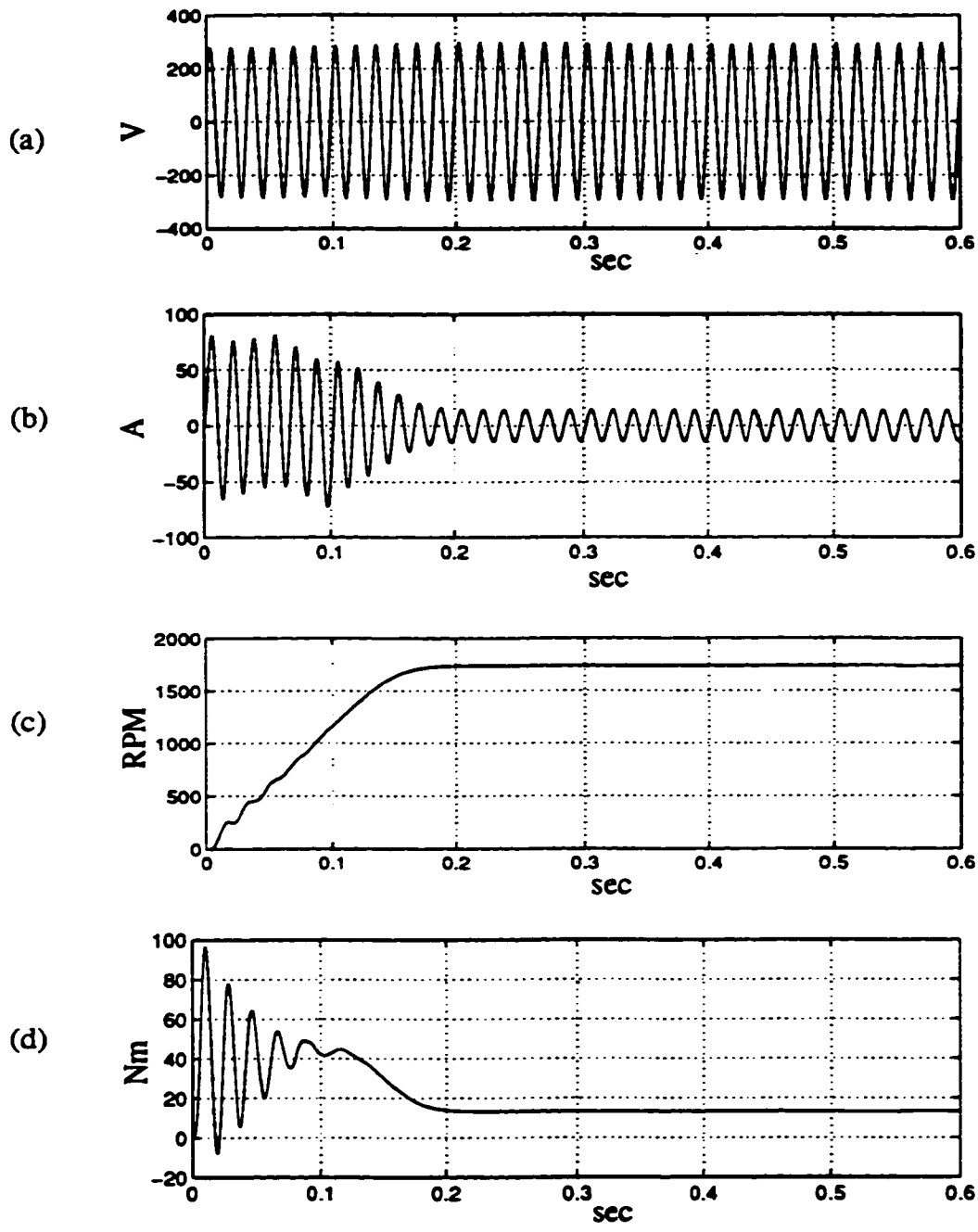

Fig. 2.3 Free acceleration of 3 hp induction motor (Simulation results)

(a) Line voltage. (b) Line current.

(c) Speed. (d) Electromagnetic torque.

At standstill, the motor is represented by its stator resistance and leakage reactance in series with the rotor resistance and leakage reactance. The terminal currents show a large value when the motor is energized. Therefore the motor requires an inrush current equal to more than four times its rated full load value in order to produce a torque level slightly greater than full load torque. During the time that the motor accelerates from zero speed to the maximum torque speed, the current remains near this high level. It drops off rapidly as the motor continues to accelerate, and settles down to its steady state value. The electromagnetic torque shows an initial oscillation that is typical for the start up of any induction motor, then it increases steadily until it reaches its maximum just before the rotor gets to its rated speed. When this speed is attained, all the machine variables attain their steady state values.

2.6 Experimental Result

The experimental result of motor input current under the normal operating conditions and during free acceleration is shown in Fig. 2.4.

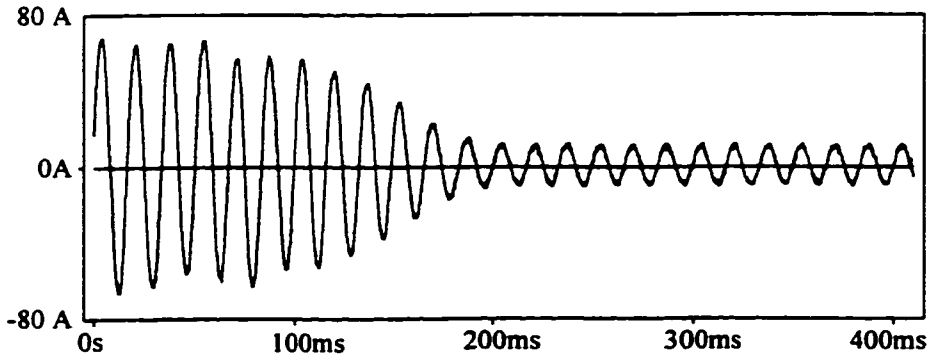

Fig. 2.4 Experimental motor input line current during free acceleration

2.7 Steady State Operation

Fig 2.5 shows the well known per phase equivalent circuit of a three phase squirrel cage induction motor in steady state when rotor equivalent resistance and reactance are referred to the stator side.

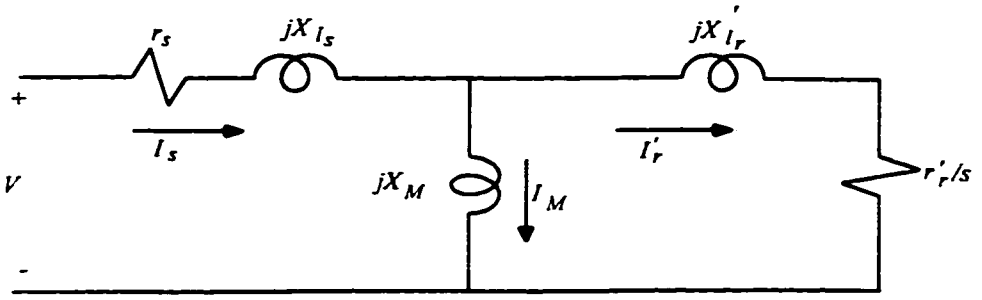

Fig. 2.5 Per phase steady state induction motor equivalent circuit.

At certain frequency f and motor slip s, the average torque developed by the motor can be calculated as [9]:

$$T = \frac{3}{4\pi}\frac{P}{f}\left[\frac{V_t^2 \frac{r'_r}{s}}{\left(R_t + \frac{r'_r}{s}\right)^2 + (X_t + X'_{l_s})^2}\right] \tag{2.4}$$

where V_t, R_t and X_t are the Thevenin's equivalent circuit parameters representing the stator and magnetizing branches in the equivalent circuit of Fig. 2.5:

$$V_t \angle \theta_t = \frac{VX_M}{\sqrt{r_s^2 + (X_{l_s} + X_M)^2}} \angle \frac{\pi}{2} - \tan^{-1}\left(\frac{X_{l_s} + X_M}{r_s}\right) \tag{2.5}$$

$$R_t + jX_t = \frac{jX_M(r_s + jX_{l_s})}{r_s + j(X_{l_s} + X_M)} \tag{2.6}$$

The motor output torque at the shaft is obtained by deducting friction, windage, and core loss torques from T in (2.4).

With appropriate modification the equivalent circuit shown in Fig. 2.5, can be used to represent the behavior of the induction motor for electric drives.

2.8 Modeling of Induction Machine for Electric Drives

Inverters used in the control circuit of induction machines apply essentially nonsinusoidal voltages to the motor. By using Fourier analysis, the motor line to line input voltage can be resolved into fundamental and harmonic components. Analysis of the performance of the motor proceeds as if there were a series of independent generators each representing one harmonic components connected in series and supplying the motor. The fundamental produces the average output torque and the harmonics produce losses and torque fluctuations [9].

The equivalent circuit for the h^{th} harmonic can be derived from the equivalent circuit of Fig. 2.5. All the reactances are modified by a factor h, and the harmonic slip is defined as:

$$s_h = \frac{(h-1)+s}{h} \qquad \textit{for positive sequence harmonics}$$

$$s_h = \frac{(h-1)-s}{h} \qquad \textit{for negative sequence harmonics} \tag{2.7}$$

If the fundamental component has the sequence *abc*, the phase sequence of the harmonic voltages and currents of order $h = 6r - 1$ (r is an integer) has a negative sequence *acb* (negative sequence harmonics). The harmonic field waves in the air gap rotate in direction opposite to that of the fundamental field with a speed equal to h times the fundamental synchronous speed. However, the phase sequence of the harmonic voltages and currents of order $h = 6r + 1$ is *abc* (positive sequence harmonics) and they produce harmonic field waves in the air gap rotating in the same direction of the motor main field with a speed equal to h times the fundamental synchronous speed [9].

The h^{th} harmonic torque can be calculated from (2.4) as:

$$T_h = \pm \frac{3}{4\pi} \frac{P}{hf} \left[\frac{V_{t_h}^2 \frac{r_r'}{s_h}}{\left(R_{t_h} + \frac{r_r'}{s_h} \right)^2 + (X_{t_h} + hX_r')^2} \right] \tag{2.8}$$

where V_{t_h} is the Thevenin equivalent harmonic voltage:

$$V_{t_h} \angle \theta_t = \frac{hV_h X_M}{\sqrt{r_s^2 + h^2 (X_S + X_M)^2}} \angle \frac{\pi}{2} - \tan^{-1} h \left(\frac{X_s + X_M}{r_s} \right) \tag{2.9}$$

and

$$R_{t_h} + jX_{t_h} = \frac{jhX_M (r_s + jhX_{l_s})}{r_s + jh(X_{l_s} + X_M)} \tag{2.10}$$

V_h in (2.9) represents the rms harmonic value.

2.9 Summary

The Universal Machine model of the EMTP allows the representation of the mechanical system of the induction machine. The start up of an unsaturated induction motor is simulated using a *type 4* UM and the results are verified experimentally. The EMTP model can be used to simulate the motor drive circuit. Thereafter, the modeling of induction machine for electric drives is discussed.

CHAPTER 3

INDUCTION MOTOR DRIVE MODELING

3.1 Introduction

Developments in power semiconductors towards an ideal switch have led to a wider use of these nonlinear devices including adjustable speed drives (ASD's). Unfortunately, the use of commercial ASD's has led to the common problem, among others, of harmonics injection into the main system in many industrial electrical systems. Modeling and analyzing ASD's has therefore become an important step to understand its behavior.

Testing of ASD's under controlled laboratory conditions can provide data on their behavior however, the behavior of the drive system can be studied in a more cost effective manner by computer simulations. It was shown in Chapter 2 that the model of induction machines using the EMTP program accurately represents the behavior of the induction motor. Using the switches and control systems available in EMTP, the complete ASD can be modeled.

This Chapter deals with the simulation of commercial ASDs and their associated problems. System harmonics, total harmonic distortion, motor and supply power factor and motor performance are obtained for different motor speed and load requirements. Simulation results are compared with those obtained experimentally.

3.2 Typical ASD Power Topology Description

The configuration of a commercial adjustable speed drive consists of diode bridge rectifier, dc filter capacitor, and a voltage source inverter. A simplified ASD configuration is shown in Fig. 3.1.

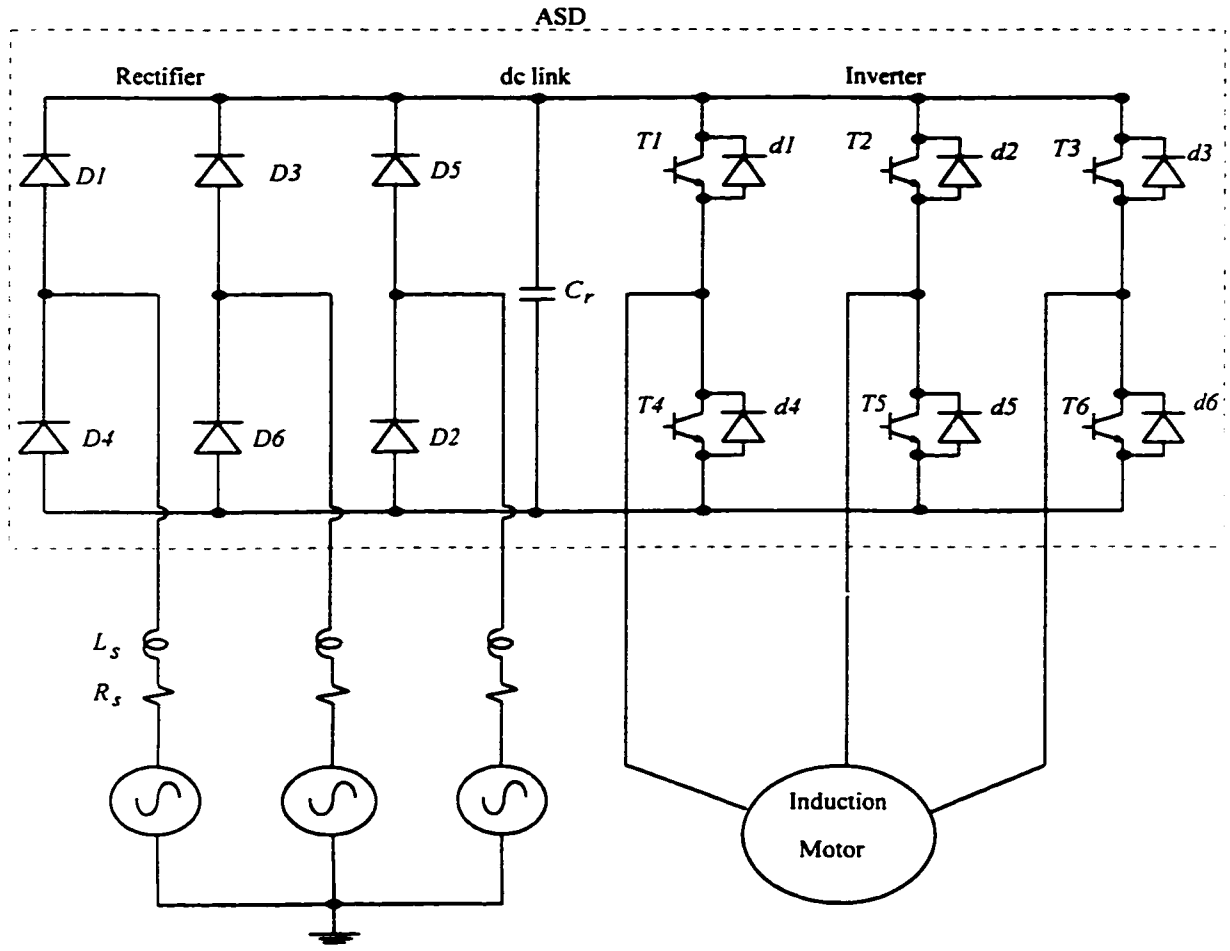

Fig. 3.1 Variable speed drive of an induction motor using a voltage source PWM.

The rectifier is made out of six diodes connected in two commutation groups consisting of valves *1-3-5*, and *4-6-2* respectively. Depending on the value of ac side inductance (L_s), the rectifier can operate in continuous or discontinuous mode. Voltage ripple in the rectifier output can be reduced by means of a filter capacitor connected at the dc side of rectifier.

The three phase voltage source inverter consists of six bipolar transistors with antiparallel diodes. In each branch, the transistors operate in a complementary function and do not conduct at the same time.

The voltage source inverter (VSI) uses pulse width modulation to produce an output voltage with a controlled fundamental rms voltage and frequency whereas the voltage harmonics are pushed to high frequencies.

The gating signals in the inverter circuit (Fig. 3.1) can be obtained by comparing three reference waves (V_{ref}) of frequency f (fundamental output voltage frequency), and amplitude m_a (pu amplitude) with a carrier waveform V_c of frequency f_c and amplitude equal to unity.

In three phase sinusoidal pulse width modulation, the reference signals in the three branches of the inverter are sinusoidal with a phase shift of 120°. The first control signal is compared with the carrier waveform and the result is applied to the first branch in the inverter circuit. By applying the same rules, the other two control signals are compared with the carrier waveform and the results are applied respectively to the second and third branches in the inverter circuit [9].

If V_{dc} represents the amplitude of the dc bus voltage in the inverter, the line to line rms voltage at the fundamental frequency is given by [9]:

$$V_{LL_1} = \frac{\sqrt{3}}{2\sqrt{2}} m_a V_{dc} \tag{3.1}$$

where m_a is also known the modulation index (control signal pu amplitude).

The frequency modulation ratio m_f can be defined as:

$$m_f = \frac{f_c}{f} \tag{3.2}$$

Since the VSI allows voltage and frequency control, it can be used to control the speed of induction motors. The motor voltage can be varied by varying the modulation index (3.1) and, the motor voltage frequency can be controlled by controlling the reference wave frequency.

3.3 Induction Motor Speed Control

The basic principle of speed control of squirrel cage induction motors using semiconductor devices is based on : (a) variable terminal voltage, and (b) variable frequency control.

In variable voltage control below the motor rated speed, speed control is obtained by varying the terminal voltage until the required torque is developed at the desired speed. For a specific slip value, the torque is proportional to the square of motor terminal voltage. The stator (and rotor) current is proportional to the motor terminal voltage. Hence, the torque to current ratio decreases with the terminal voltage. Consequently, the torque available for a given thermal loading of the motor also decreases. Moreover, the

maximum torque decreases in proportion to the square of terminal voltage. Low speed operation of the machine, therefore, is possible only if the load torque decreases with speed.

In variable frequency control, speed control is achieved by changing the motor input frequency. The voltage induced in the stator of the machine is given by:

$$E_s = k_s f \varphi \tag{3.3}$$

where φ is the air gap flux, f is the frequency and k_s is a fixed constant.

For motor operation below the rated frequency and speed control, both f and E_s in (3.3) must be controlled. Controlling only f causes an increase in the air gap flux, leading to saturation of the motor. This will increase the core loss and the stator copper loss. Therefore, the variable frequency operation below the rated frequency is possible only if the air gap voltage to frequency ratio is kept constant.

Neglecting the voltage drop across the stator resistance, the back *emf* can be assumed to be equal to the motor terminal voltage. Therefore, it is a good approximation if control can be easily applied to the terminal voltage instead of the air gap voltage. In such a simplification the V/f ratio should be constant, but this method presents difficulties at low frequencies. In fact the assumption of a small drop across the stator resistance is not valid any more, and the difference between V and E_s is considerable. Additional voltage has to be impressed to compensate this effect.

The operation at a frequency higher than the rated frequency takes place at a constant rated terminal voltage. Since the terminal voltage is maintained constant, the motor flux decreases. The motor, therefore, operates in the field weakening mode [3][9].

3.4 Simulation Results

Figs. 3.2 to 3.3 show the simulation results at rated operation for the squirrel cage induction motor given in Chapter two, using sinusoidal PWM pattern and a constant *V/f* ratio. The inverter is operated in the overmodulation mode (m_a = 1.7) and switching frequency is 1260 Hz (m_f = 21). The following base values are defined:

$V_{base} = V_{a1}$, rated value of the fundamental component of the Sinusoidal PWM voltage source inverter (line to neutral voltage) or motor rated voltage (120 V).

$I_{base} = I_{a1}$, rated value of the fundamental component of the Sinusoidal PWM voltage source inverter ac current or motor rated current (10 A).

$f_{base} = f_s$, supply frequency or motor rated frequency (60 Hz).

Figs. 3.4 to 3.7 show the simulation results for the motor at constant torque and variable speed. The chosen output torque is 8 N.m. At 862 RPM, the motor is supplied at a frequency of 30 Hz. The modulation index is 0.6 and the switching frequency is 1020 Hz (m_f = 34). At 411 RPM, the motor is supplied at a frequency of 15 Hz, the modulation index is 0.3 and switching frequency is also 1020 Hz (m_f = 68).

Fig. 3.8 shows the spectrum of dc link voltage when the motor is operated under various frequencies (V_{dc} = 286 V).

The motor is simulated using the dynamic model in EMTP program. Mechanical losses are assumed to vary with speed, and the converter switches are ideal. Table 3.1 shows the supply impedance and the dc link capacitor presented in Fig. 3.1.

Table 3.1

Inverter Circuit Parameters

Per phase line resistance, R_s	0.11 Ω
Per phase line inductance, L_s	0.15 mH
dc link capacitor, C_r	1200 μF

The motor input current and voltage waveforms contain sideband harmonics centered around multiples of f_c and given by:

$$f_h = Kf_c \pm kf \tag{3.8}$$

where f_h is the frequency of the sidebands, K and k are integers and $(K+k)$ is always an odd number. The sideband harmonics are listed in Table 3.2. They are centered around the carrier frequency and its odd multiples comprise of upper and lower sideband components of approximately equal amplitudes and displaced by even multiples of the reference frequency. The bands centered around the even multiples have upper and lower sidebands displaced by odd multiples of the reference frequency.

Table 3.2

Harmonics In Sinusoidal PWM

Harmonics	$K=1$, $k = 2, 4, 6,..$	$K=2$, $k=1, 3, 5,..$	$K=3$, $k=2, 4, 6, ..$
Sidebands	$f_c \pm 2f$	$2f_c \pm f$	$3f_c \pm 2f$
	$f_c \pm 4f$	$2f_c \pm 3f$	$3f_c \pm 4f$
	..	..	..

At 60 Hz operation, the inverter is operated in PWM overmodulation mode. The peak of the reference voltages are allowed to exceed the peak of the carrier waveform and the magnitude of the fundamental frequency does not increase proportionally with the modulation index. At 30 and 15 Hz, the inverter is operated in the PWM modulation region (linear region), and unlike the overmodulation region, the fundamental frequency magnitude increases or decreases proportionally to the modulation index.

In the overmodulation operation compared with the linear operation, the output voltage contains more harmonics in the sidebands.

In the rectifier input side (supply side), the input current contains the fundamental (at 60 Hz), plus the harmonics which are odd multiples of the fundamental. The order of these harmonics are determined by:

$$h = 6r \pm 1 \tag{3.9}$$

where r is an integer.

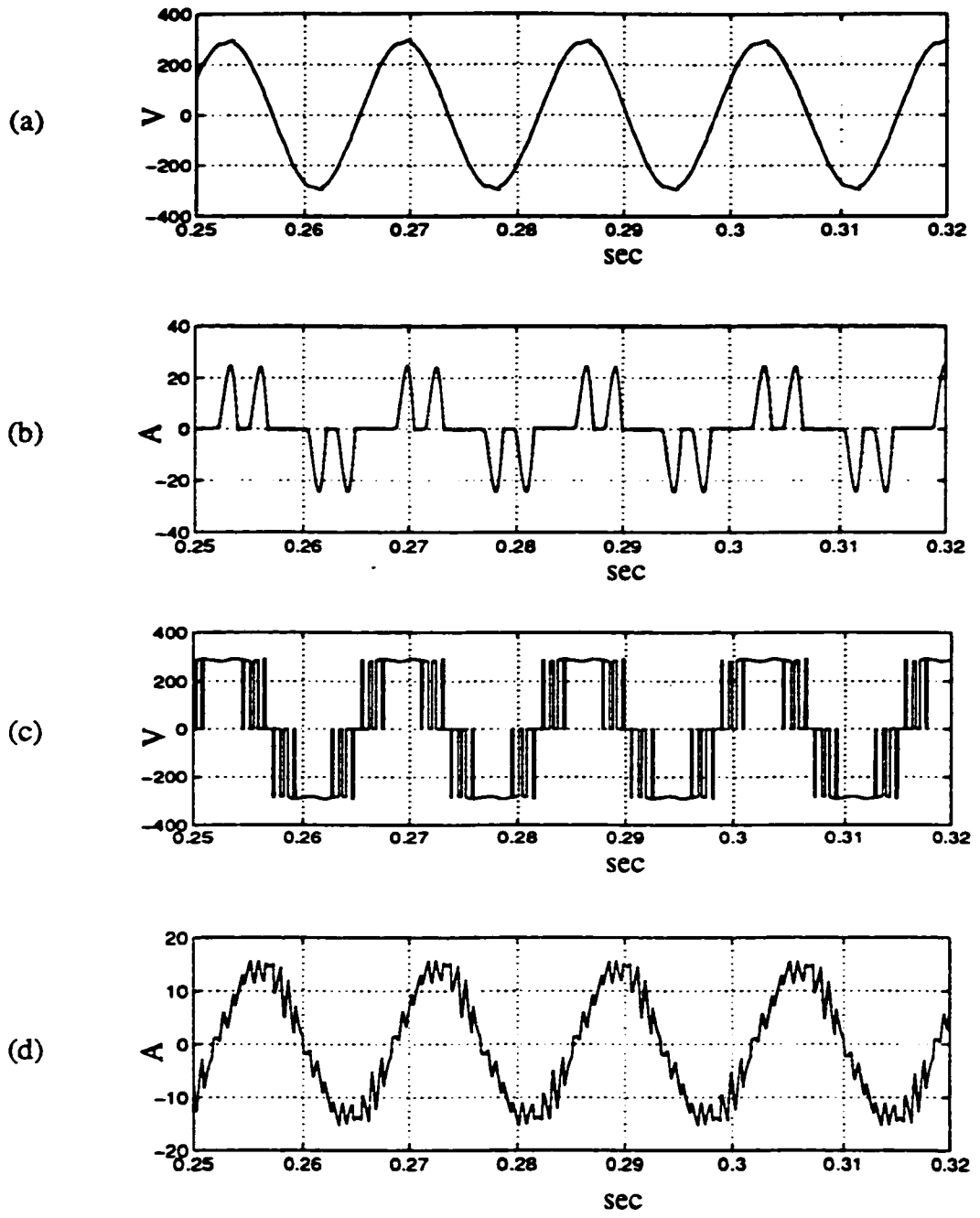

Fig. 3.2 Simulation results at 60 Hz motor operation (balanced supply).

(a) Rectifier input line to line voltage. (b) Rectifier input line current.

(c) Motor input line to line voltage. (d) Motor input line current.

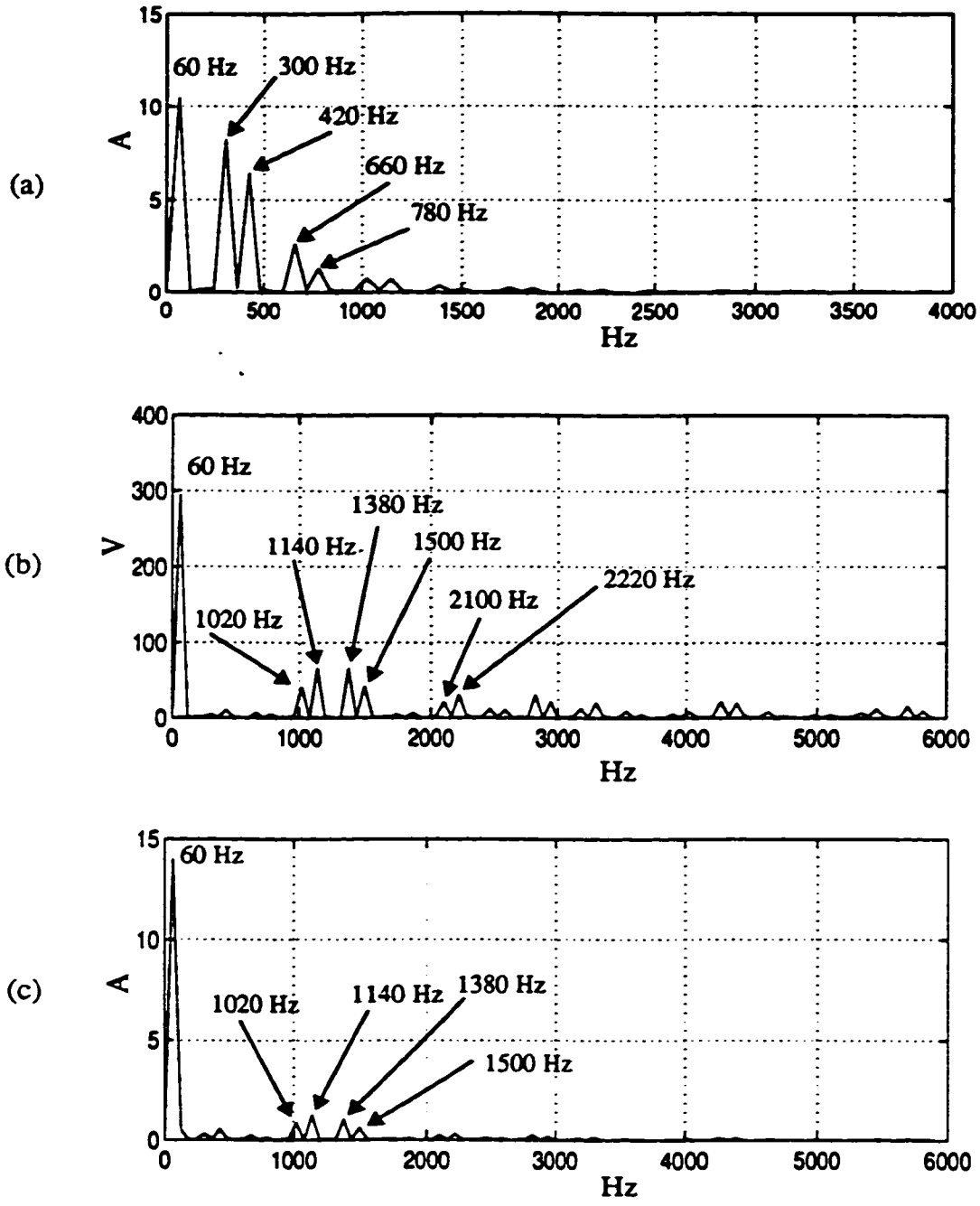

Fig. 3.3 Simulation results showing frequency spectrum at 60 Hz motor operation (balanced supply).

(a) Rectifier input line current. (b) Motor input line to line voltage.

(c) Motor input line current.

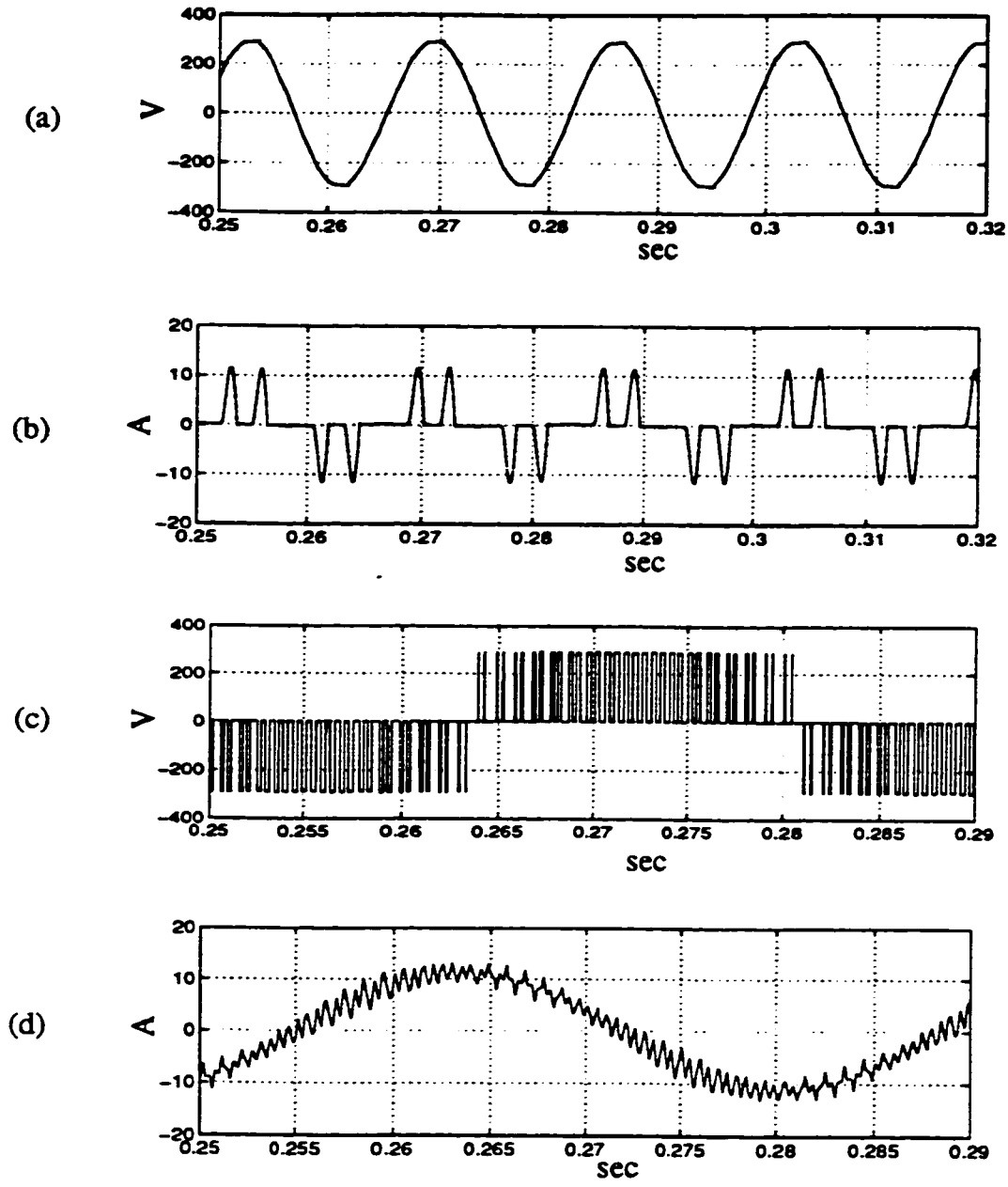

Fig. 3.4 Simulation results at 30 Hz motor operation (balanced supply).

(a) Rectifier input line to line voltage. (b) Rectifier input line current.

(c) Motor input line to line voltage. (d) Motor input line current.

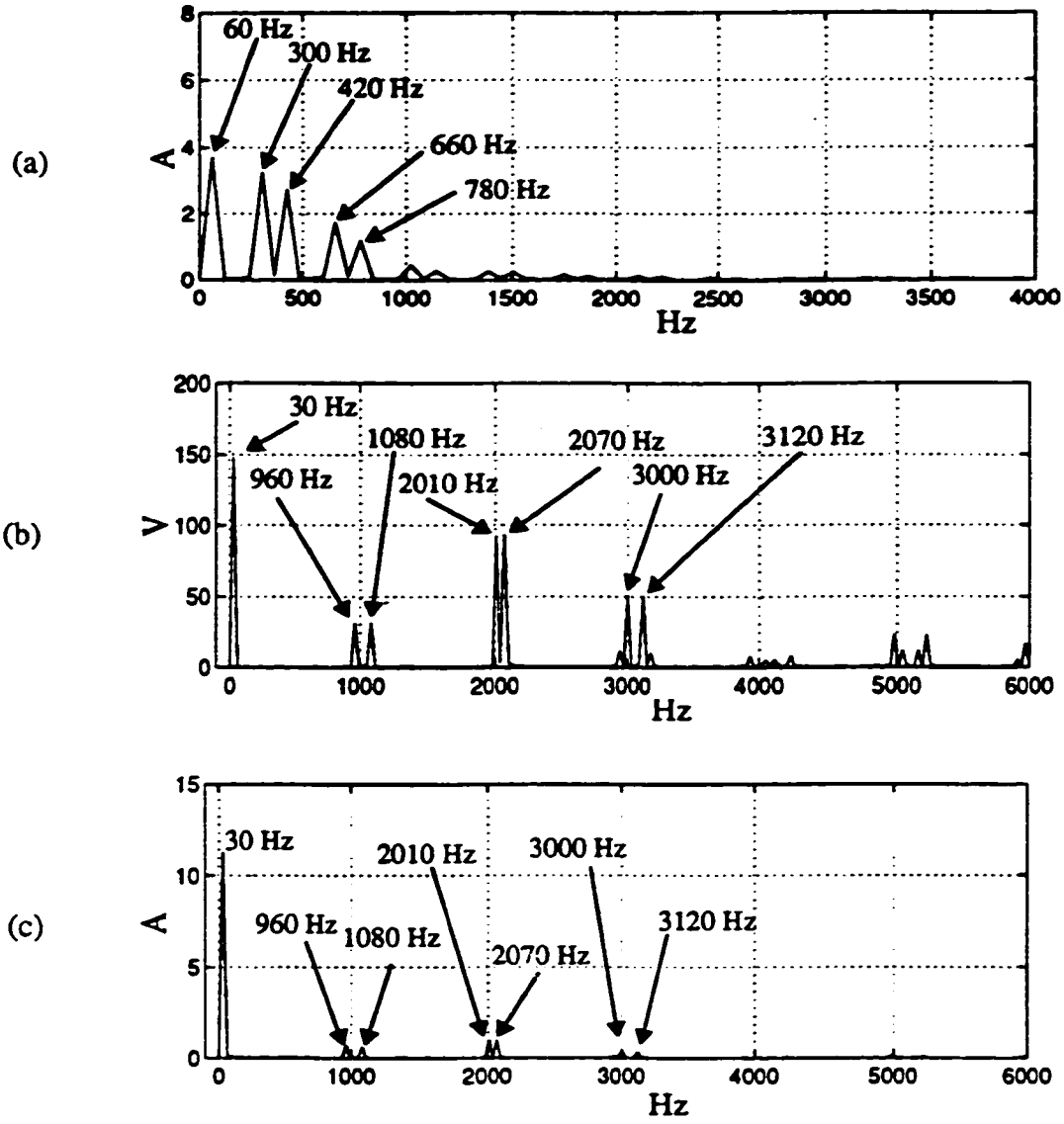

Fig. 3.5 Simulation results showing frequency spectrum at 30 Hz motor operation (balanced supply).

(a) Rectifier input line current. (b) Motor input line to line voltage.

(c) Motor input line current.

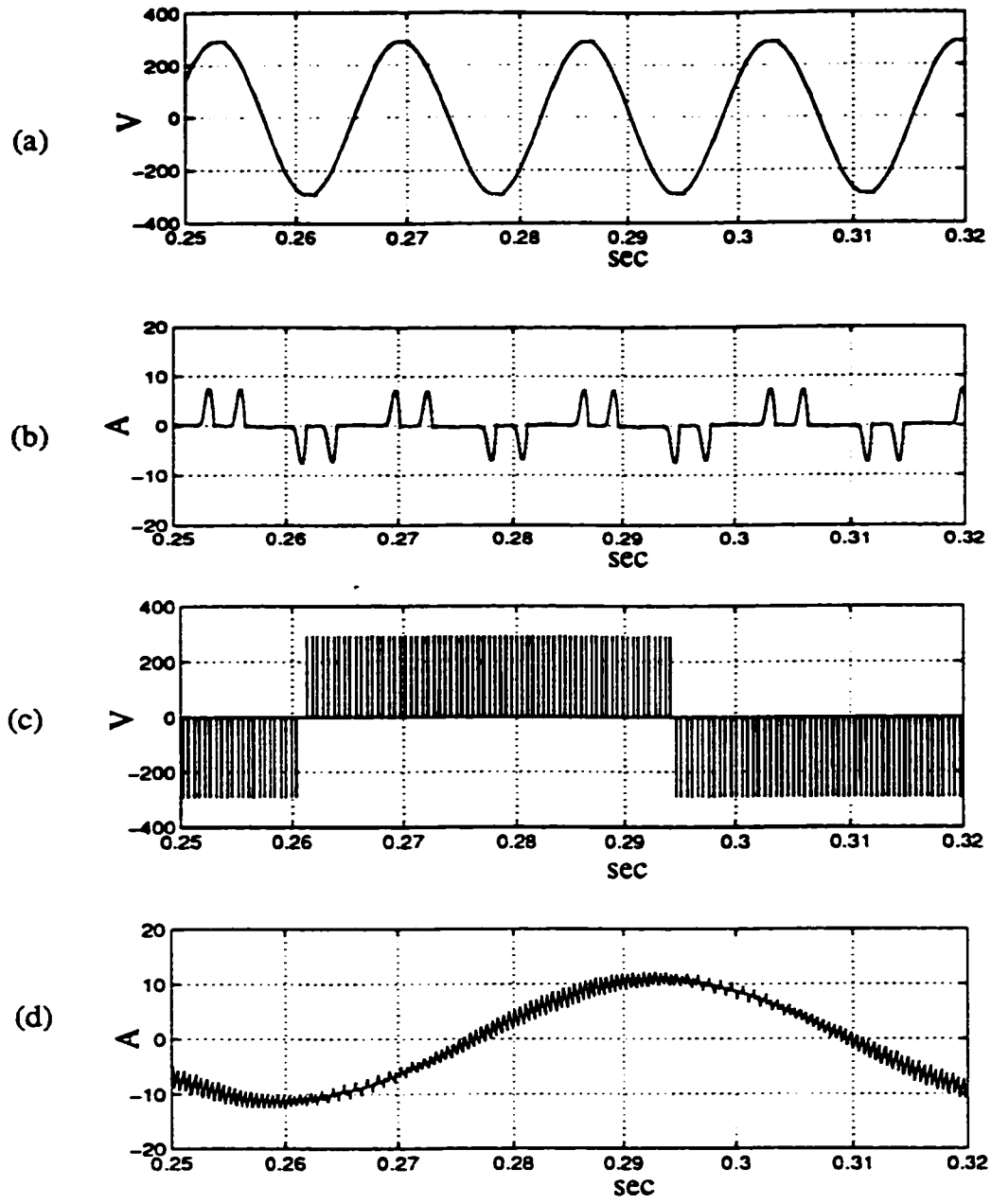

Fig. 3.6 Simulation results at 15 Hz motor operation (balanced supply).

(a) Rectifier input line to line voltage. (b) Rectifier input line current.

(c) Motor input line to line voltage. (d) Motor input line current.

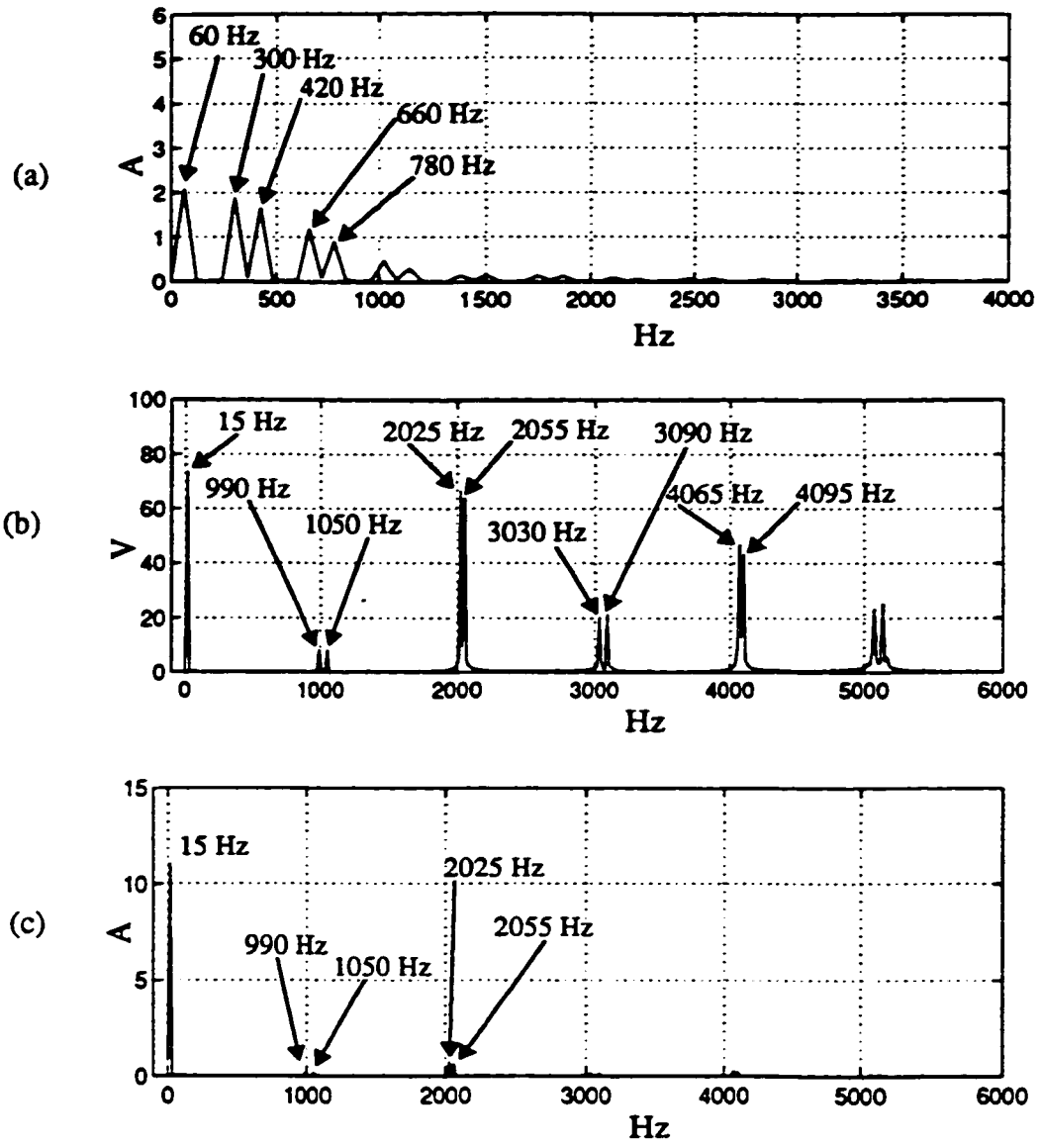

Fig. 3.7 Simulation results showing frequency spectrum at 15 Hz motor operation (balanced supply).

(a) Rectifier input line current. (b) Motor input line to line voltage.

(c) Motor input line current.

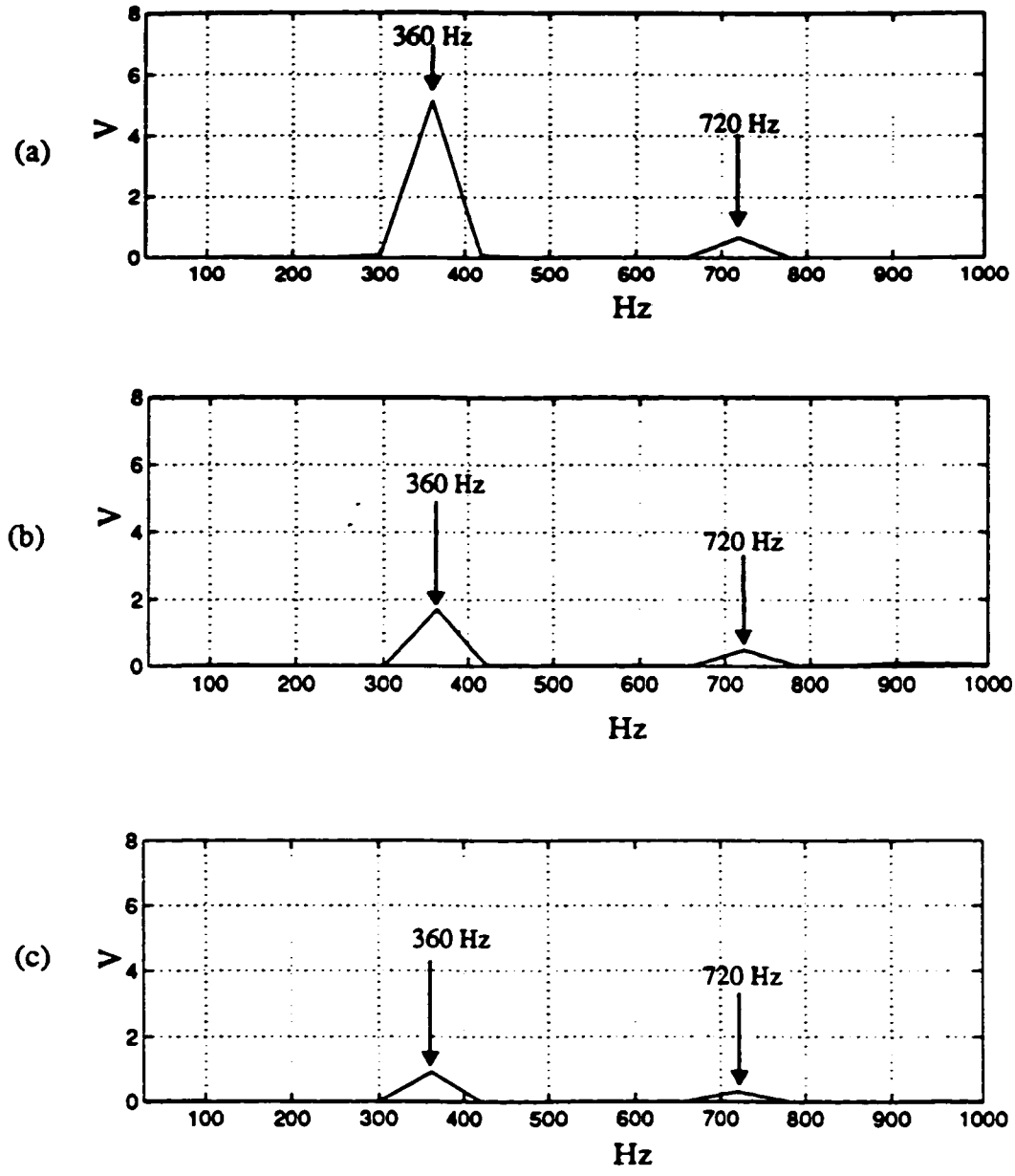

Fig. 3.8 Simulation results showing frequency spectrum of dc link voltage (balanced supply)

(a) At 60 Hz motor operation. (b) At 30 Hz motor operation.

(c) At 15 Hz motor operation.

3.5 Experimental Results

Experimental results for the 3 hp, 1740 RPM squirrel cage induction motor obtained in Chapter 2 are shown in Figs. 3.9 to 3.15. The rectifier output voltage (V_{dc}) was 282 V. The load at the motor shaft is a dc generator connected to a resistive load. The torque at the motor shaft is kept constant by keeping the generator current constant for different operating frequencies of the motor. The simulation and experimental results are in agreement with each other. However, due to the unbalanced supply voltage a little difference of the order and the amplitude of certain harmonics is observed. The magnitude of these inevitable harmonics varies with the degree of unbalance in the power supply. The tripplen harmonics in the rectifier input current, and the unexpected harmonics in the dc link voltage and motor inputs, result from the unbalanced input voltage. The difference in harmonic components and magnitudes, between simulation and experimental results for rectifier and motor inputs, are summarized using the tables shown in the following section.

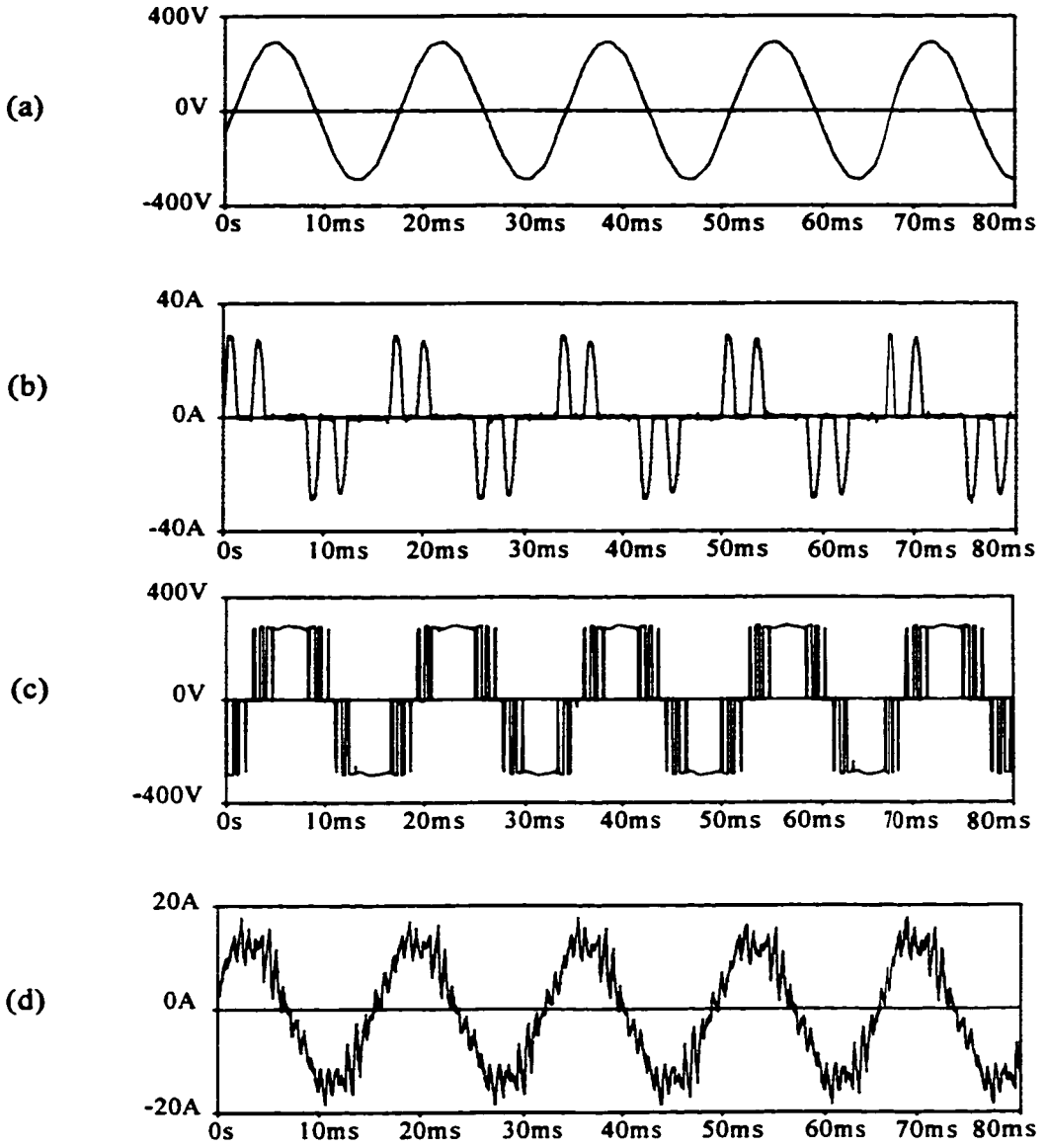

Fig. 3.9 Experimental results at 60 Hz motor operation (unbalanced supply).

(a) Rectifier input line to line voltage.

(b) Rectifier input line current.

(c) Motor input line to line voltage.

(d) Motor input line current.

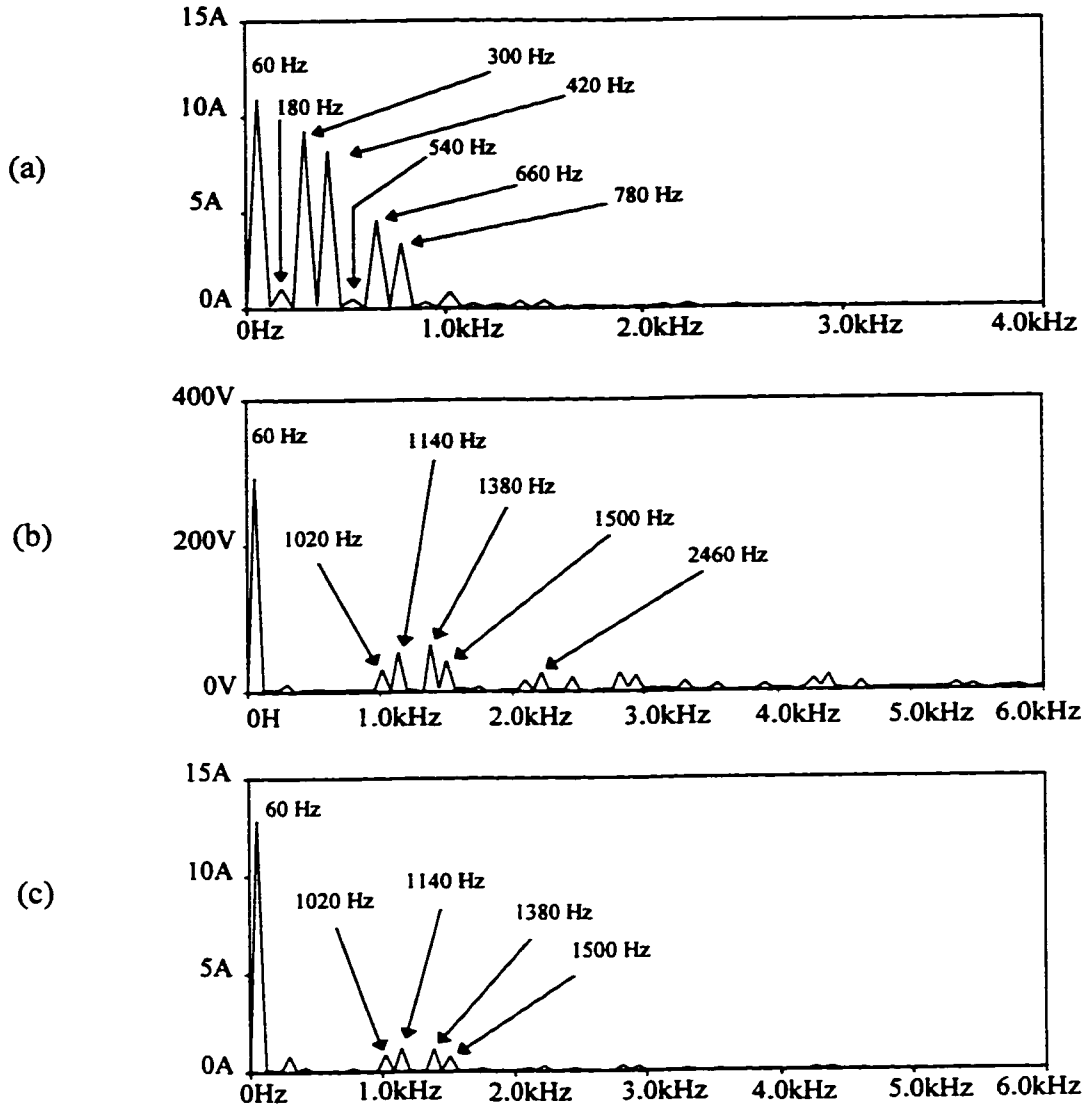

Fig. 3.10 Experimental results showing frequency spectrum at 60 Hz motor operation (unbalanced supply).

(a) Rectifier input line current.

(b) Motor terminal line to line voltage.

(c) Motor input line current.

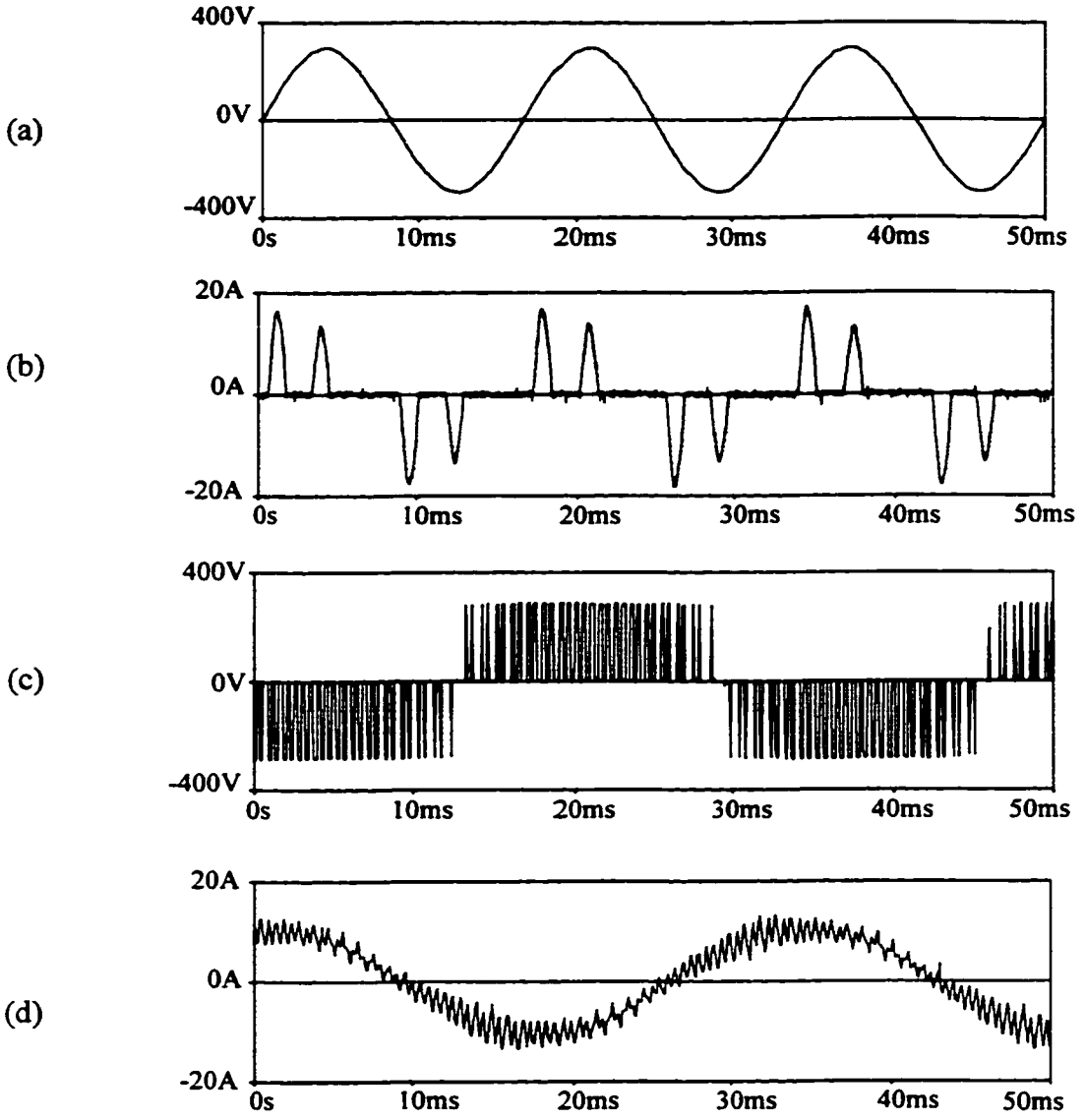

Fig. 3.11 Experimental results at 30 Hz motor operation (unbalanced supply).

(a) Rectifier input line to line voltage.

(b) Rectifier input line current

(c) Motor input line to line voltage.

(d) Motor input line current.

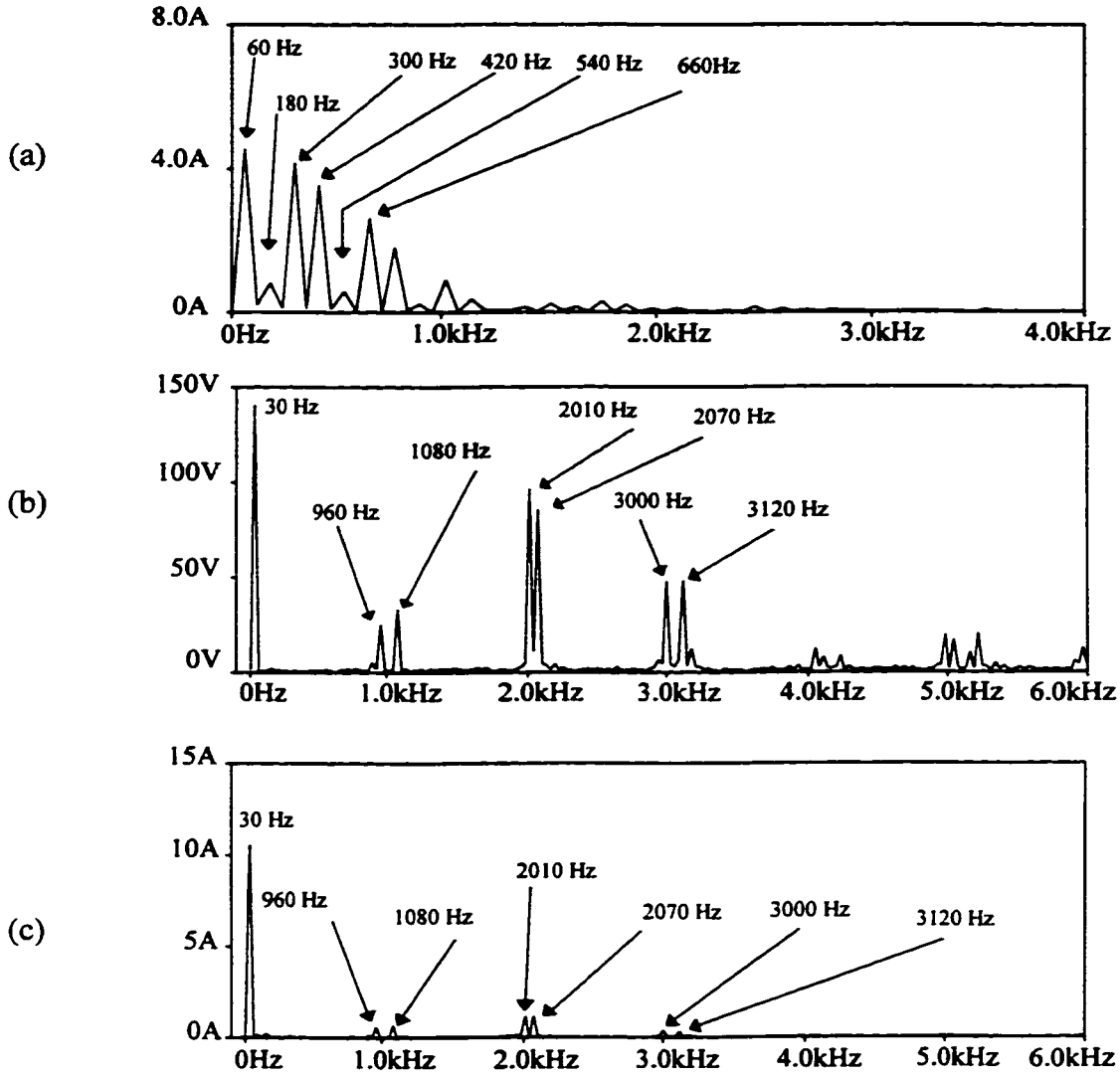

Fig. 3.12 Experimental results showing frequency spectrum at 30 Hz motor operation (unbalanced supply).

(a) Rectifier input line current.

(b) Motor terminal line to line voltage.

(c) Motor input line current.

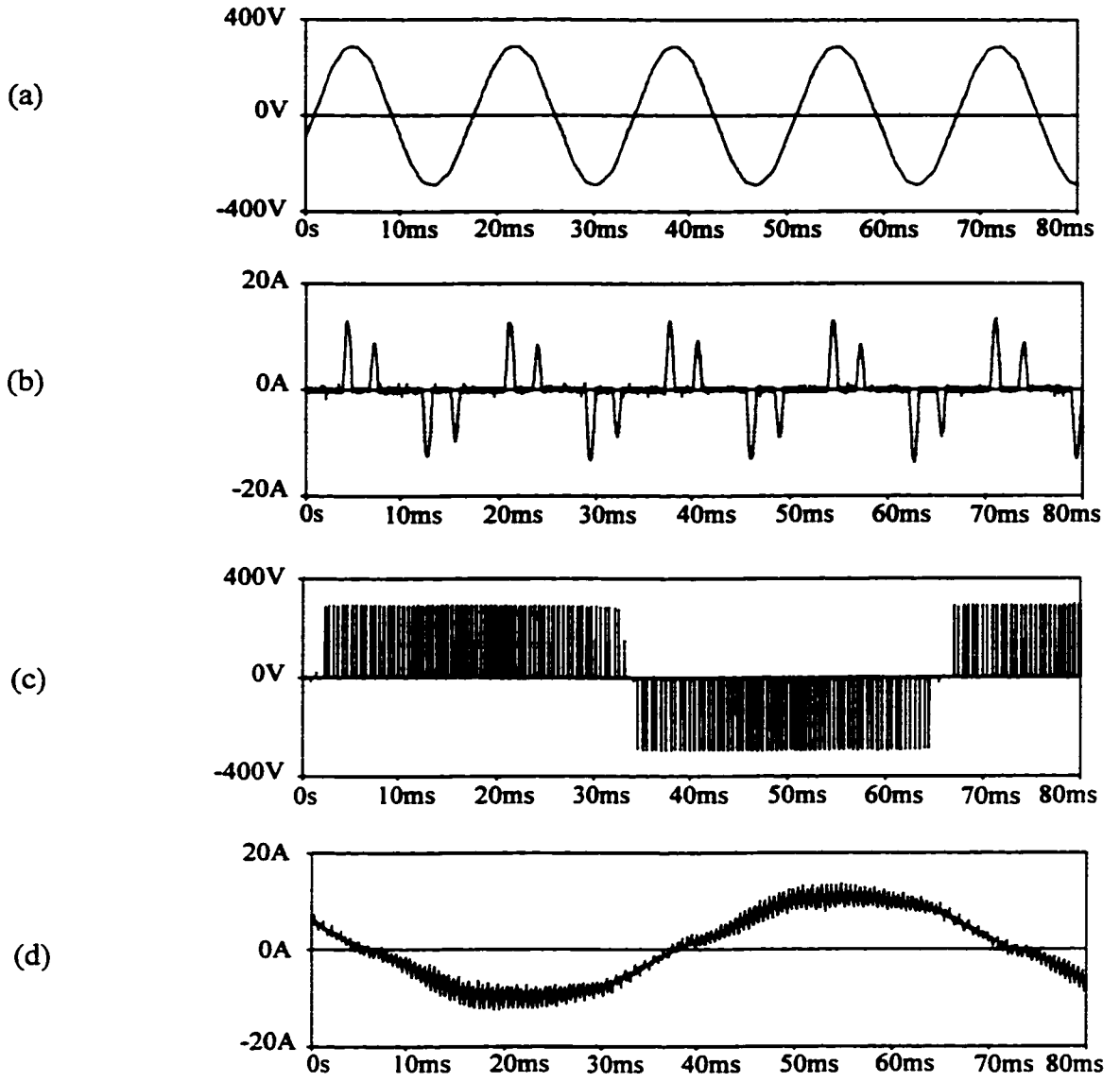

Fig. 3.13 Experimental results at 15 Hz motor operation (unbalanced supply).

(a) Rectifier input line to line voltage.

(b) Rectifier input line current

(c) Motor input line to line voltage.

(d) Motor input line current.

(a)

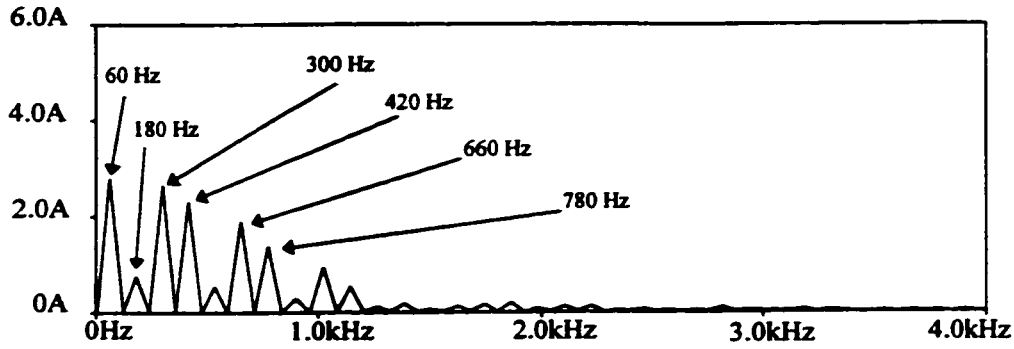

(b)

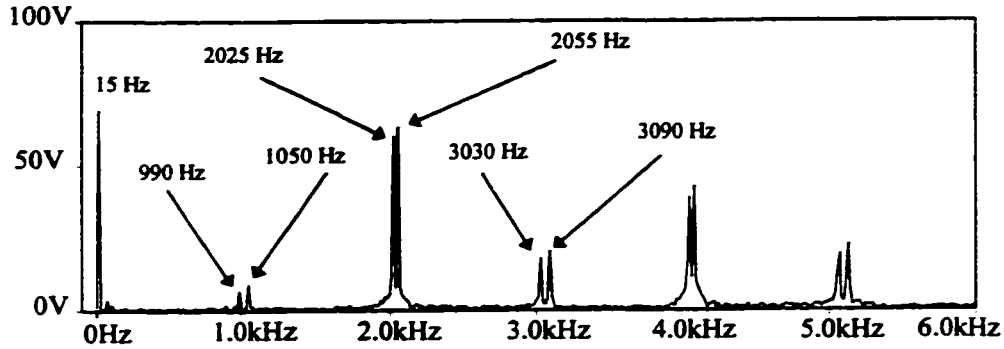

(c)

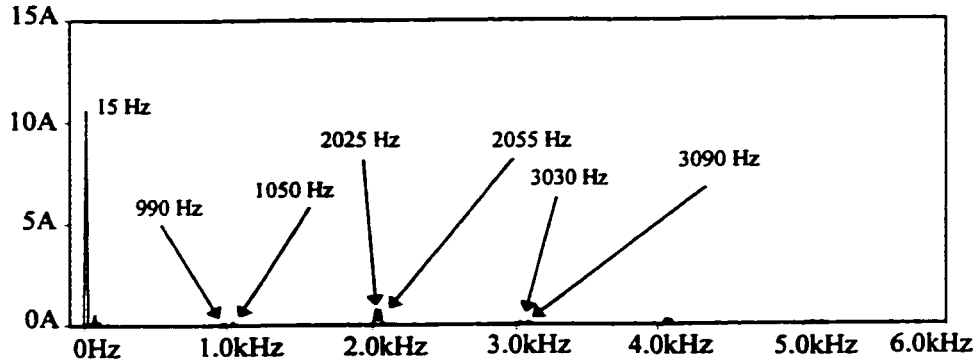

Fig. 3.14 Experimental results showing frequency spectrum at 15 Hz motor operation (unbalanced supply).

(a) Rectifier input line current.

(b) Motor terminal line to line voltage.

(c) Motor input line current.

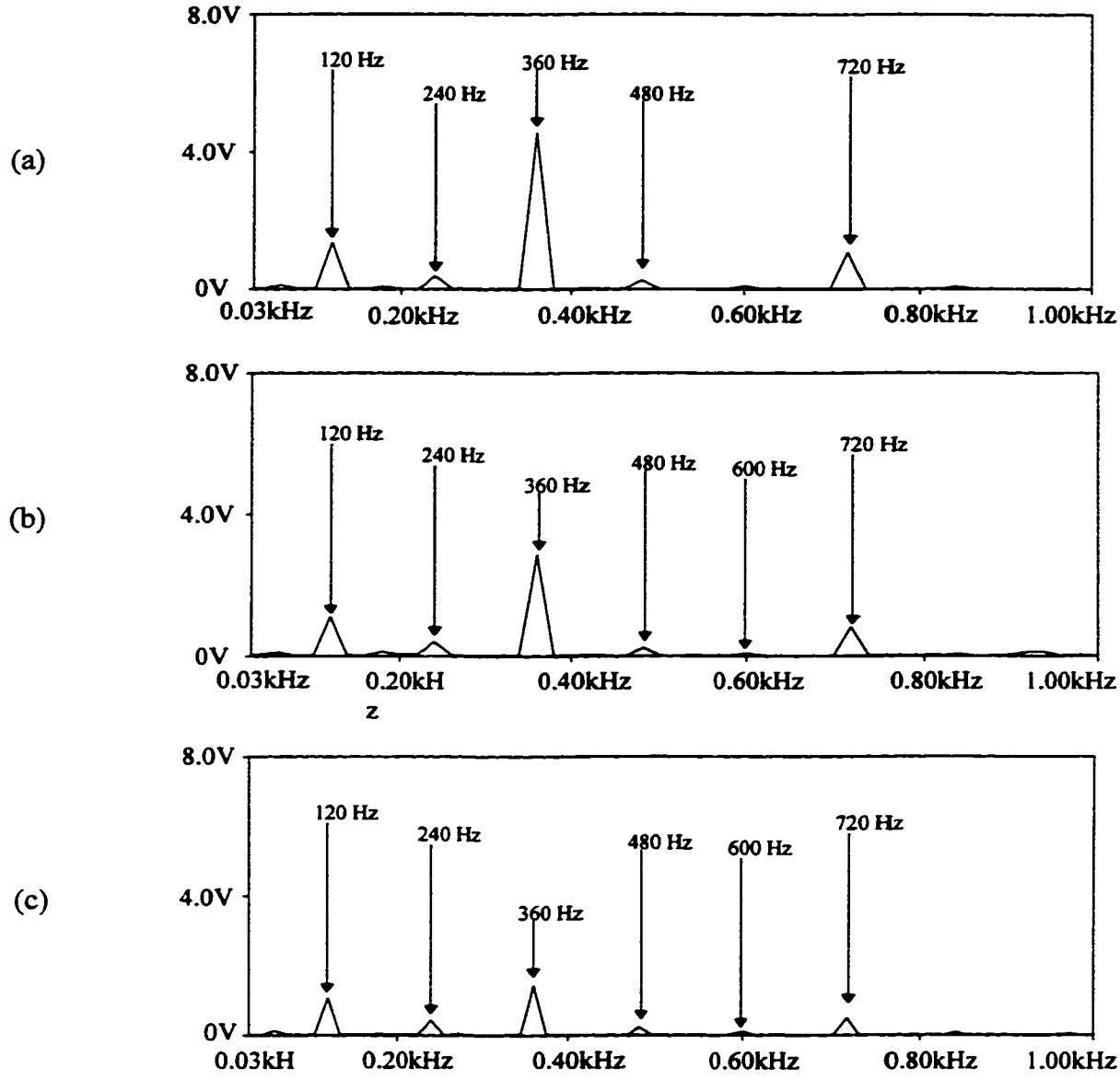

Figure 3.15 Experimental results showing frequency spectrum of dc link voltage (Unbalanced supply).

(a) At 60 Hz motor operation.

(b) At 30 Hz motor operation.

(c) At 15 Hz motor operation.

3.6 Experimental Verification

Table 3.3 shows the comparison between the normalized simulated and experimental harmonics of the rectifier input current at 60, 30 and 15 Hz motor operation.

Table 3.3

Normalized Frequency Spectrum Of

Rectifier Input Line Current At

60, 30 and 15 Hz Motor Operation

	Simulation results			Experimental results		
Order h	60 Hz	30 Hz	15 Hz	60 Hz	30 Hz	15 Hz
1	1.0	0.35	0.198	1.0	0.41	0.25
3	---	---	---	0.09	0.07	0.07
5	0.79	0.311	0.173	0.84	0.381	0.244
7	0.64	0.261	0.153	0.74	0.319	0.210
9	---	---	---	0.05	0.021	0.051
11	0.29	0.164	0.113	0.42	0.24	0.174
13	0.17	0.111	0.055	0.31	0.171	0.125
15	---	---	---	0.03	0.022	0.023
17	0.07	0.041	0.055	0.07	0.071	0.08
19	0.06	0.024	0.037	0.02	0.03	0.051
21	---	---	---	0.01	0.004	0.01
23	0.04	0.024	0.014	0.03	0.012	0.015
$\%THD_i$	108.4	130.2	150.5	122.5	142.4	165.2

Table 3.4 shows the comparison between the normalized simulated and experimental harmonics of the motor terminal line to line voltage and input line current at 60 Hz operation.

Table 3.4

Normalized Frequency Spectrum Of

Motor Terminal Line To Line Voltage And

Input Line Current At 60 Hz Operation

	Simulation results		Experimental results	
Order h	Motor voltage	Motor current	Motor voltage	Motor current
1	1.0	1.0	1.0	1.0
5	0.015	0.021	0.028	0.065
7	0.035	0.037	0.168	0.018
11	0.021	0.02	0.005	0.0051
13	0.014	0.007	0.016	0.011
17	0.14	0.006	0.12	0.068
19	0.22	0.086	0.177	0.095
23	0.22	0.078	0.21	0.091
25	0.14	0.043	0.138	0.062
29	0.025	0.006	0.028	0.008
	$\%THD_v = 44.7$	$\%THD_i = 17.6$	$\%THD_v = 38.3$	$\%THD_i = 20.1$

Table 3.5 shows the comparison between the normalized simulated and experimental harmonics of the motor terminal line to line voltage and input line current at 30 Hz operation.

Table 3.5

Normalized Frequency Spectrum Of

Motor Terminal Line To Line Voltage And

Input Line Current At 30 Hz Operation

	Simulation results		Experimental results	
Order *h*	Motor voltage	Motor current	Motor voltage	Motor current
1	0.5	0.8	0.48	0.82
5	---	---	0.006	0.017
7	---	---	0.003	0.003
11	0.002	0.003	0.002	0.004
32	0.105	0.049	0.087	0.045
36	0.106	0.043	0.107	0.053
67	0.314	0.069	0.332	0.089
69	0.317	0.068	0.294	0.087
98	0.004	0.006	0.019	0.003
100	0.172	0.027	0.165	0.034
104	0.170	0.025	0.165	0.026
106	0.034	0.004	0.042	0.005
131	0.027	0.003	0.011	0.001
	$\%THD_v = 115.5$	$\%THD_i = 18.5$	$\%THD_v = 111.2$	$\%THD_i = 23.6$

Table 3.6 shows the comparison between the normalized simulated and experimental harmonics of the motor terminal line to line voltage and input line current at 15 Hz operation.

Table 3.6

Normalized Frequency Spectrum Of

Motor Terminal Line To Line Voltage And

Input Line Current At 15 Hz Operation

	Simulation results		Experimental results	
Order *h*	Motor voltage	Motor current	Motor voltage	Motor current
1	0.25	0.8	0.24	0.81
5	---	---	0.011	0.033
7	---	---	0.006	0.013
11	---	---	0.002	0.004
66	0.027	0.011	0.023	0.012
70	0.021	0.010	0.031	0.015
135	0.227	0.051	0.211	0.061
137	0.217	0.045	0.217	0.053
202	0.069	0.009	0.061	0.012
206	0.073	0.013	0.071	0.011
271	0.159	0.017	0.131	0.018
273	0.146	0.015	0.128	0.021
338	0.067	0.007	0.059	0.01
	$\%THD_v = 177.8$	$\%THD_i = 10.7$	$\%THD_v = 171.1$	$\%THD_i = 14.2$

Table 3.7 shows the power factor of the drive (PF_i) and the motor (PF_m), for different motor operating frequencies.

Table 3.7

Drive And Motor Power Factor At 60, 30 and 15 Hz

Motor Operation

	Simulation results				Experimental results			
f	PF_i	PF_m	T_M	N	PF_i	PF_m	T_M	N
60 Hz	0.68	0.67	12.3	1740	0.64	0.65	11.1	1753
30 Hz	0.61	0.45	8	862	0.56	0.41	7.5	854
15 Hz	0.57	0.36	8	411	0.52	0.37	7.5	402

T_M = Mechanical torque (N.m)

N = Mechanical speed (RPM)

3.7 Motor Harmonic Torques

The harmonic torques produced in the motor at rated operation are shown in Table 3.8. These harmonic torques are quite small compared to the fundamental torque of the motor. Also, they are alternately negative and positive for the harmonics listed in ascending order, and the total is a negligibly small. For different motor operating torques and speeds, the harmonic torques are found negligible.

Table 3.8

Harmonic Torques Produced At

Motor Rated Operation

Harmonic torque, T_h	Value, N.m
1	12.3
5	-0.0012
7	0.0038
11	-0.0003
13	0.0001
17	-0.003
19	0.007
23	-0.004
25	0.002

3.8 Variations of Switching Frequency for Motor Drives

Fig. 3.16 shows the modes of induction motor operation with sinusoidal PWM inverter control. In this figure, the frequency of the carrier wave f_c has been plotted against the motor fundamental frequency f.

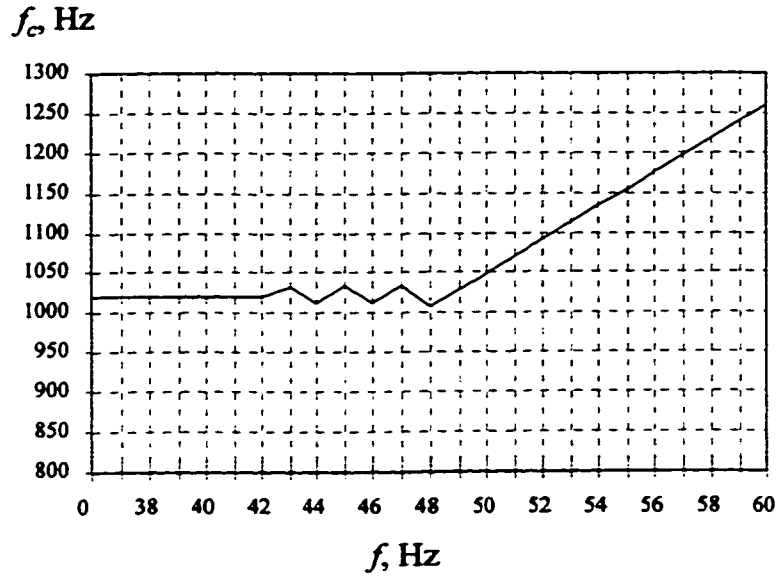

Fig. 3.16 Variation of the carrier frequency f_c with motor fundamental frequency f.

At low speeds, for which f is low, the asynchronous operation is employed in which the frequency of the carrier waveform is kept constant (1020 Hz) for different values of f (up to 42 Hz). The subharmonics introduced due to asynchronous operation have negligible magnitude because of high m_f. As the motor frequency is increased to increase the speed, the operation is shifted to synchronous modulation in which, f and f_c are synchronized with each other. Synchronous PWM requires that the carrier frequency f_c be a multiple of motor fundamental frequency f.

3.9 Summary

In this chapter, induction motor drive modeling is investigated. The motor drive circuit is implemented using a diode bridge rectifier, filter and voltage source type

inverter. The speed control of the motor is achieved using the *V/f* ratio control. The speed of a 3 hp squirrel cage induction motor is controlled for different operating points at a constant torque. The motor drive circuit characteristics are discussed. Harmonic torques are studied, and carrier frequency variations are discussed. Simulation results are verified experimentally.

CHAPTER 4

MODELING AND SIMULATION OF TRAVELING WAVES IN INDUCTION MOTOR DRIVES

4.1 Introduction

Adjustable speed induction motor drives are used more and more often in industry, particularly as an energy saving measure. In many industrial applications, the motor and the inverter must be at separate locations, thus requiring long motor leads. A number of motor windings failures have been recorded and attributed to overvoltages resulting from the high *dv/dt* inverter output waveforms.

The traveling wave phenomenon has been identified as a potential cause of overvoltage across the motor winding, associated with this *dv/dt* phenomena. The traveling wave problem is further compounded when the PWM inverter and the motor are separated by substantial distances. Long cables, with their distributed leakage reactance and coupling capacitance, result in high frequency poorly damped voltage oscillations.

This chapter is concerned with the modeling and simulation of the traveling wave phenomenon in induction motor drives. It investigates the modeling options for the feed cable, particularly by means of distributed parameters, the influence of line length and power semiconductor switching times on the magnitude of overvoltages. Solutions are proposed and a filter design procedure is given. Selected results are verified experimentally.

4.2 The Traveling Wave Phenomenon

Fig. 4.1 shows the standard configuration of a three phase induction motor supplied from a PWM inverter using long cable.

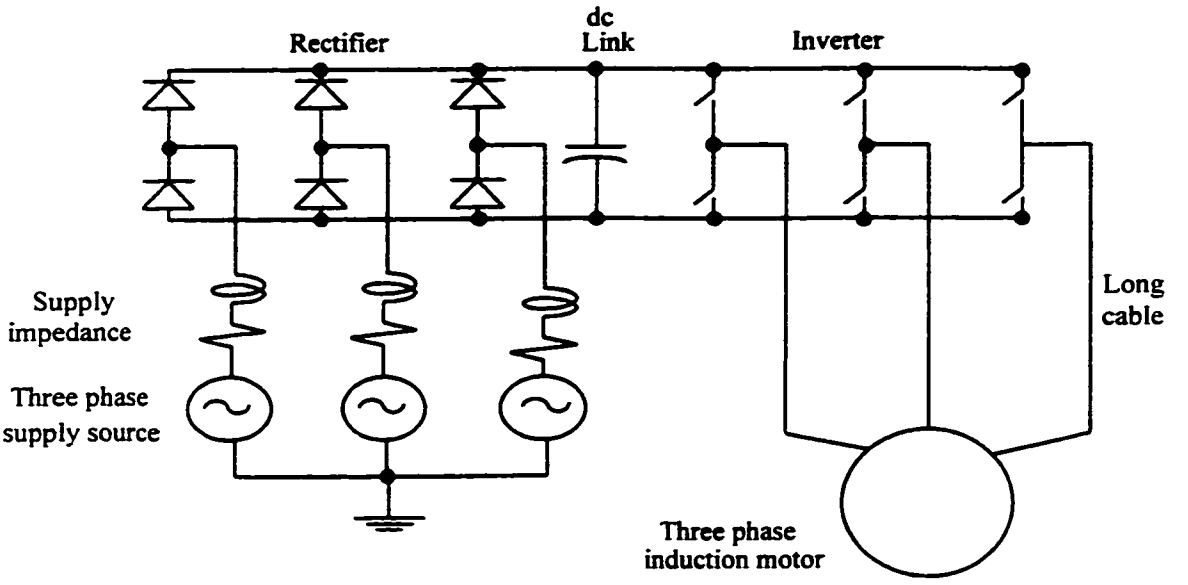

Fig. 4.1 PWM inverter supplying three phase induction motor using long cable.

Assuming that L (Henries per meter) and C (Farads per meter) are the inductance and the capacitance of a lossless cable respectively, the traveling wave voltage E and current I satisfy a relation called the wave equation at any point of the cable [41]:

$$\frac{\partial^2 E}{\partial x^2} = LC\frac{\partial^2 E}{\partial t^2} \tag{4.1}$$

and

$$\frac{\partial^2 I}{\partial x^2} = LC\frac{\partial^2 I}{\partial t^2} \tag{4.2}$$

The solution of (4.1) and (4.2) give:

$$E(x,t) = e_1\left(x - \frac{1}{\sqrt{LC}}t\right) + e_2\left(x + \frac{1}{\sqrt{LC}}t\right) \tag{4.3}$$

$$I(x,t) = i_1\left(x - \frac{1}{\sqrt{LC}}t\right) + i_2\left(x + \frac{1}{\sqrt{LC}}t\right) \tag{4.4}$$

At any distance x in the cable measured from the sending end, the voltage is the sum of two waves, e_1 and e_2, the first of which is a wave traveling in the positive x direction, and the second is a wave traveling in the opposite or negative x direction. The speed of each wave is giving by:

$$v = \frac{1}{\sqrt{LC}} \tag{4.5}$$

which has the dimension of speed.

The voltage and current waves in (4.3) and (4.4) are related to each other by the cable characteristic impedance Z_0:

$$\frac{e_1}{i_1} = \sqrt{\frac{L}{C}} = Z_0 \tag{4.6}$$

and

$$\frac{e_2}{i_2} = -\sqrt{\frac{L}{C}} = -Z_0 \tag{4.7}$$

which has the dimension of resistance.

The reflection in the cable can be studied using the boundary conditions at its terminals. Assuming that the cable is terminated by an inductance L_m in series with a resistance R_m, and an ideal incident wave of magnitude E is suddenly applied to the

sending end of the cable. For a cable length l, the time required for the pulse E to travel along the cable in one direction is l/v. The boundary condition at the point of connection between the load and the cable gives [49]:

$$v_m = R_m i_m + L_m \frac{di_m}{dt} \tag{4.8}$$

Operating characteristics of the cable are now computed by substituting (4.3) through (4.7) in (4.8); the following equation is obtained which is applicable to the receiving end of the cable:

$$e_1 + e_2 = R_m\left(\frac{e_1}{Z_0} - \frac{e_2}{Z_0}\right) + L_m \frac{d}{dt}\left(\frac{e_1}{Z_0} - \frac{e_2}{Z_0}\right) \tag{4.9}$$

Solution of e_2 in terms of e_1 gives:

$$(R_m + Z_0)e_2 + L_m \frac{de_2}{dt} = (R_m - Z_0)e_1 + L_m \frac{de_1}{dt} \tag{4.10}$$

In (4.10), e_1 as a function of time is presumably known, for e_1 is the incident wave that is arriving from the sending end of the cable. The right-hand side of (4.10) may therefore be treated as a known function with constant coefficients.

By considering the incident wave as a flat-topped wave of constant voltage E, (4.10) becomes, for each wave:

$$(R_m + Z_0)e_2 + L_m \frac{de_2}{dt} = (R_m - Z_0)E \tag{4.11}$$

Separating the variables in (4.11), the solution can be written as:

$$-\frac{L_m}{R_m + Z_0} \ln[(R_m - Z_0)E - (R_m + Z_0)v_2] = t + a_1 \tag{4.12}$$

where a_1 is a constant of integration.

In the exponential form, (4.12) becomes:

$$(R_m - Z_0)E - (R_m + Z_0)e_2 = a_2 e^{-\frac{(R_m+Z_0)}{L_m}t} \tag{4.13}$$

The constant a_2 can be calculated by applying the boundary condition at the cable terminal. At the instant of arrival of the incident wave, the load cannot carry current because of its inductance; consequently, the wave is fully reflected, and the voltage of the reflected wave (at that instant) is equal to the voltage of incident wave. The value of a_2 is equal to:

$$a_2 = -2Z_0E \tag{4.14}$$

Substituting the value of a_2 in Eq. (4.13) gives:

$$e_2 = E\frac{R_m - Z_0 + 2Z_0 e^{-\frac{R_m+Z_0}{L_m}t}}{R_m + Z_0} \tag{4.15}$$

Equation (4.15) generates a traveling wave and it becomes the equation of the traveling wave if $(t + \sqrt{LC}x)$ is substituted for t:

$$e_2 = E\frac{R_m - Z_0 + 2Z_0 e^{-\frac{R_m+Z_0}{L_m}(t+\sqrt{LC}x)}}{R_m + Z_0} \tag{4.16}$$

Equation (4.16) shows that when a cable is terminated by an impedance (in this case a resistance in series with an inductor), the reflected wave is not any more a constant fraction of the incident wave and it varies with time. Two assumptions were made to obtain this equation: (a) the pulse is flat-topped with zero rise time or in general the pulse takes longer than half the rise time to travel from the inverter to the motor; (b) the cable is loss less.

In (4.16), $\sqrt{LC}$ has the dimensions second/meter, and x has the dimensions meter, therefore, $t_0 = \sqrt{LC}x$ has the dimensions second, and it equals the time that the pulses take to travel from one end side of the cable to the other. So, $2t_0$ is the associated time for the total distance traveled to and fro. Table 4.1 shows how the reflection coefficient varies with time for a 85 m cable length ($t_0 = 0.79\mu s$, $Z_0 = 51.6\ \Omega$) feeding the 3 hp induction motor obtained in Chapter two.

Table 4.1

Reflection Coefficient For 85 m Cable Length

Time	Reflection coefficient
t_0	0.99
$5t_0$	0.98
$20t_0$	0.9
$100t_0$	0.57
$200t_0$	0.26

Special cases of (4.16) can be characterized by four cable terminations:

(1) If the cable is open at the end ($R_m = L_m = \infty$), then from (4.16) we have:

$$e_2 = E \tag{4.17}$$

The reflected voltage at the end of the cable will be equal in magnitude with the same sign, resulting in two times the magnitude of the incident voltage at the cable terminals.

(2) If the cable is terminated by a resistive load (or cable with characteristic impedance) R, the reflected voltage at the point of connection is calculated from (4.17) as:

$$e_2 = E\frac{R - Z_0}{R + Z_0} \tag{4.18}$$

The reflection coefficient becomes constant and the reflected voltage will depend on R and Z_0 only.

An important case of (4.18) can be concluded if the cable terminal resistor R is equal to the cable characteristic impedance Z_0. The reflection coefficient in (4.18) is zero, and therefore there is no reflected wave. This means that the incident wave is completely absorbed.

(3) If the cable is short circuited ($R_m = L_m = 0$), then the reflected voltage is given by:

$$e_2 = -E \tag{4.19}$$

The reflected voltage at the end of the cable will be equal in magnitude but has a negative sign resulting in zero voltage at the cable terminals [42].

(4) If the cable is terminated by an inductance L_m, then the reflected voltage at the point of connection is given by:

$$e_2(t) = E\left(2e^{-\frac{Z_0}{L_m}(t+\sqrt{LC}x)} - 1\right) \tag{4.20}$$

At the first instant of impact of the incident wave the current through the inductance is zero, and therefore the cable acts as an open circuit at that first instant and the voltage is doubled if the wave front is abrupt.

At the sending end of the cable, the reflection coefficient is defined as [37] [41]:

$$\gamma = \frac{R_i - Z_0}{R_i + Z_0} \tag{4.21}$$

where R_i is the sending end resistance.

4.3 EMTP Cable Representation

The EMTP program has the capability of representing cables with typical overhead line parameters. The formulation is based on the method of distributed parameters [30]. Multiplying (4.3) by Z_0 and adding it to or substracting it from Eq. (4.4) gives:

$$E(x,t) + Z_0 I(x,t) = 2Z_0 i_1(x - \frac{1}{\sqrt{LC}}t) \tag{4.22}$$

$$E(x,t) - Z_0 I(x,t) = -2Z_0 i_2(x + \frac{1}{\sqrt{LC}}t) \tag{4.23}$$

In (4.22), $(E + Z_0 I)$ is constant if $(x - t/\sqrt{LC})$ is constant, and in (4.23), $(E - Z_0 I)$ is constant if $(x + t/\sqrt{LC})$ is constant.

For an observer traveling along the cable in a forward direction at velocity v, $(x - t/\sqrt{LC})$ and consequently $(E + Z_0 I)$ along the cable will be constant. Similarly, $(x + t/\sqrt{LC})$ and consequently $(E - Z_0 I)$ are constant to an observer traveling in the backward direction.

Fig. 4.2 shows the corresponding equivalent impedance network which describes fully the loss less cable at its terminals *m* and *n* [39].

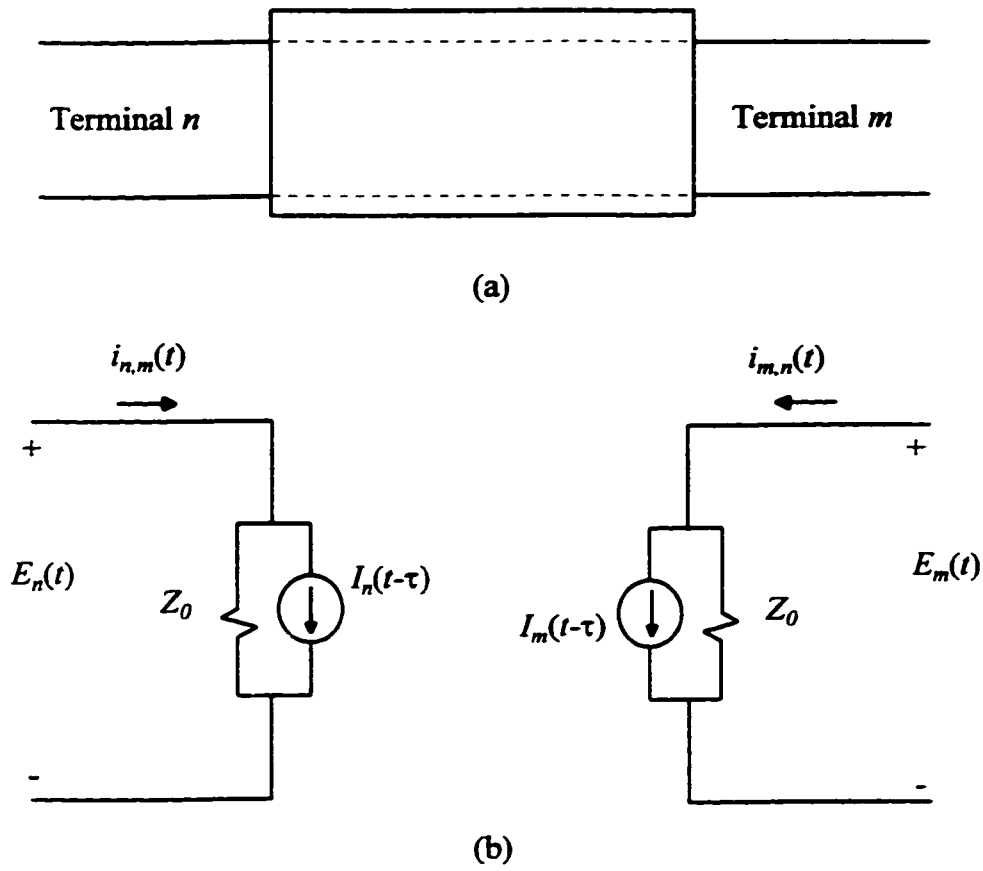

Fig. 4.2 (a) Loss less cable. (b) Equivalent circuit network.

If the travel time to get from one end of the cable to the other is τ, then $(E + Z_0 I)$ encountered by the observer when he leaves node *m* at time $(t - \tau)$ must still be the same when node *n* is reached at time *t*, that is:

$$E_m(t-\tau) + Z_0 i_{m,n}(t-\tau) = E_n(t) + Z_0(-i_{n,m}(t)) \tag{4.24}$$

The simple two port equations for $i_{n,m}$ from this equation are:

$$i_{n,m} = \frac{1}{Z_0} E_n(t) + I_n(t-\tau) \tag{4.25}$$

and

$$i_{m,n}(t) = \frac{1}{Z_0} E_m(t) + I_m(t-\tau) \tag{4.26}$$

with equivalent current sources I_n and I_m, which are known at state t from the past history at time (t-τ):

$$I_n(t-\tau) = -\frac{1}{Z_0} E_m(t-\tau) - i_{m,n}(t-\tau) \tag{4.27}$$

$$I_m(t-\tau) = \frac{1}{Z_0} E_n(t-\tau) - i_{n,m}(t-\tau) \tag{4.28}$$

The distributed series resistance of the cable is represented as a lumped element. The program automatically cuts the cable in two, inserting half of the resistance in middle, and one fourth at each end [39].

4.4 Simulation Results

To compare the voltage at the motor terminals for different cable lengths and for different inverter rise times, the inverter-cable-motor circuit (Fig. 4.1) is simulated using the EMTP program. The Three-Conductor Belted Paper-Insulated cable used in the inverter motor circuit is modeled using distributed elements, and their parameters per meter at 60 Hz are shown in Table 4.2 [40]. The inverter drives the standard 3 hp induction motor data given in Chapter 1. The inverter pulse (or wave) travels at a speed of 107 m/μs (from Eq. (4.5)) and the cable characteristic impedance is equal to 51.6 Ω.

Table 4.2

Per Phase Three-Conductor Belted Paper-Insulated

Cable Parameters

Cable resistance	4.65 mΩ/m
Cable inductance	0.48 μH/m
Cable capacitance	0.18 nF/m

The simulation results are close to the experimental results for the frequency of oscillation, but they are completely different from the experimental results in the sense of damping. Further study showed that assuming a constant resistor for the cable is not the case especially for a short length of the cable.

The traveling wave is somehow similar to the resonance in a simple *L-C* circuit. The pulse travels between two ends, and as a result the output voltage at the cable terminal has a period equal to $4l/v$ resulting in a very high frequency which increases as the cable length decreases. This high frequency voltage will damp out through the cable resistance when it goes back and forth. Because of the cable skin effect, this high frequency voltage sees a variable resistance during this process. This variable resistor changes between a maximum value which corresponds to the maximum skin effect, and a minimum value which corresponds to the normal cable resistor when the high frequency component is completely damped out.

Simulation of the system without taking into account the skin effect will give results which are different from the experimental in the terms of damping. To model the

skin effect of the cable, a variable resistor which varies with time is added to the cable. The maximum value of such a resistor (R_{max}) is obtained from the testing of the cable whereas the minimum value (R_{min}) equals that of the cable resistor.

The maximum values of the selected variable resistor for different cable length are shown at Table 4.3.

Table 4.3

Skin Effect Cable Resistor Variations

Cable length	R_{max}
10 m	0.95 Ω/m
40 m	0.27 Ω/m
85 m	0.087 Ω/m

Table 4.4 illustrates the effect of inverter output rise time and the cable length on the voltage at the motor terminals (V_p) when the motor is fully loaded. The results show that the motor terminals voltage increases as the cable length increases. Overvoltages are also sensitive to the pulse rise time; higher voltage is obtained for smaller rise time and longer cable lengths.

Table 4.4

Normalized Motor Terminal Peak Voltage (*Vp/E*) Resulting From Distributed Parameter

Cable Length	Inverter output pulse rise time, μs	Peak voltage at the motor
10 m	0.1	1.63
10m	0.2	1.52
10 m	0.4	1.1
10 m	0.8	1.07
10 m	1.6	1.04
10 m	2.0	1.03
10 m	2.5	1.02
40 m	0.1	1.67
40 m	0.2	1.67
40 m	0.4	1.67
40 m	0.8	1.67
40 m	1.6	1.52
40 m	2.0	1.12
40 m	2.5	1.08
85 m	0.1	1.73
85 m	0.2	1.73
85 m	0.4	1.73
85 m	0.8	1.72
85 m	1.6	1.7
85 m	2.0	1.43
85 m	2.5	1.21

To see the effect of modeling, the cable is modeled using one, two and three pi equivalent lumped parameter circuit. However, from the simulation results it is observed that modeling the cable by a few number of pi equivalent circuits are insufficient to correctly represent the behavior of the cable. To show this, for 40 m cable length, the cable has also been modeled by ten pi equivalent circuit. Fig. 4.3 shows the pi equivalent circuit for cable circuit, where R_t, L_t and C_t are respectively the total resistance, inductance and capacitance of the cable.

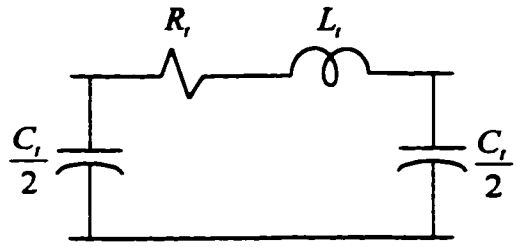

Fig. 4.3 One pi cable equivalent circuit.

Table 4.5 shows the obtained results for different cable lengths.

Table 4.5

Normalized Motor Terminal Peak Voltage (*Vp/E*) Resulting From Lumped Parameter

		Peak voltage at the motor		
Cable length	Inverter output rise time, μs	One pi	Two pi	Three pi
10 m	0.2	1.53	1.73	1.74
40 m	0.2	1.76	1.94	1.95
85 m	0.2	1.85	2.07	2.08

The inverter output line to line voltage (expanded) is shown in Fig. 4.4. Using the distributed parameter model of the cable, the simulation results of motor terminal line to line voltages (expanded) for 10 m, 40 m and 85 m respectively are shown in Fig. 4.5. Figs. 4.6 to 4.8 show the simulation results of the motor terminal line to line voltage using lumped parameter for the cable, at 10 m, 40 m and 85 m cable length, respectively.

As shown from Fig. 4.7, at 40 m cable length, the peak voltage at the motor terminals starts to decrease when the cable is modeled using ten pi lumped parameter. Therefore to have the motor overvoltages obtained from the distributed parameter model, more than a three pi equivalent circuit is needed. Comparing the normalized motor peak voltage obtained from three pi and ten pi, it is seen that the peak at the motor terminal is reduced from 1.95 to 1.81.

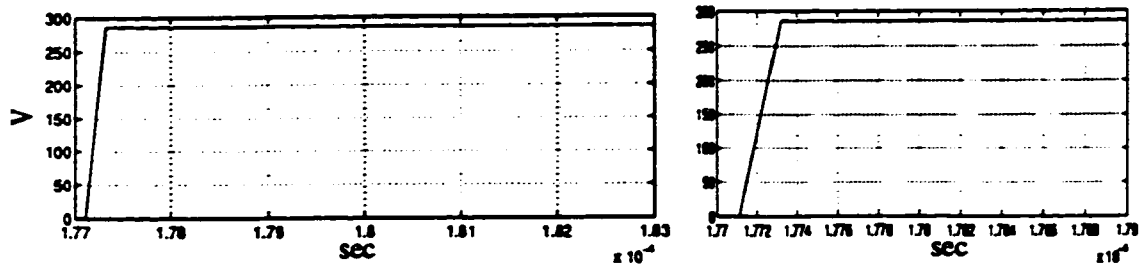

Fig. 4.4 Inverter output line to line voltage (expanded in the right).

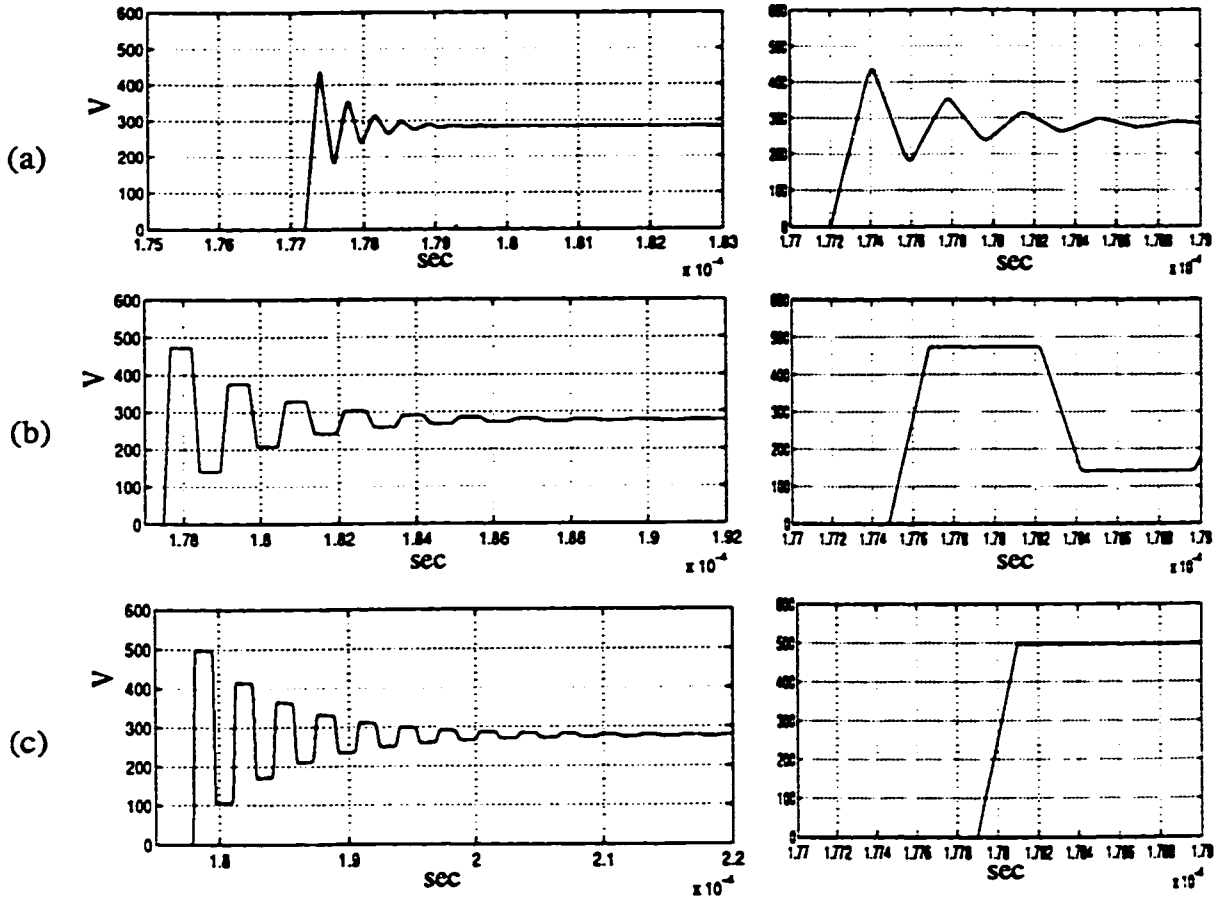

Fig. 4.5 Simulation results showing line to line voltage at motor terminal (expanded in the right) using distributed parameter cable model.

(a) With 10 m of cable.

(b) With 40 m of cable.

(c) With 85 m of cable.

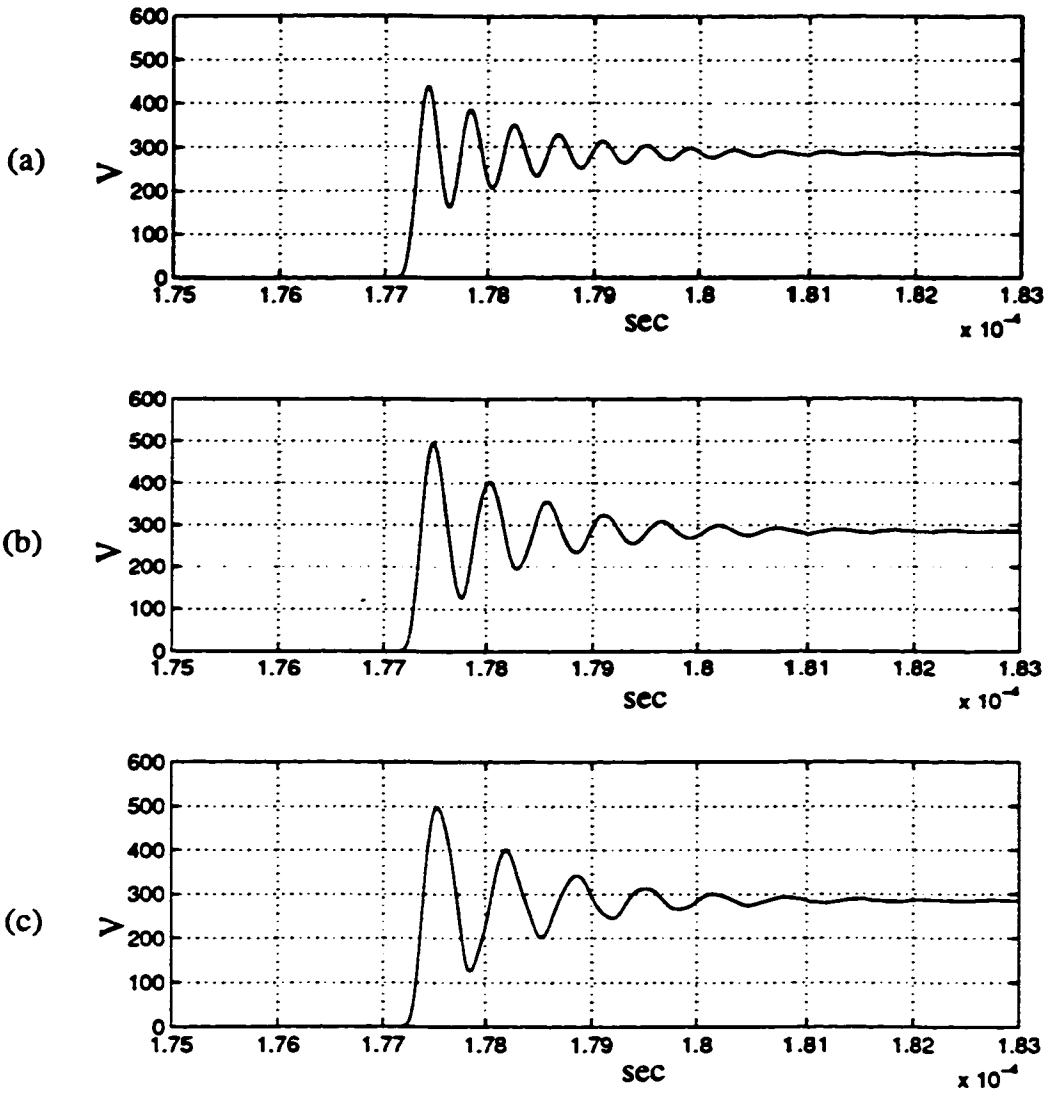

Fig. 4.6 Simulation results showing line to line voltage at motor terminal (expanded) with a 10 m cable.

(a) One pi.

(b) Two pi.

(c) Three pi.

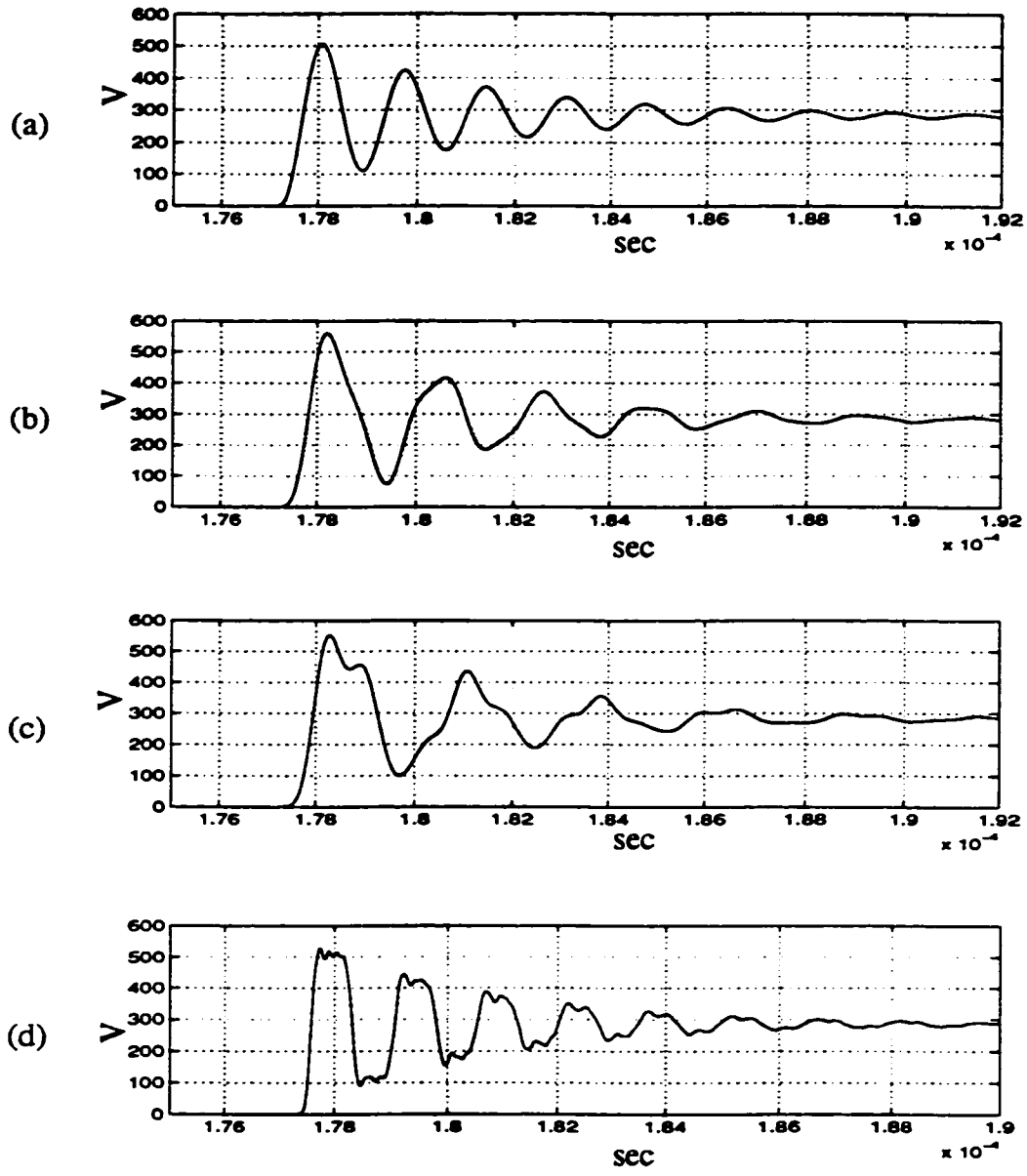

Fig. 4.7 Simulation results showing line to line voltage at motor terminal (expanded) with 40 m cable.

(a) One pi.

(b) Two pi.

(c) Three pi.

(d) Ten pi.

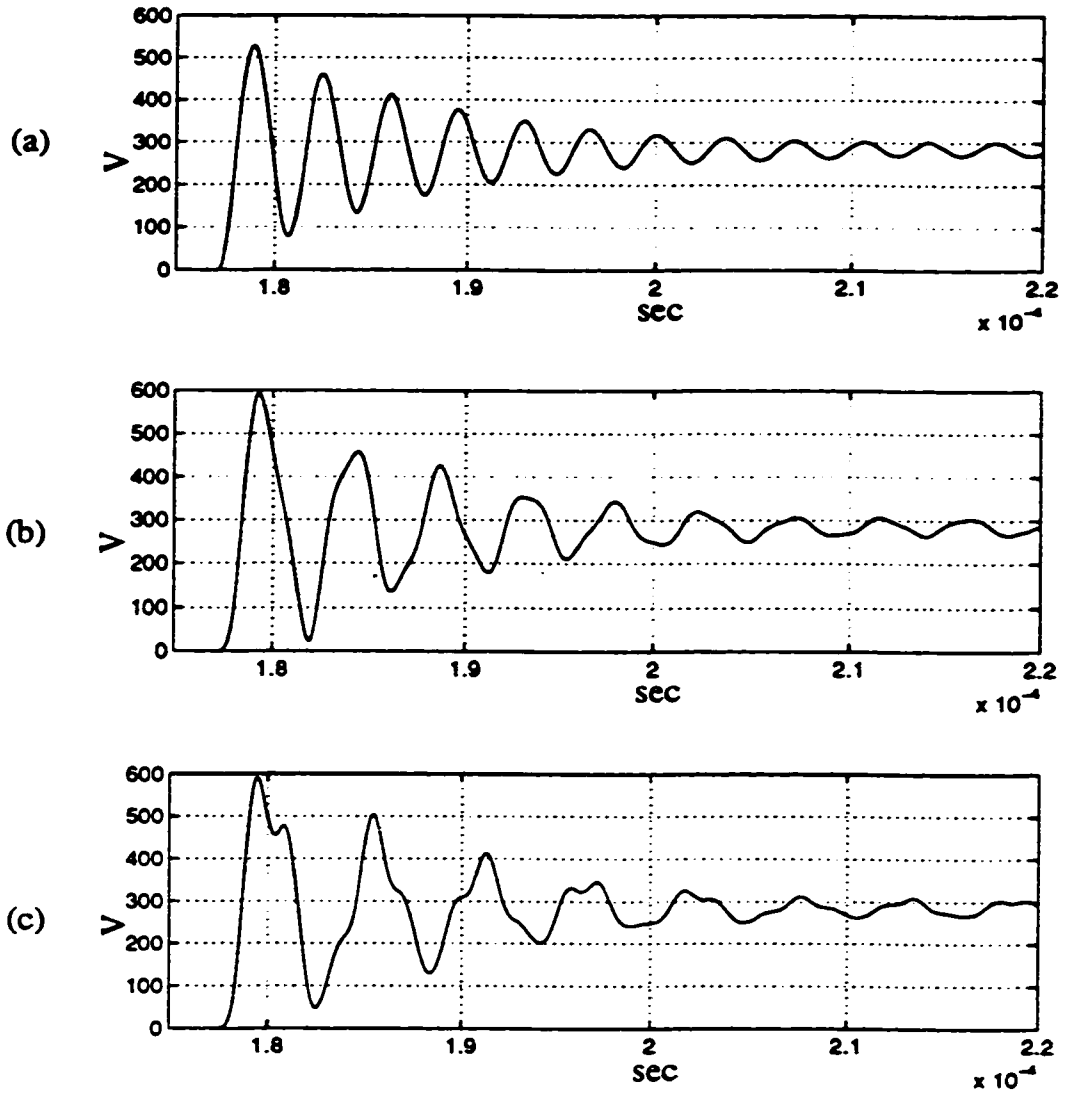

Fig. 4.8 Simulation results showing line to line voltage at motor terminal (expanded) with a 85 m cable.

(a) One pi.

(b) Two pi.

(c) Three pi.

4.5 Experimental Results

Fig. 4.9 shows the experimental results obtained from a Hitachi static converter type HFC-VW. The inverter is supplied from three phase diode bridge rectifier connected to 208 V, 60 Hz and operated at 1260 Hz (21 pu) carrier frequency. The three phase, standard 3 hp motor is connected to the inverter using a Three-Conductor Belted Paper-Insulated cable [40]. The inverter rise time is 0.2 μs.

There is a good agreement between experimental results in Fig. 3.9 and the simulation results shown in Fig. 4.5. Table 4.6 illustrates the difference between the motor peak voltages obtained from experimental and simulation results using distributed parameter and three pi lumped parameter.

Table 4.6

Normalized Experimental Motor Peak Voltage (V_P/E)

At Full load

		Percentage variation to simulation	
Cable length	Peak voltage at the motor	Distributed parameter	Lumped parameter (3 pi)
10 m	1.43	- 6 %	- 21 %
40 m	1.61	- 4 %	- 21 %
85 m	1.71	- 3 %	- 22 %

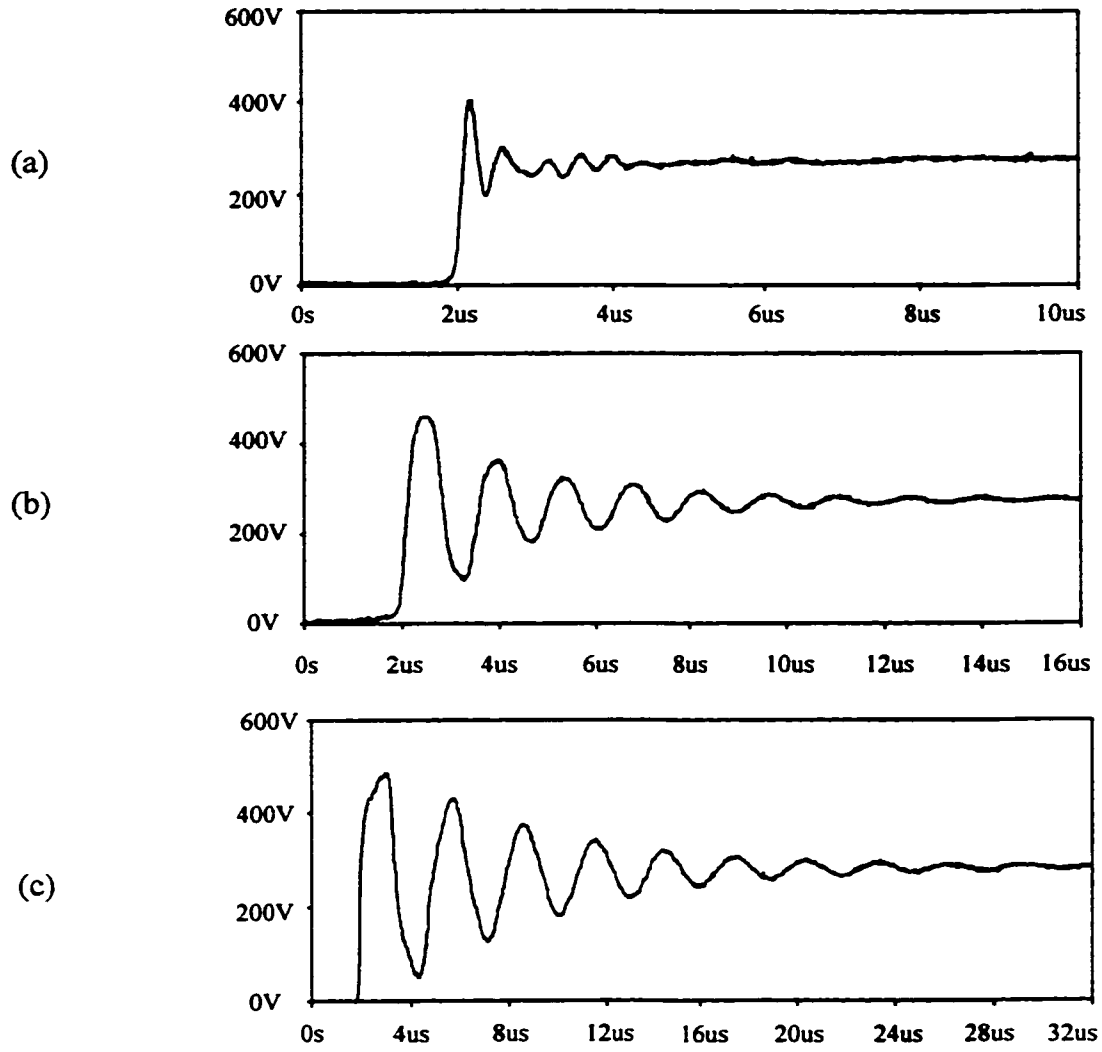

Fig. 4.9 Experimental results showing line to line voltage at motor terminal (expanded).

(a) With 10 m of cable.

(b) With 40 m of cable.

(c) With 85 m of cable.

The overvoltages at the motor terminals are not substantially influenced by the load. In comparison to the low surge impedance of the cable, the motor impedance is high and is equivalent to an open circuit at high frequencies. The maximum overvoltage at the motor terminals for no load test and for different length of cable is experimentally measured and depicted in Table 4.7. There is little difference with the results of Table 4.6.

Table 4.7

Normalized Experimental Motor Peak Voltage (V_P/E)

At No Load

Cable length	Peak voltage at the motor
10 m	1.44
40 m	1.68
85 m	1.73

4.6 Filter Design and Justification

Fig. 4.10 shows the circuit topology for a first order R_f - C_f filter used to reduce the overvoltage at the terminal of the motor. The filter resistance, selected to be equal to the cable characteristics impedance, is used in series with a small 60 Hz blocking capacitor. The equivalent impedance of this filter is closely matched with the cable surge impedance. If the cable is terminated by this filter circuit design, the reflection coefficient becomes zero, and no overvoltage will appear at the motor terminals. The filter

performance was verified for all cable lengths using the EMTP simulation to ensure that a proper cable termination and overvoltage attenuation is achieved.

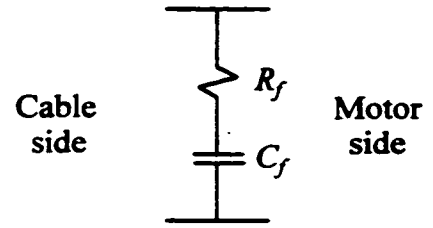

Fig. 4.10 First order filter circuit.

The values of the filter components are shown in Table 4.8.

Table 4.8

First Order Filter Components

Filter components	Values
R_f	51.6 Ω
C_f	0.073 μF

At 60 Hz operation, the filter impedance becomes very high thereby the current flowing in the filter is small. Furthermore, the filter losses are negligible.

The simulation results for the voltages across the motor terminals before and after filtering using the first order filter, are shown in Fig. 4.11 for 10m, 40m and 85 m cable length, respectively.

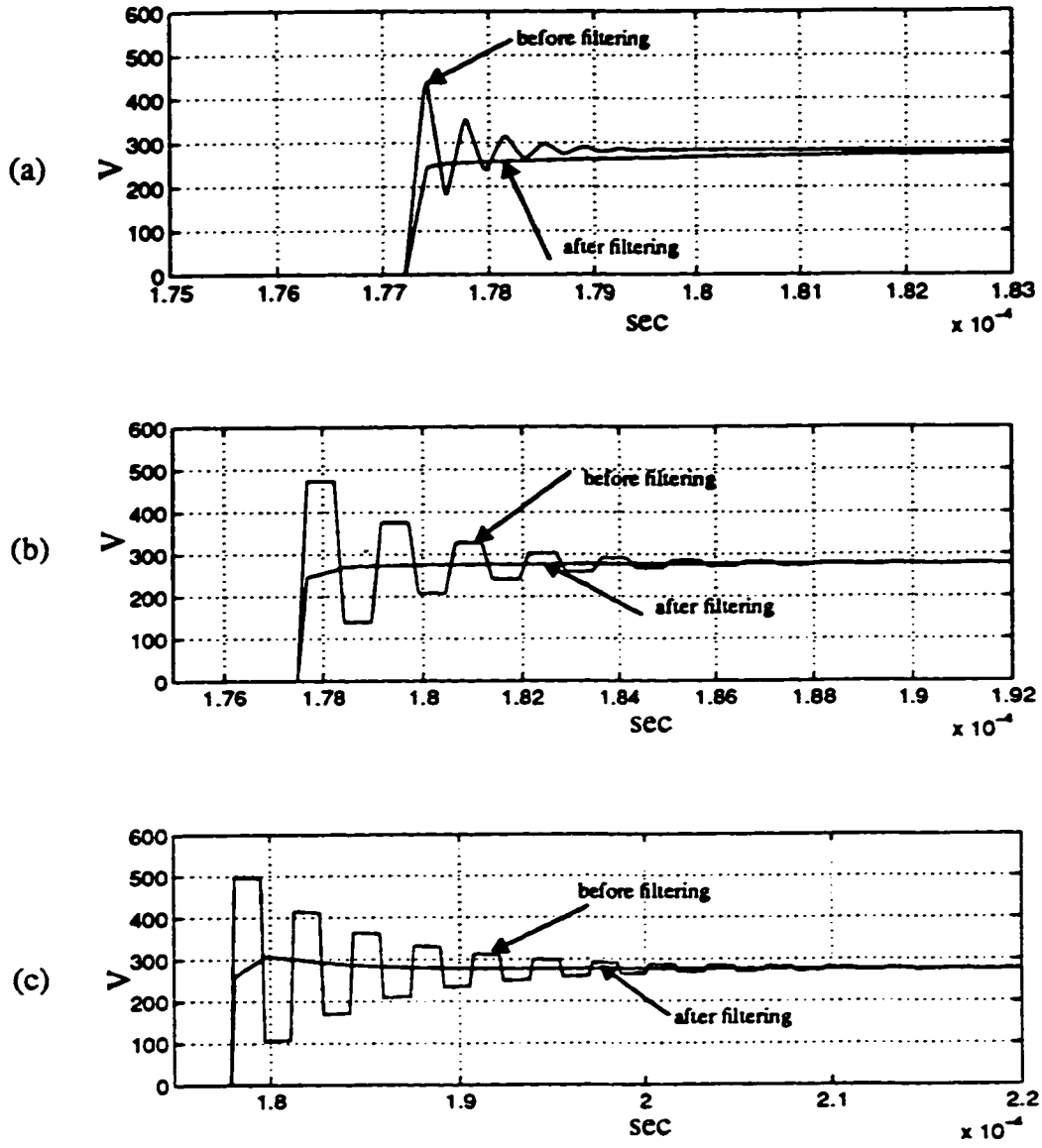

Fig. 4.11 Simulation results showing motor terminal line to line voltage (expanded) before and after filtering.

(a) With 10 m of cable.

(b) With 40 m of cable.

(c) With 85 m of cable.

Fig. 4.12 shows the experimentally obtained motor input line to line voltage after filtering when the motor is fed by a cable of 40 m length.

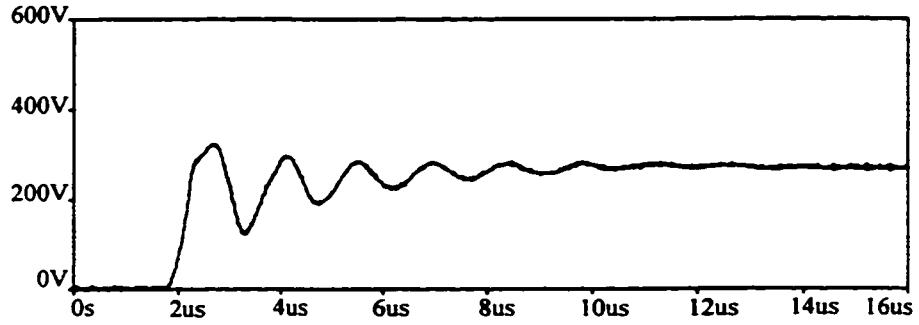

Fig. 4.12 Experimental motor terminal line to line voltage for 40 m of cable after filtering.

The voltage at the motor terminals is significantly reduced from 462 V to 338 V; however the results deviated from the simulation results. This is due to the fact that at very high frequency the conventional capacitors and resistors do not behave like ideal elements. Their internal inductance, at very high frequency, creates a reflection coefficient at the cable terminal different from zero, which will further cause new overvoltages across the motor terminal. Table 4.9 shows the measuring of internal parameters of the filter at 682 kHz (40 m cable length).

Table 4.9

Measurements Of Internal Parameters For First Order Filter

At 682 kHz

	R_i	L_i	C_i
R_f	65.2 Ω	20.14 μH	200 pF
C_f	113 mΩ	263 nH	73.2 nF

4.7 Alternative Filters

Two different types of filters can be used to reduce the overvoltages at motor terminals:

i. Second order shunt filter

ii. Tuned *L-C* filter

4.7.1 Second Order Shunt Filter

Fig. 4.13 shows the circuit topology of a second order filter used to reduce the overvoltage at the motor terminals. The filter components values are selected such that the equivalent impedance of the filter closely matches the surge impedance of the cable as shown in Eq. (4.28) [38]:

$$Z_f = \sqrt{\left[\frac{R_f \omega_f^2 L_f}{R_f^2 + \omega_f^2 L_f^2}\right]^2 + \left[\frac{R_f^2 \omega_f L_f}{R_f^2 + \omega_f^2 L_f^2} - \frac{1}{\omega_f C_f}\right]^2} \approx Z_0 \qquad (4.28)$$

where ω_f is the resonant frequency of the filter.

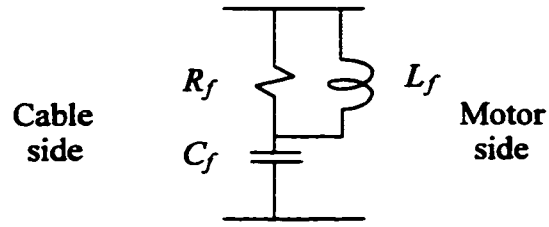

Fig. 4.13 Second order shunt filter.

Experimental results of the application of this filter have shown that it is less effective in attenuating the overvoltages than the first order filter. This can be attributed to the behavior of the resistance, inductance and capacitance at high frequencies.

4.7.2 Tuned *L-C* Filter

A third type of output filter, the *L-C* filter, is shown in Fig. 4.14. It efficiently produces a sine wave voltage output when applied to inverters using a high modulating frequency approaching 10 kHz. Cost and size of these type of filters are important considerations in its applications [44].

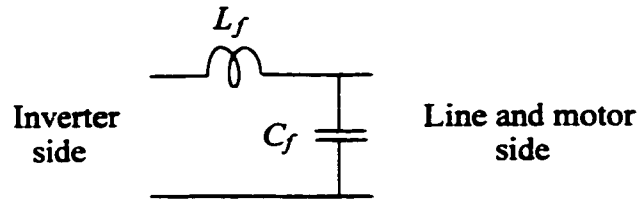

Fig. 4.14 The *L-C* filter.

4.8 Summary

This chapter investigates the winding overvoltages effect of traveling waves on induction motors. From the theoretical consideration, EMTP simulation and experimental results, it may be concluded that: (a) theoretical considerations define the traveling wave phenomenon, its speed and reflection coefficient and the effect of the cable termination or motor impedance on the phenomenon; (b) simulation by means of distributed parameter cable models accurately predicts the overvoltage generated as a result of pulse rise time and cable length, results that are confirmed by experimental measurements; and (c) terminating the cable on the motor side by a small first order $R_f C_f$ filter effectively damps voltage oscillations.

CHAPTER 5

EFFECT OF LINE TRANSIENTS ON DIODE BRIDGE RECTIFIERS

5.1 Introduction

In industrial applications, the rectifier is normally a three phase bridge circuit. This is because of its low ripple content in the output waveforms and a higher power handling capability. As the rectifier is connected to the ac supply, its characteristics are affected externally by the ac circuit components.

A study of the following two effects was carried out : (i) Effect of line inductance on the input and output of the rectifier; (ii) Effect of ac power factor correction capacitor switching.

In the first part of this chapter, the effect of the line inductance on the diode bridge rectifier characteristics is studied for the continuous and discontinuous mode of operation. In the second part, the effect of switching capacitor on power factor correction on the intermediate dc link voltage is simulated for a variable dc link capacitor and variable rectifier associated inductance. Rectifier and capacitor switching waveforms are obtained.

5.2 Effect of the Line Inductance on the Diode Rectifier Characteristics

Fig. 5.1 shows the circuit configuration of three phase diode bridge rectifier supplying a resistive load R_L, where the line impedance is represented by its inductance L_s, and the rectifier filter is represented by the capacitor connected on the dc side of the rectifier.

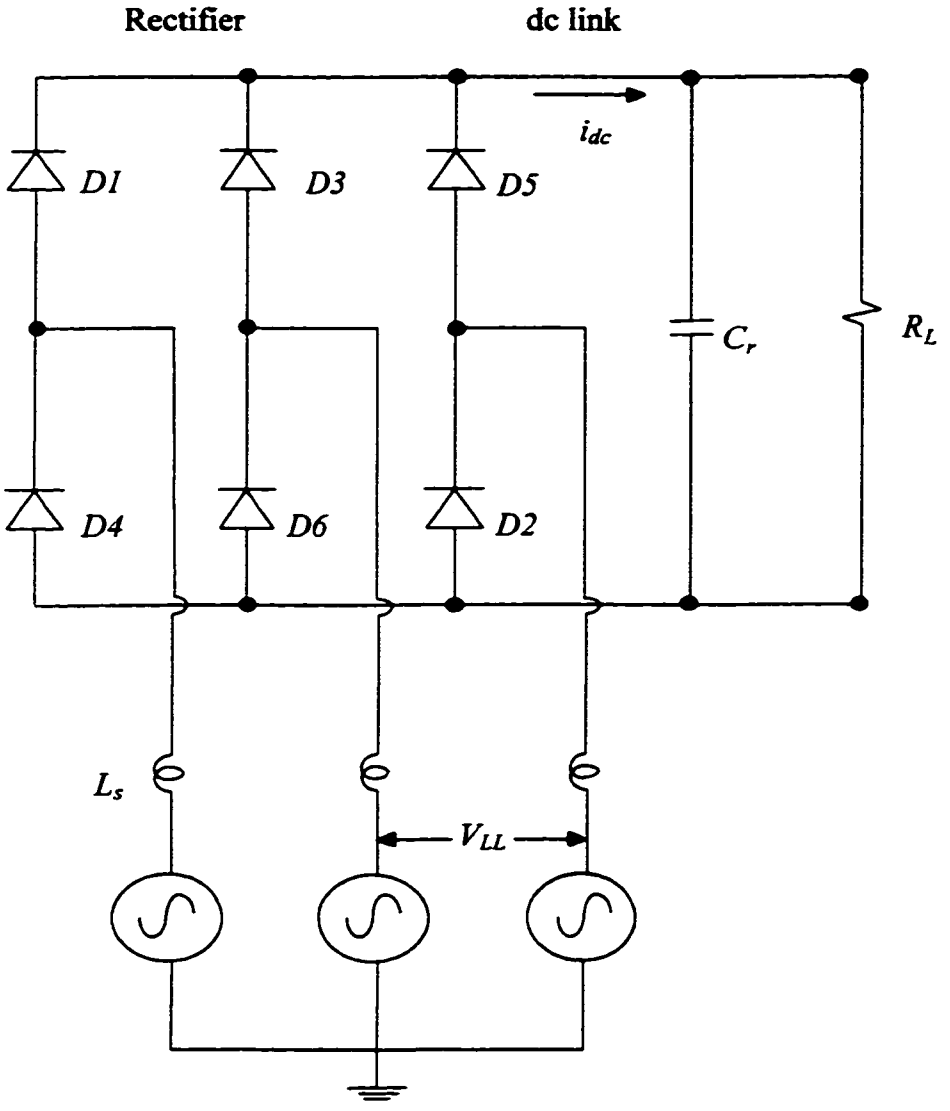

Fig. 5.1 Three phase diode bridge rectifier.

Depending on the value of the ac side inductance in the rectifier circuit, the operation of the bridge rectifier can be classified into two modes of operation: (i) Continuous and, (ii) Discontinuous.

In the discontinuous mode of operation, the intermediate dc link current is discontinuous when the ac side has a small inductance L_s. The displacement power factor which is defined as the cosine of angle between the fundamental components of rectifier input voltage and current, is very high and becomes unity when the supply is ideal, it starts to decrease as L_s increases. As opposed to this, the distortion factor which is the ratio between the rectifier fundamental input current to its total input current is very small and becomes high as L_s is increased. Rectifier power factor which is the result of these two factors, becomes very poor at a small L_s and improves when L_s increases.

With a small L_s, rectifier average output voltage V_{dc} approaches the peak of the rectifier supply line to line voltage ($\sqrt{2}V_{LL}$), and starts to decrease when L_s increases and the dc link current i_{dc} goes from discontinuous to continuous mode.

Total harmonic distortion of the line current (THD_i) decreases with the increase of L_s and becomes considerably low if the rectifier operates in the continuous mode.

Rectifier input voltage total harmonic distortion (THD_v) has low values in the discontinuous mode of operation as compared with the continuous mode, due to absence of commutation in the diodes and low values of L_s during this mode.

The effect of the ac source inductance on the bridge rectifier is shown in Figs. 5.2 to 5.4 where the discontinuous mode of operation is depicted by thin line. The rectifier load is assumed equal 30.5 Ω.

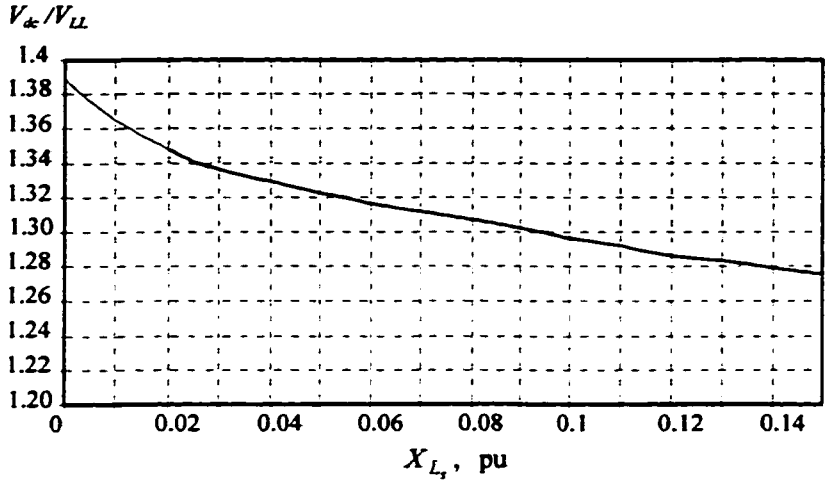

Fig. 5.2 Average rectifier output voltage as function of V_{LL} vs X_{L_s}.

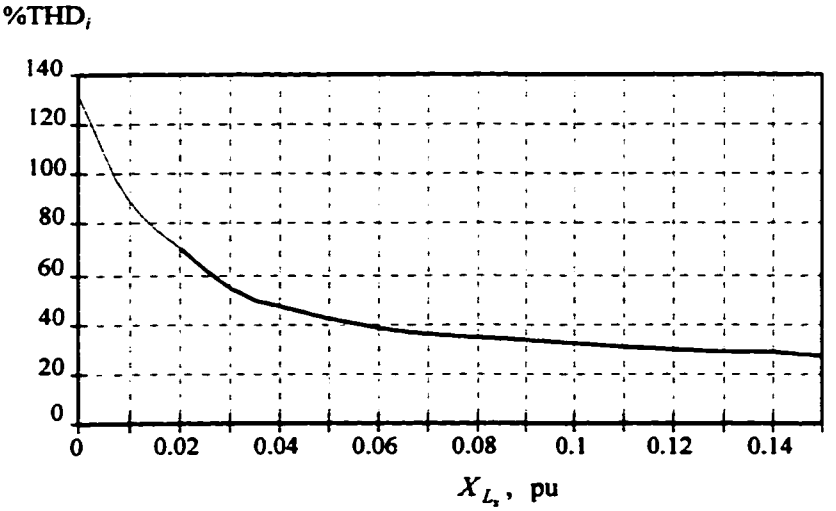

Fig. 5.3 Rectifier input current total harmonic distortion vs X_{L_s}.

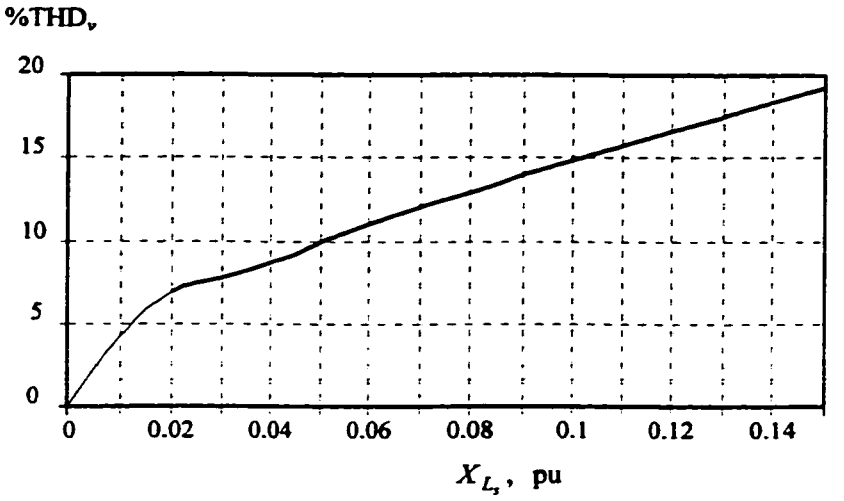

Fig. 5.4 Rectifier input voltage total harmonic distortion vs X_{L_s}.

5.3 Effect of ac Supply Capacitor Switching in Power Factor Correction on Rectifier Operation

If a linear load is connected to the supply point of diode bridge rectifier, an overvoltage will appeared in the intermediate dc link voltage (capacitor peak voltage), when the power factor in the linear load is corrected using a switching capacitor.

Assume L_{s_2} is the per phase inductance associated of the rectifier and a three phase, star connected 208 V, 60 Hz, 12.5 kVA, 0.8 PF (lagging) linear load is connected at the same supply point of the rectifier, as shown in Fig. 5.5.

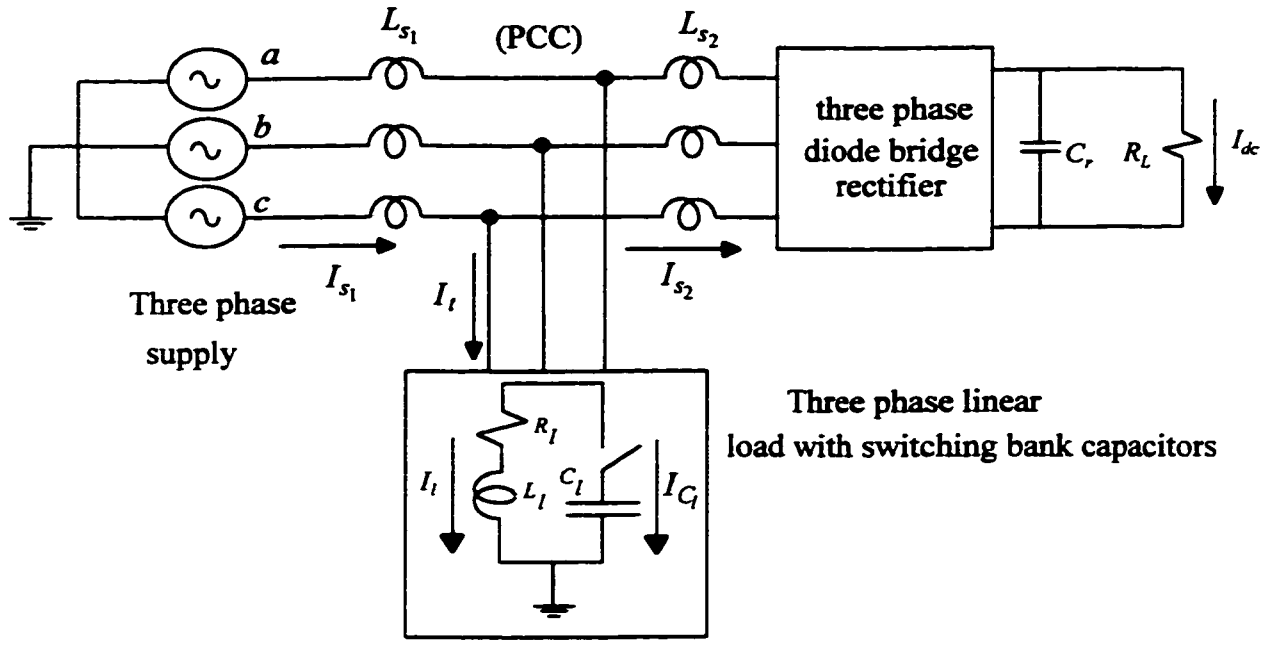

Fig. 5.5 Three phase bridge rectifier with linear load capacitor switching.

If S_l (in VA) and V_l (in V) are, respectively, the apparent power and terminal phase voltage of the linear load shown in Fig. 5.5, the magnitude of its impedance can be calculated as:

$$|Z_l| = \sqrt{R_l^2 + (2\pi f L_l)^2} = \frac{3|V_l|^2}{S_l} \tag{5.1}$$

and its phase angle is:

$$\phi = \tan^{-1} \frac{2\pi f L_l}{R_l} \tag{5.2}$$

The active and reactive power P_l and Q_l absorbed by the linear load are:

$$P_l = S_l \cos\phi \tag{5.3}$$

and

$$Q_l = S_l \sin\phi \tag{5.4}$$

To bring the power factor to unity a capacitance is needed. Its generated reactive power Q_c must be equal to the reactive power absorbed by the load. Therefore:

$$Q_{c_l} = Q_l \tag{5.5}$$

Assuming a star connected capacitor bank, the magnitude of its impedance is:

$$|Z_c| = \frac{3|V_l|^2}{Q_{c_l}} \tag{5.6}$$

Table 5.1 shows the values of the linear load and its switching capacitor when the power factor is corrected to unity.

Table 5.1

Linear Load And Its Switching Capacitor Parameters

Parameter	Value, Ω
Linear load resistance	2.77
Linear load inductance	2.07
Switching capacitor reactance	5.77

Fig. 5.6 shows the effect of the inductance L_{s_2} on the ratio of (V_{C_r} / V_{LL}) where V_{C_r} is the capacitor peak voltage and V_{LL} is the supply line to line voltage, for different values of C_r. The bank capacitors are assumed to be discharged when they are switched in the circuit.

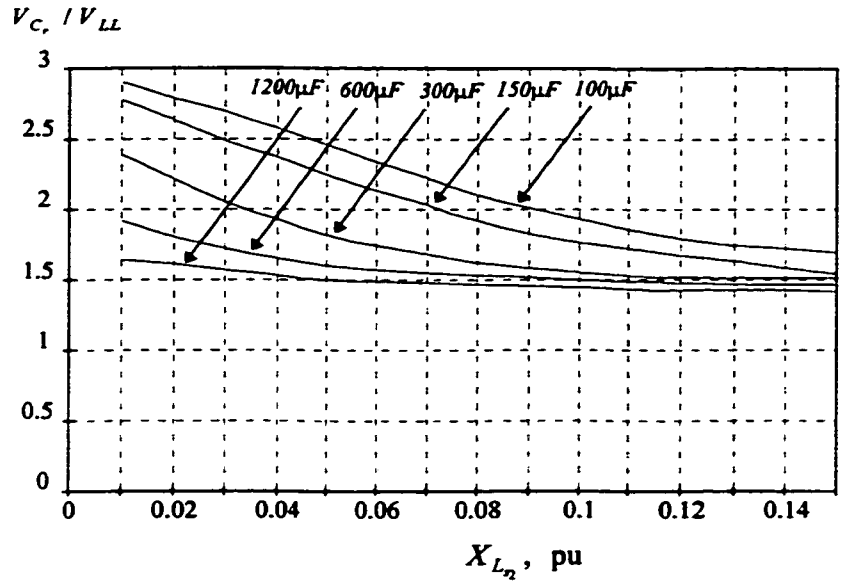

Fig. 5.6 Effect of the rectifier associated inductance L_{s_2} on the capacitor peak voltage (V_{C_r}) for different values of dc rectifier filter capacitor C_r

Fig. 5.6 shows that the overvoltages across the rectifier output capacitor can be reduced by either of the two methods:

(i) By increasing the value of L_{s_2}, or

(ii) By increasing the value of the rectifier output capacitor C_r

Figs 5.7 to 5.10 show the voltage and current waveforms for the linear load and bridge rectifier, when the capacitor banks are switched at the instant where one of the three phase supply voltages is zero (t = 50 ms). The rectifier associated reactance equals 0.1 mH.

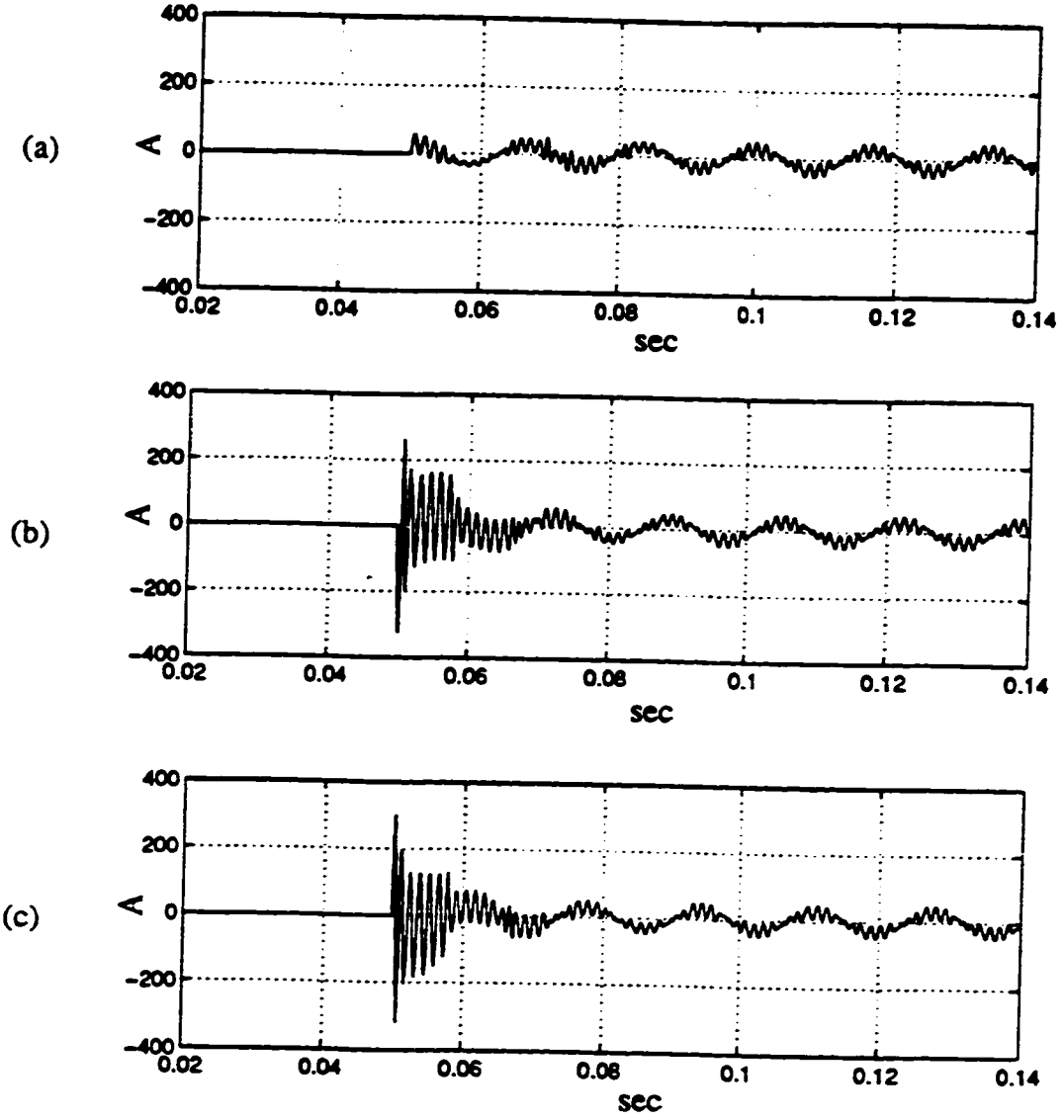

Fig. 5.7 Simulation results of capacitor bank phase current (I_{C_l}).

(a) Phase *a*.

(b) Phase *b*.

(c) Phase *c*.

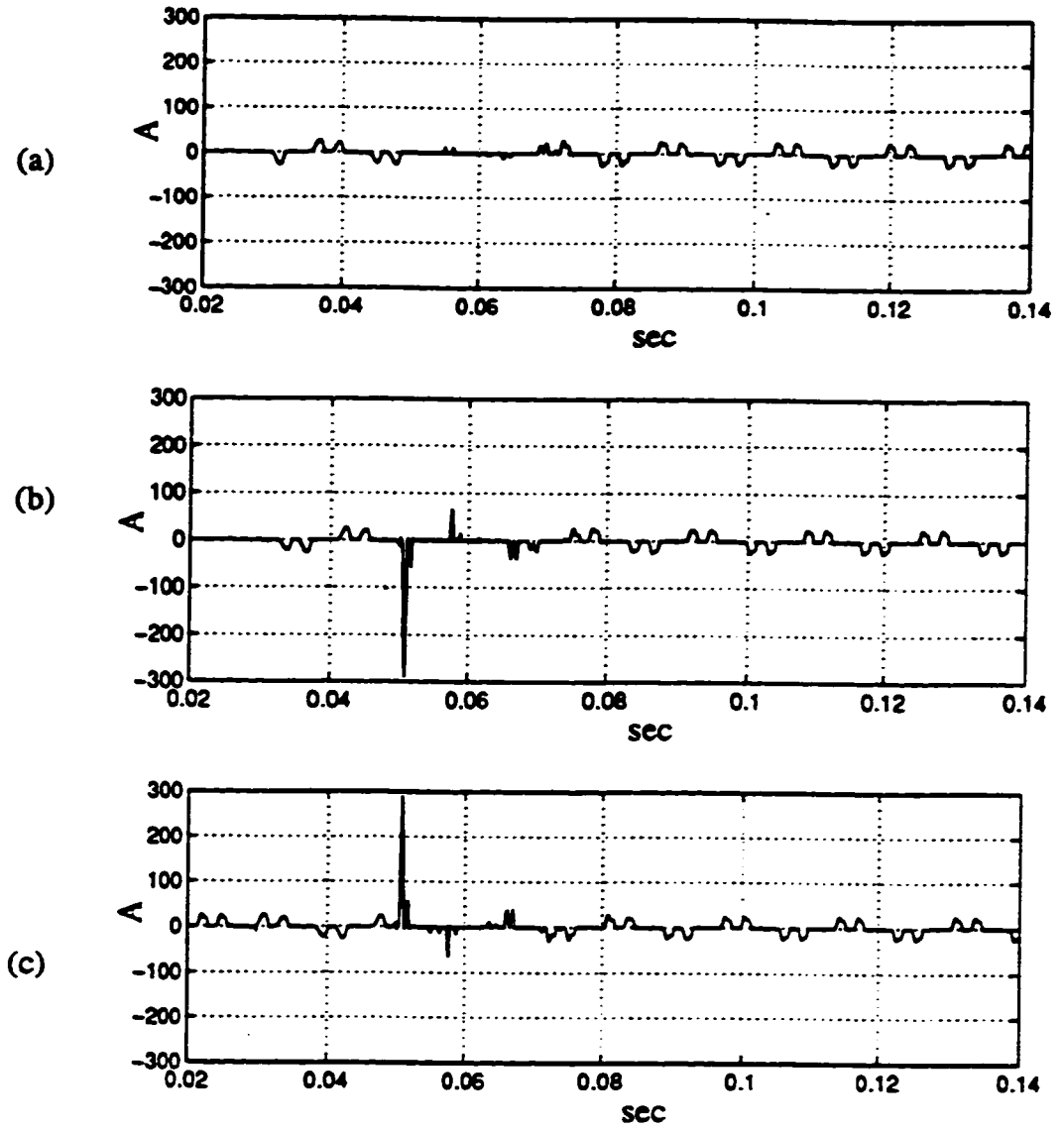

Fig. 5.8 Simulation results of rectifier input phase current (I_{s_2}).

(a) Phase *a*.

(b) Phase *b*.

(c) Phase *c*.

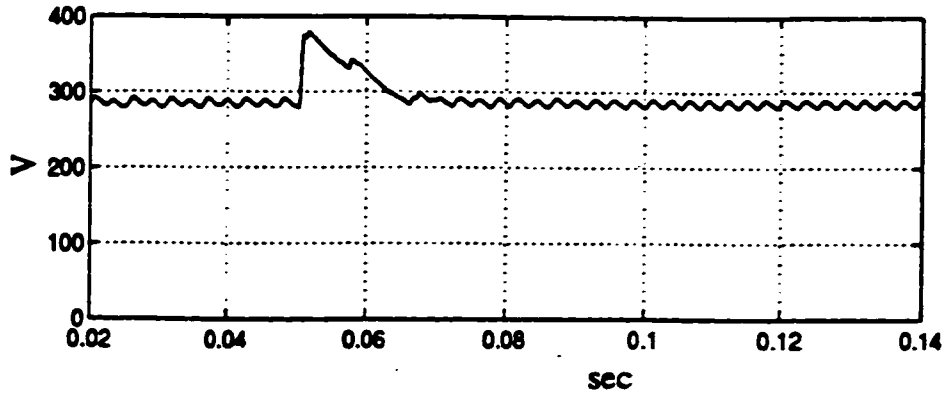

Fig. 5.9 Simulation result of rectifier output voltage.

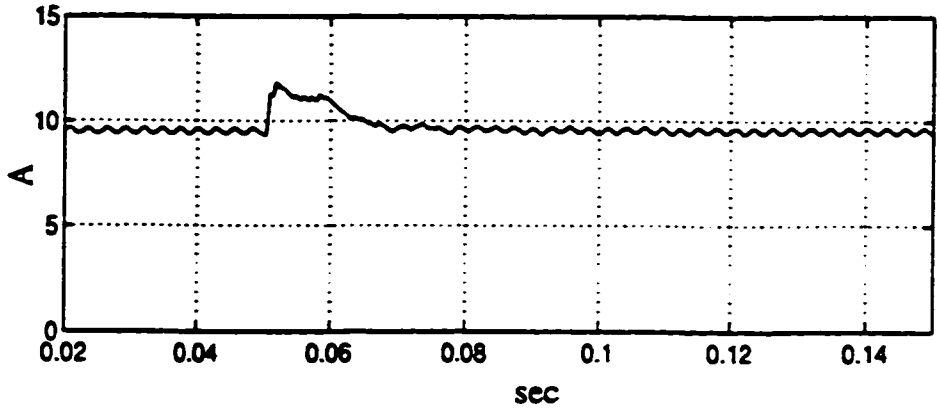

Fig. 5.10 Simulation result of rectifier output current.

Capacitor switching effect on the rectifier circuit can be viewed by dividing the time duration of switching current into three time periods. This division is based on events during each period beginning at the capacitors bank switching time and ending when a new steady state is reached.

In the first period, called the subtransient period, a rapid decay of both the ac and dc components of switching current exists. During the second period, also called transient period, a low decay of components with small magnitude will be obtained as compared with the first one. Steady state is reached in the last period and a new output voltage will appear across the capacitor filter.

5.4 Experimental Results

Figs. 5.11 (a) and (b) show, respectively, the experimental results of capacitor and rectifier output current waveforms, obtained for a 33 V, 60 Hz, 0.85 PF (lagging) linear load connected at the supply point of the rectifier shown in Fig. 5.5. The rectifier associated inductance, and, the line resistance and inductance are 1mH, 0.17 Ω and 0.21 mH, respectively.

The simulation results of capacitor and rectifier output current waveforms are shown respectively in Fig. 5.12 (a) and (b) respectively.

(a)

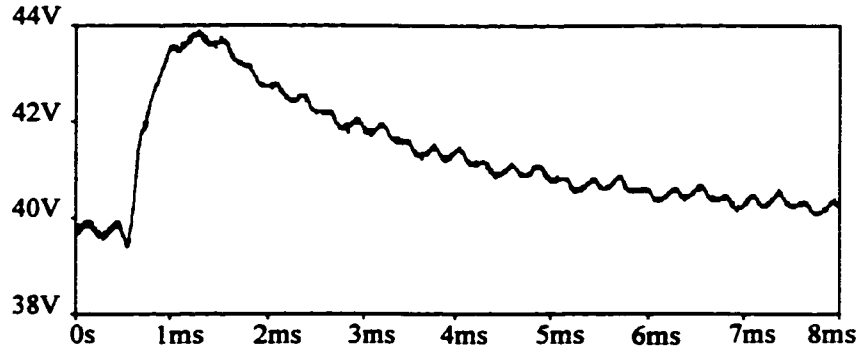

(b)

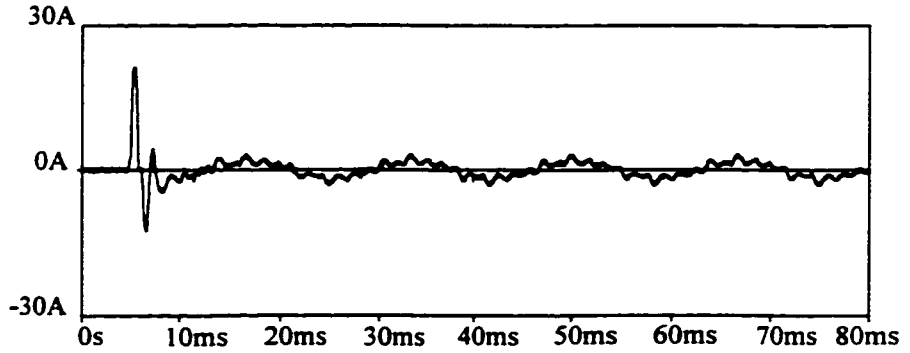

Fig. 5.11 Experimental results with a scaled linear load.

(a) Rectifier output voltage (expended).

(b) Capacitor current.

(a)

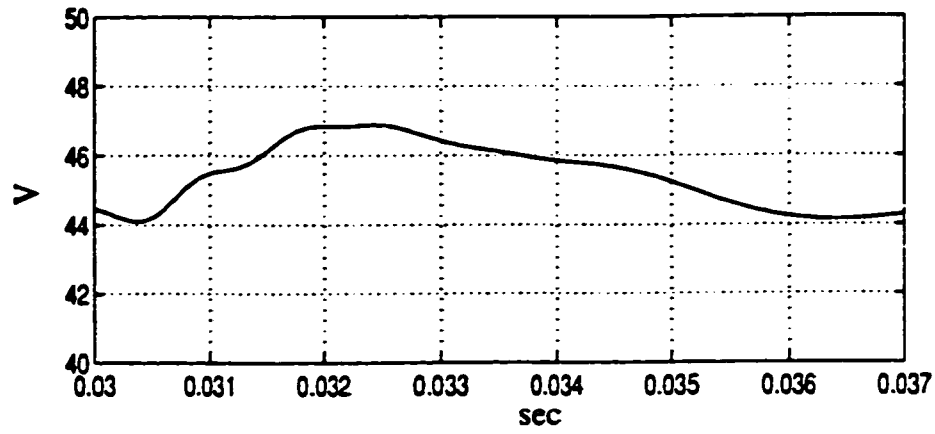

(b)

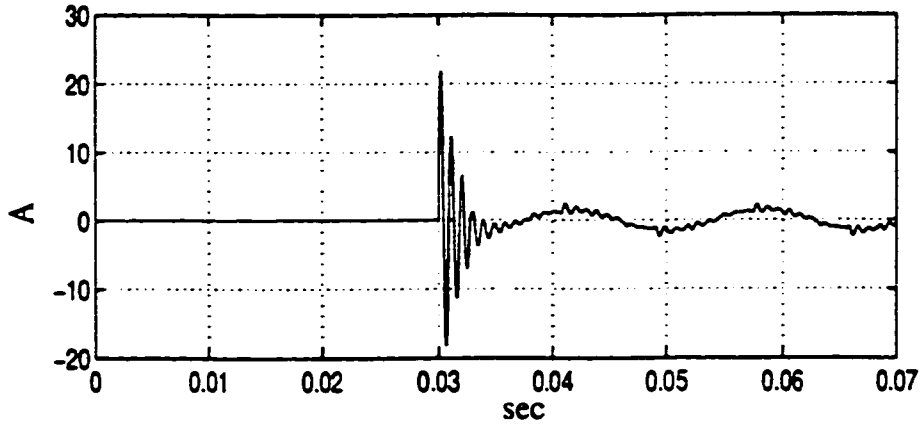

Fig. 5.12 Simulation results with a scaled linear load.

(a) Rectifier output voltage.

(b) Capacitor phase current

5.5 Summary

In this chapter, the effect of line inductance on the characteristics of the three phase diode bridge rectifier is obtained for continuous and discontinuous mode of operation. Overvoltages across the rectifier capacitor filter due to capacitor switching are investigated for variable rectifier associated inductance and dc filter. The simulation and experimental results of the circuit leads us to the conclusion of a high input pulse current to the rectifier circuit.

CHAPTER 6

SUMMARY AND CONCLUSIONS

6.1 Summary

A complete study of induction motor drive systems has been presented. The compelling reason for the increased interest in this field lies in the fact that the squirrel cage induction motor is the one most used in industrial applications. The contents of this thesis can be summarized as follows:

In Chapter 2, modeling techniques for induction motors in electric drives using the EMTP program have been presented. It is shown that the Universal Machine model in EMTP allows a detailed analysis of the machine characteristics. The shaft dynamics are represented by an equivalent analog electric circuit. The validity of the model has been verified by simulation and experimental results.

In Chapter 3, modeling of the induction motor drive supplied by a PWM voltage source inverter is investigated. The motor drive circuit is implemented by means of a diode bridge front - end rectifier, a dc capacitive filter, and a voltage source type inverter. The harmonic contents of the motor and ac line voltages and currents, total harmonic distortion, and system power factor are obtained for different operating speeds. Simulation results are validated experimentally.

In Chapter 4, the effects of long leads on PWM inverter fed induction motors are analyzed. The overvoltage across the motor terminals is obtained for different cable

lengths and different inverter output voltage rise times. The following two cable models are investigated: (i) distributed parameter model, and, (ii) lumped parameter model. The simulation results are verified experimentally for three different cable lengths. It is also shown that voltage oscillations are effectively damped using a small first order filter across the motor terminals.

In Chapter 5, two effects on diode bridge front - end rectifier characteristics are studied : (i) the effect of line inductance for continuous and discontinuous modes of operation, and, (ii) the effect of ac side capacitor switching for different dc link capacitor and line inductance values is investigated. These effects are verified on an industrial drive.

6.2 Conclusions

(i) Despite the fact that the Electromagnetic Transient Program (EMTP) was originally designed for power system studies, it has the flexibility of handling power electronics systems, modeled of the converter level. Moreover, since the EMTP has excellent models for the cables, transmission lines and machines, more realistic studies considering frequency dependent parameters, traveling wave phenomena, and machine dynamics can be performed with grater ease and completeness than with electronic circuit simulators such as PSPICE. In particular, EMTP studies confirmed by experimental verifications have shown adjustable speed drives inject nonsinusoidal current waveforms into the power system and generate nonsinusoidal voltage waveforms across the

induction motor. On the line side, this results in high total current harmonic distortion and poor power factor.

(ii) By using PWM control, the voltage harmonics on the motor side are moved to higher frequencies. This reduces torque harmonics and heating in the motor. However, feeding the motor from a PWM inverter using long cables, produces overvoltages across the motor terminals. These overvoltages can be greater than the rated voltage of the motor. The traveling wave phenomenon can be effectively used to explain the experimental results and simulate cable performance. A first order output filter can effectively attenuate overvoltages and the traveling wave phenomenon can be used to explain its operation.

(iii) The line impedance has a considerable effect on the diode bridge front - end rectifier performance. With a small supply inductance, the current in the dc link of the rectifier becomes discontinuous. This results in a higher average output voltage and higher input current total harmonic distortion, which in turn results in poor rectifier power factor. This effect was carefully studied using EMTP and an optimum value for the line inductance was determined.

(iv) Switching power factor correction capacitors in the ac system will result in overvoltages on the rectifier output capacitor. These overvoltages vary with the rectifier dc side capacitor and line inductance. Values for the dc side capacitor and line inductance were determined to limit the overvoltage taking into account the complete distribution system.

6.3 Suggestions for Future Research Work

The following are suggestions for further research:

(i) The increasing use of adjustable speed drives dictates that the effect of harmonic pollution on other equipment in the power system be considered. The EMTP program provides a good environment to study these effects.

(ii) The motor model available in EMTP can be improved by introducing frequency dependent parameters.

(iii) The EMTP provides other options for cable modeling including frequency dependent modeling. Therefore a further study covering the effect of the variations of cable parameters with frequency could be carried out.

(iii) The first order filter which is used to remove the overvoltages resulting from the traveling wave phenomenon across the motor terminal, does not work as well in practice as in simulation. The reason is the variation in the values of the filter components at high frequencies. Alternative configurations could be investigated.

REFERENCES

[1] F. L. Alvarado, H. Dommel, V. Brandwajn, R. De La Rosa and L. Marti, "*Electromagnetic Transients Program (EMTP), Volume 2, Workbook II*", EPRI, Palo Alto, California, June 1989.

[2] S. Lefebvre, "*Three-phase induction machines in The EMTP*", IREQ-94-091, Hydro-Quebec, Mar. 1994.

[3] S. B. Dewan, G. R. Slemon and A. Straghen, "*Power semiconductors drives*", Jone Wiley, New York, 1989.

[4] P. C. Sen, "*Principles of electric machines and power electronics*", Jone Wiley, New York, 1989.

[5] P. C. Krause, "*Analysis of electric machinery*", McGraw - Hill, New York, 1986.

[6] J. J. Pollack, "Some guidelines for the application of adjustable speed ac drives", *IEEE Trans. Ind. Appl.*, vol. IA-9, no. 6, pp. 704-710, Nov./Dec. 1973.

[7] P. Enjeti and W. Shireen, "A new techenique to reject dc-link voltage ripple for inverters operating on programmed PWM waveforms", in *Conf. Rec. IEEE PESC'90*, pp. 705-713, June 1990.

[8] R. H. Daugherty and C. H. Wennerstrom, "Need for industry standards for ac induction motors intended for use with adjustable-frequency controllers", *IEEE Trans. Ind. Appl.*, vol. 27, no. 6, pp. 1175 - 1185, Nov./ Dec. 1991.

[9] G. K. Dubey, "*Power semiconductor controlled drives*", Prentice Hall, New Jersy, 1989.

[10] P. M. Espelage, J. A Chiera, and F. G. Turnbull, "A wide range static inverter suitable for ac induction motors drives", *IEEE Trans. Ind. Gen. Appl.*, vol. IGA-5, no.4, pp. 438-445, Jul./Aug. 1969.

[11] J. M. D. Murphy and M. G. Egan, "A comparison of PWM strategies for inverter-fed induction motors", *IEEE Trans. Ind. Appl.*, vol. IA-19, no. 1, pp. 363-368, May/June 1983.

[12] E. A. Klingshirn and H. E. Jordan, "Polyphase induction motor performance and losses on nonsinusoidal voltage sources", *IEEE Trans. Power. App. Syst.*, vol. PAS-87, no. 4, pp. 624-631, Mar. 1968.

[13] G. S. Buja and G. B. Indri, "Optimal pulse width modulation for feeding ac motor", *IEEE Trans. Ind. Appl.*, vol. IA-13, no.2, pp. 38-44, Jan./Feb. 1977.

[14] I. Takahashi and H. Mochikawa "A new control of PWM waveform for minimum loss operation of an induction motor", *IEEE Trans. Ind. Appl.*, vol. IA-21, no. 4, pp. 580-587, May/June 1985.

[15] H. Mochikawa and I. Takahashi, "Optimum PWM waveforms of an inverter for decreasing acoustic noise of an induction motor", *IEEE trans. Ind. Appl.*, vol. IA-22, no. 5, pp. 828-834, Sep./Oct. 1986.

[16] G. R. Slemon, "Modeling of induction machines for electric drives", *IEEE. Trans. Ind. Appl.*, vol. IA-25, no. 6, pp. 1126-1131, Nov./Dec. 1989.

[17] G. R. Slemon, "Electrical machine for variable-frequency drives", *Proc. IEEE*, vol. 82, no. 8, pp. 1123-1135, Aug. 1994.

[18] P. C. Krause and L. T. Woloszyk, "Comparison of computer and test results of a static ac drive system", *IEEE Trans. Ind. Gen. Appl.*, vol. IGA-4, no. 6, pp. 583-588, Nov./Dec. 1968.

[19] S. R. Bowes and R. R. Clements, "Computer-aided design of PWM inverter systems", *IEE Proc. B-Elect. Power Appl., 129*, pp. 1-17, 1982.

[20] S. R. Bowes and R. R. Clements, "Digital computer simulation of variable-speed PWM inverter drives", *IEE Proc. B-Elect. Power Appl., 130*, pp. 229-244, 1983.

[21] J. D. Lavers and R. W. Y. Cheung, "A software package for the steady state and dynamic simulation of induction motor drives", *IEEE Trans. Power Syst.*, vol. PWRS-1, no. 2, pp. 167-175, May 1986.

[22] B. Wu, G. R. Slemon and S. B. Dewan, "PWM-CSI inverter for induction motor drive", in *Conf. Rec. IEEE IAS'89*, pp. 508-513, Oct. 1989.

[23] H. Jin, B. Wu, J. D. Lavers and S. H. Dewan, "Simulation of PWM CSI induction motor drive system", in *Conf. Rec. IEEE IECON'89*, pp. 225-231, Nov. 1989.

[24] N. Mohan, *"Computer exercises for power electronics education"*, Jan. 1990.

[25] C. L. Johnson, *"Analog computer techniques"*, McGraw-Hill, New York 1963.

[26] H. A. Peterson, P. C. Krause, J. F. Luini and C. H. Thomas, "An analog computer study of a parallel ac and dc power system", *IEEE Trans. Power App. Syst.*, vol. PAS-85, pp. 191-209, Mar. 1966.

[27] H. K. Lauw and W. Meyer, "Universal machine modeling for the representation of rotating electric machinery in an electrmagnetic transients program", *IEEE Trans. App. and Sys.*, vol. PAS-101, no. 6, pp. 1342-1351, June 1982.

[28] H. K. Lauw, " Interfacing for universal multi-machine system modeling in an electromagnetic transient program", *IEEE Trans. Power App. and Sys.*, vol. PAS-104, no. 9, pp. 2367-2373, Sept. 1985.

[29] G. J. Rogers and D. Shirmohammadi, "Induction motor modelling for Electromagnetic Transient Program", *IEEE Trans. Eng. Conv.*, vol. 2, no. 4, pp. 622-627, Dec., 1988.

[30] F. L. Alvarado, H. Dommel, V. Brandwajn, R. De La Rosa and L. Marti, "*Electromagnetic Transients Program (EMTP), Volume 1, Workbook III*", EPRI, Palo Alto, California, June 1989.

[31] L. Salazar and G. Joos, "Pspice simulation of three-phase inverters by means of switching functions", *IEEE Trans. Power Electr.*, vol. 9, no. 1, pp. 35-42, Jan. 1994.

[32] H. Jin, M. Pande, "*Instruction manual for Power Electronics Circuit Analysis (PECAN) simulation package*", Concordia University, June 1992.

[33] R. H. Lasseter, K. Fehrle, B. Lee, "*Electromagnetic Transients Program (EMTP), Volume 4, Workbook IV*", EPRI, Palo Alto, California, June 1989.

[34] P. Wood, "*Theory of switching power converter*", Van Nostrand-Reihold, New York, 1981.

[35] P. D. Ziogas, "Synthesis of optimum gain functions for static power converters", *IEEE Trans. Ind. Appl.*, vol. IA-19, pp. 401-408, May/June 1983.

[36] E. P. Wiechmann, P.D. Ziogas and V. R. Stefanovic, "Generalized functional model for three phase PWM inverter/rectifier converters", in *Conf. Rec. IEEE IAS'86*, pp. 984-993, Oct. 1986.

[37] A. V. Jouanne, O. Enjeti and W. Gray, "The effect of long motor leads on PWM inverter fed ac motor drive system", in *Conf. Rec. IEEE APEC' 95*, pp. 592-597, Mar. 1995.

[38] A. V. Jouanne, P. Enjeti and W. Gray, "Filtering techniques to minimize the effect of long motor leads on PWM inverter fed AC motor drive systems", *IEEE IAS'95*, pp. 592-597, Oct. 1995.

[39] H. W. Dommel, "Digital computer solution of electromagnetic transients in single-and multiphase Networks", *IEEE Trans. on App. and Sys.*, vol. PAS-88, no. 4, pp. 388-398, Apr. 1969.

[40] H. N. Muller, "*Electrical Transmission and Distribution Reference book*", Westinghouse Electric Corporation, Pennsylvania, 1964.

[41] E. Persson, "Transient effects in application of PWM inverters to induction motors", *IEEE Trans. Ind. Appl.*, vol. IA-28, no. 5, pp. 1095-1101, Sept./Oct. 1992.

[42] Greenwood, "*Electrical transients in power system*", Wiley, New York, 1991, 2nd eddition.

[43] A. Bradley, "*IGBT technology, Application note 114*", Mar. 1994.

[44] B. Mokrytzki, "Filters for adjustable frequency drives", in *Conf. Rec. IEEE APEC' 94*, pp. 542-548, Mar. 1994.

[45] D. E. Rice, "Adjustable speed drive and power rectifier harmonics--Their effect on power system components", *IEEE Trans. Ind. Appl.*, vol. IA-22, no. 1, pp. 161-177, Jan./Feb. 1986.

[46] J. Arrillaga, D. A. Bradley and P. S. Bodger, *"Power system harmonics"*, John Wiley ans Sons, New York, 1985.

[47] R. F. Chu and J. J. Burns, "Impact of cycloconverter harmonics", *IEEE Trans. Ind. Appl.*, vol. 25, no. 3, pp. 427-435, May/June 1989.

[48] *"IEEE Recommended practices and requirements for harmonic control in electrical power systems"*, IEEE Standard 519, Apr. 1993.

[49] A. Hussein and G. Joos, "Modeling and simulation of traveling waves in induction motor drives", Submitted to *IEEE APEC'97.*

APPENDIX

A.1 Listing of EMTP Programs Used in this Thesis.

A.1.1 EMTP Program to Simulate a 3 Phase Squirrel Cage Induction Motor (*Type 4*)

```
C INDUCTION MOTOR MODELING
  1.5E-4    0.6
    1000        1                                                        1
TACS HYBIRD
90BUSMG
88SLIP      = 1- BUSMG/(377/2)
90BUSA
90BUSB
88VA2       = BUSA - BUSB
88IR      65+VA2                                        60.
33SLIP
BLANK
00VA      BUSA                  0.001
00VB      BUSB                  0.001
00VC      BUSC                  0.001
00NA1                           1.E+9
00BUSA    INA                   .11    .15
00BUSB    INB     BUSA   INA
00BUSC    INC     BUSA   INA
00BUSMG                                  .033E6
00        BUSMG               202.97
00BUSMS   BUSMG               1.0E-6
00NEUT                        1.0E+9
97NA      NA1                           -1
            0.0000                 1.3
            0.01                   1.17
            0.02                   1.04
            0.03                   0.91
            0.04                   0.78
            0.05                   0.65
            0.06                   0.52
            0.08                   0.26
            0.09                   0.13
            0.1                    0.1
              9999
97NB      NA1     NA     NA1
97NC      NA1     NA     NA1
BLANK
BLANK
14VA           170.         60.0     -90.                                -1.
14VB           170.         60.0     -210.                               -1.
14VC           170.         60.0     30.                                 -1.
14BUSMS -1     -12.3      0.00001                                        -1.
```

```
19 UM
 0
BLANK
 4 1 1111BUSMG          2
                0.0483
                0.0483
0.40            0.0018          INA     NEUT
0.40            0.0018          INB     NEUT
0.40            0.0018          INC     NEUT
0.50            0.0027          NA      NA1
0.50            0.0027          NB      NA1
0.50            0.0027          NC      NA1
BLANK
BLANK
  INA    INB
BLANK
BLANK
BLANK
```

A.1.2 EMTP Program to Simulate a 3 Phase Squirrel Cage Induction Motor Drive

```
C INDUCTION MOTOR DRIVE MODELING (60 Hz Operation)
  1.5E-6  0.275
    1000        1                                                          1
TACS HYBIRD
98FS        =1260.0
23PULS        2.0          0.794E-3  0.397E-3
98SQPUL     = (UNITY - PULS)
98VTRI   58+SQPUL                                          5040.0    0.0  1.0
14VCONTA        1.7          60.0      -90.0
14VCONTB        1.7          60.0      - 210.0
14VCONTC        1.7          60.0       30.0
98SIGA      = VCONTA .GT. VTRI
98SIGAP     = .NOT. SIGA
98SIGB      = VCONTB .GT. VTRI
98SIGBP     = .NOT. SIGB
98SIGC      = VCONTC .GT. VTRI
98SIGCP     = .NOT. SIGC
77VTRI         1.0
BLANK
00VSA    VA                      0.11    0.15
00VSB    VB      VSA     VA
00VSC    VC      VSA     VA
00NEUT                           1.E+9
00NA1            NEUT
00VA1    A1                      0.001
00VB1    B1                      0.001
00VC1    C1                      0.001
00NA     NA1     VA1     A1
00NB     NA1     VA1     A1
00NC     NA1     VA1     A1
00POS    POSP                            0.01
00POSP   VA                      33.0           1.0
00POSP   VB      POSP    VA
00POSP   VC      POSP    VA
00VA     NEG     POSP    VA
```

```
00VB     NEG    POSP  VA
00VC     NEG    POSP  VA
00POSP   NEG                                  1200.
00BUSMG                                       .03E6
00       BUSMG              202.97
00BUSMS  BUSMG              1.0E-6
BLANK
00NEG1   NEG                                                MEASURING
11VA     POS
11VB     POS
11VC     POS
11NEG    VA
11NEG    VB
11NEG    VC
13POSP   VA1                                               CLOSED          SIGA
13POSP   VB1                                                               SIGB
13POSP   VC1                                               CLOSED          SIGC
13VA1    NEG1                                                               SIGAP
13VB1    NEG1                                              CLOSED          SIGBP
13VC1    NEG1                                                               SIGCP
BLANK
14BUSMS -1 -12.3      0.00001
19 UM
 0
BLANK
 4 1 1110BUSMG         2
                0.0483
                0.0483
0.4             0.0018          A1      NEUT
0.4             0.0018          B1      NEUT
0.4             0.0018          C1      NEUT
0.50            0.0027          NA      NA1
0.50            0.0027          NB      NA1
0.50            0.0027          NC      NA1
BLANK
14VSA       170.0       60.0       -90.0
14VSB       170.0       60.0       -210.0
14VSC       170.0       60.0        30.0
BLANK
 2POSP        144.0
 2NEG        -144.0
  VA     VB     VA1    VB1
BLANK
BLANK
BLANK
BLANK
```

A.1.3 EMTP Program to Simulate a 3 Phase Squirrel Cage Induction Motor Drive with Long Cable (Distributed Parameter Cable Model)

```
C INDUCTION MOTOR DRIVE MODELING WITH LONG CABLE (DISTRIBUTED PARAMETER)
C CABLE LENGTH = 40 m
  .10E-7  0.5E-3
       1       1                                                        1
TACS HYBIRD
90A1
90A2
90B1
90B2
90C1
90C2
98SIGA     = A1 + A2
98SIGB     = B1 + B2
98SIGC     = C1 + C2
98A        = (2.0 * SIGA - 1.0 )*143.
98B        = (2.0 * SIGB - 1.0 )*143.
98C        = (2.0 * SIGC - 1.0 )*143.
33SIGA  SIGB  SIGC
BLANK
00A1     NEUT1              2.7E9
00A2     NEUT1              2.7E9
00B1     NEUT1              2.7E9
00B2     NEUT1              2.7E9
00C1     NEUT1              2.7E9
00C2     NEUT1              2.7E9
97A      VA1
        1.7775E-4           10.8
          1.92E-4           10.8
         1.925E-4            .186
            9999
97B      VB1
        1.7775E-4           10.8
          1.91E-4           10.8
         1.925E-4            .186
            9999
97C      VC1
        1.7775E-4           10.8
          1.91E-4           10.8
         1.925E-4            .186
            9999
-1VA1    VA2               .01E-64.8E-4.18E-3 40.    0 0 0
-1VB1    VB2               .01E-64.8E-4.18E-3 40.    0 0 0
-1VC1    VC2               .01E-64.8E-4.18E-3 40.    0 0 0
00VA2    NEUT              8.78  21.75
00VB2    NEUT  VA2   NEUT
00VC2    NEUT  VA2   NEUT
C 00VAF1                                  .073
C 00VBF1         VAF1
C 00VCF1         VAF1
C 00VA2   VAF1                51.6
C 00VB2   VBF1  VA2   VAF1
C 00VC2   VCF1  VA2   VAF1
BLANK
BLANK
```

```
60A
60B
60C
12A1        1.                          0.2E-6                      1.771E-4   6.877E-4
12A2        1.                          0.2E-6                      8.786E-4   0.007E-4
12B1        1.                          0.2E-6                       0.0043    0.0044
12B2        1.                          0.2E-6                       0.005     0.0053
12C1        1.                          0.2E-6                        2.3E-6   0.0015
12C2        1.                          0.2E-6                      0.0016     0.0023
BLANK
  VA2    VB2    A       B
BLANK
BLANK
BLANK
BLANK
```

A.1.4 EMTP Program to Simulate a 3 Phase Squirrel Cage Induction Motor Drive with Long Cable (Lumped Parameter Cable Model)

```
C INDUCTION MOTOR DRIVE MODELING WITH LONG CABLE
C                    (LUMPED PARAMETER - 3 pi)
C CABLE LENGTH = 40 m
  .10E-7 2.93E-4
       1        1
TACS HYBIRD
90A1
90A2
90B1
90C1
90C2
98SIGA     = A1 + A2
98SIGB     = B1 + B2
98SIGC     = C1 + C2
98A        = (2.0 * SIGA - 1.0 )*143.
98B        = (2.0 * SIGB - 1.0 )*143.
98C        = (2.0 * SIGC - 1.0 )*143.
33SIGA  SIGB  SIGC
BLANK
00A1     NEUT1                  2.7E9
00A2     NEUT1                  2.7E9
00B1     NEUT1                  2.7E9
00B2     NEUT1                  2.7E9
00C1     NEUT1                  2.7E9
00C2     NEUT1                  2.7E9
97A      M1
        1.7775E-4               3.6
          1.92E-4               3.6
         1.925E-4               .062
             9999
97B      N1
        1.7775E-4               3.6
          1.92E-4               3.6
         1.925E-4               .062
             9999
97C      P1
        1.7775E-4               3.6
          1.92E-4               3.6
         1.925E-4               .062
             9999
```

```
97M2     M3
       1.7775E-4                3.6
         1.92E-4                3.6
        1.925E-4                .062
            9999
97N2     N3
       1.7775E-4                3.6
         1.92E-4                3.6
        1.925E-4                .062
            9999
97P2     P3
       1.7775E-4                3.6
         1.92E-4                3.6
        1.925E-4                .062
            9999
97M4     M5
       1.7775E-4                3.6
         1.92E-4                3.6
        1.925E-4                .062
            9999
97N4     N5
       1.7775E-4                3.6
         1.92E-4                3.6
        1.925E-4                .062
            9999
97P4     P5
       1.7775E-4                3.6
         1.92E-4                3.6
        1.925E-4                .062
            9999
00M1     M2                                .0064
00M3     M4      M1      M2
00M5     VA2     M1      M2
00N1     N2      M1      M2
00N3     N4      M1      M2
00N5     VB2     M1      M2
00P1     P2      M1      M2
00P3     P4      M1      M2
00P5     VC2     M1      M2
00M2                                               .0072
00M4             M2
00N2             M2
00N4             M2
00P2             M2
00P4             M2
00VA2                                              .0036
00VB2            VA2
00VC2            VA2
00VA2    NEUT                      8.78   21.75
00VB2    NEUT    VA2     NEUT
00VC2    NEUT    VA2     NEUT
BLANK
BLANK
60A
60B
60C
12A1       1.                                0.2E-6          1.771E-4   6.877E-4
12A2       1.                                0.2E-6          8.786E-4   0.007E-4
12B1       1.                                0.2E-6           0.0043    0.0044
12B2       1.                                0.2E-6           0.005     0.0053
12C1       1.                                0.2E-6            2.3E-6   0.0015
12C2       1.                                0.2E-6          0.0016     0.0023
BLANK
```

```
  VA2    VB2    A      B
BLANK
BLANK
BLANK
BLANK
```

A.1.5 EMTP Program to Simulate Three Phase Diode Bridge Rectifier with Capacitor Switching

```
C 3 PHASE DIODE BRIDGE RECTIFIER WITH CAPACITOR SWITCHING
  2.5E-6 150.E-3
    1000        1                                                        1
TACS HYBIRD
90POS
90NEG
98ALI      = POS-NEG
98IDSUM 58+ALI                                          1.0        0.0 1.0
98IDAVG    = IDSUM / TIMEX
33IDAVG
BLANK
00VSA    VLA                        .15
00VSB    VLB                        .15
00VSC    VLC                        .15
00VLA    VA                          .1
00VLB    VB      VLA    VA
00VLC    VC      VLA    VA
00VLA    VLA1                0.001
00VLB    VLB1    VLA    VLA1
00VLC    VLC1    VLA    VLA1
00VLA1                       2.77   5.507
00VLB1           VLA1
00VLC1           VLA1
00VLA2                                  459.83
00VLB2                                  459.83
00VLC2                                  459.83
00POSP   VA                  33.0        1.0
00POSP   VB      POSP   VA
00POSP   VC      POSP   VA
00VA     NEG     POSP   VA
00VB     NEG     POSP   VA
00VC     NEG     POSP   VA
00POSP   POS                 0.001
00POS    NEG                                1200.0
00POS    NEG                 30.5
BLANK
00NEG1   NEG                                                  MEASURING
11VA     POSP
11VB     POSP
11VC     POSP
11NEG    VA
11NEG    VB
11NEG    VC
00VLA1   VLA2        50.E-3   9999.0
00VLB1   VLB2        50.E-3   9999.0
00VLC1   VLC2        50.E-3   9999.0
BLANK
14VSA       170.0        60.0      -90.0
14VSB       170.0        60.0     -210.0
14VSC       170.0        60.0       30.0
BLANK
BLANK
BLANK
```

A.2 Lists of Equipments Used for Experimental Testing

(i) Three Phase Squirrel Cage Induction Motor

3 hp, 1740 RPM, 208 V, 10 A, 60 Hz.

(ii) DC Motor/Generator

2 hp, 1750 RPM, 180 V, 8.5 A.

(iii) Three Phase Static Converter HFC-VWS$_3$ U (Hitachi)

Input voltage	200-220 V/ 200-300 V
Input frequency	50/60 Hz
Control system	Voltage source type (SPWM)
Output Frequency range	1→120 Hz
Rating	4.1 kVA

(iv) Three-Conductor Belted Paper Insulated Cable

Voltage class	1 kV
Circular Mils	6
Weight per 1000 Feet	1500 Lbs.
Type of conductor	Standard round

(v) Resistive Load

Maximum voltage/phase	208 V (rms)
Maximum current/phase	50 A (rms)
Rating	31.2 kVA

A.3 DC Generator Equations Used to Calculate the Shaft Torque and Speed

Assuming I_g and V_g are respectively the generator output voltage and current, the relation between V_g and I_g is:

$$V_g = E_g - I_g R_g \tag{A.1}$$

where

E_g = The induced voltage,

R_g = The armature resistance.

Neglecting the mechanical losses on the generator shaft, E_g and I_g can be defined as:

$$E = K_g \omega_m \tag{A.2}$$

$$T_M = K_g I_g \tag{A.3}$$

where K_g is a constant can be calculated from the machine name plate data.

For the generator data given in section (A.2):

$$K_g = 0.95 \text{ and } R_g = 0.5\ \Omega$$